SCRATCH AND MECHANICAL BEHAVIORS OF POLYROTAXANE-MODIFIED POLY(METHYL METHACRYLATE)

A Dissertation

by

GLENDIMAR MOLERO

Submitted to the Office of Graduate and Professional Studies of
Texas A&M University
in partial fulfillment of the requirements for the degree of

DOCTOR OF PHILOSOPHY

Chair of Committee,	Hung-Jue Sue
Committee Members,	Homero Castaneda-Lopez
	Lei Fang
	Mohammad Naraghi
Head of Department,	Ibrahim Karaman

May 2021

Major Subject: Materials Science and Engineering

ABSTRACT

The susceptibility of polymers to surface damage like scratch significantly limits their use in applications where both surface structural integrity and aesthetics are important. The present study employs a standardized progressive load scratch test to investigate the fundamental physical and mechanistic origins of scratch-induced deformation in polymers with the purpose of applying the gained knowledge to design polymers with superior scratch resistance. The key aspects of polymer scratch behavior in this study are the scratch cracking resistance and the scratch visibility resistance. Previous experimental and numerical studies have shown that there is a correlation between mechanical properties and scratch deformation mechanisms. In order to obtain a more comprehensive understanding on how the mechanical properties affect the scratch behavior, this research focuses on experimental analysis of a set of well controlled polymer systems to establish structure-property relationships, leading to effective design of polymers with superior scratch-proof properties.

A scratch can be considered a single-pass sliding of a single-asperity across the surface of a polymer under an applied normal load. Understanding the scratch-induced deformation of polymers is complicated due to the viscoelastic nature of polymers. The ASTM scratch test has enabled significant progress in the understanding of the scratch behavior of polymers. This test consists of a linearly increasing normal load, which generates continuous progression of deformation, allowing for the observation of damage formation and evolution. This allows to conduct a straightforward analysis and to develop structure-property relationships. Another challenging aspect of scratch testing is unambiguously evaluating the scratch visibility. Assessing the scratch visibility merely based on human observation is troublesome. Quantitative evaluation

of scratch resistance requires the elimination of ambiguity and subjectivity. Employing a reliable testing and analysis methodology that is based upon the principles of material science facilitates the fundamental understanding of polymer scratch behavior.

To successfully design polymers with high scratch resistance, the first step is to fundamentally understand what factors influence the scratch behavior. To do so, a set of model epoxy systems with varying crosslinking density were prepared to investigate how the scratch behavior, specifically, the onset of crack formation, might be influenced. The findings indicate that both the tensile strength and compressive yield stress determine the resistance against scratch damage formation. Moreover, the scratch behavior of a set of injection molded model PC systems with different tensile and compressive constitutive behavior was investigated. The findings suggest that the scratch visibility of the model PC systems is closely linked to the compressive yield stress, which dictate the magnitude of the scratch depth and shoulder height.

Novel material design concepts are required to develop polymers with superior scratch resistance. Polyrotaxane (PR) is a supramolecule with rings threaded onto a backbone linear chain that is capped by bulky end groups. The ring structure, cyclodextrin (CD), can slide along the backbone, allowing for stress redistribution. Due to its dynamic structure, PR has shown to induce significant self-recovery abilities after scratch-type of damage, leading to improvements in the scratch resistance. PR has been extensively investigated in elastomeric coating systems. In this work, the effect of PR on the scratch behavior of more rigid polymers networks like poly(methyl methacrylate) (PMMA) were investigated. Dielectric relaxation spectroscopy, dynamic mechanical analysis, tensile and compressive true stress-strain tests, in conjunction with ASTM scratch test, were conducted to fundamentally understand how PR influences the mechanical and scratch behaviors of PMMA.

DEDICATION

To:

My husband, Ezequiel

&

My parents, Glenda and Martin

ACKNOWLEDGEMENTS

I would like to express my deepest appreciation to my advisor, Dr. Hung-Jue Sue, for his guidance and support throughout these years. Thanks to Dr. Michael Mullins for his mentorship. I would also like to recognize the generous support from the Texas A&M Scratch Behavior of Polymers Consortium.

I would like to sincerely thank my husband, Ezequiel Cisneros, for his encouragement and endless love and support during this journey. Thanks to my parents, Glenda Rondon and Martin Molero, my sister, Loreana Molero, and my grandmother, Nelis Molero, without their guidance, love and support, this would never have been possible.

Special thanks to Dr. Shuang Xiao, Dr. Cong Liu, Dr. Shuoran Du and Dr. Joseph Baker for their mentorship and help. I would also like to thank my colleagues Chia-Ying Tsai, Zewen Zhu and Qihui Chen for their friendship and support.

Thanks to Shuntaro Uenuma and Professor Kohzo Ito for their constant support during our research collaboration.

I would like to thank Dr. Karen Lozano, for being a role model and inspiring me to become a scientist. Thanks to Dr. David Fiscus for his valuable guidance and friendship.

CONTRIBUTORS AND FUNDING SOURCES

Contributors

This work was supervised by a dissertation committee consisting of Professor Hung-Jue Sue, advisor and committee chair, and Professor Homero Castaneda-Lopez of the Department of Materials Science & Engineering, Professor Lei Fang of the Department of Materials Science & Engineering and of the Department of Chemistry, and Professor Mohammad Naraghi of the Department of Aerospace Engineering.

Funding Sources

All work for the dissertation was completed independently by the student and funded by Texas A&M Scratch Behavior of Polymers Consortium.

TABLE OF CONTENTS

Page

LIST OF FIGURES

Page

LIST OF TABLES

Page

CHAPTER I

INTRODUCTION & LITERATURE REVIEW

1.1 Overview of Polymer Scratch Research

Surface quality in polymer products has become a critical property in many applications. The three main areas of concern are aesthetics, structural integrity and durability. Polymer products with a visually appealing surface are valuable to consumers. Surface scratches reduce the value of products even if their functionality is unaffected. For example, in interior and exterior vehicle components, scratches reduce surface quality, thus lowering its perceived value. From a structural integrity perspective, resistance against scratch deformation is of extreme importance for food packaging applications. Thin polymers layers of food packaging films must retain their structural integrity during shipping and handling to protect the contents. From a durability point of view, protective polymer coatings on metal surface must withstand surface scratches during transportation and service to prevent or slow down corrosion and extend the service life of the metal substrate.

Compared to other materials, polymers are extremely susceptible to surface damage. Yet, due to their lightweight, low cost, ease of processing and versatile properties, polymers remain the best candidate for most applications in the microelectronics, packaging, automotive and aerospace industries. In most of these applications, polymers are subjected to scratching, resulting in surface damage at various scales. Understanding scratch-induced damage is complicated due to viscoelastic nature and complex constitutive behavior of polymers, which plays an important role

in the material response when a polymer is scratched. This brings the additional challenge of developing test methods that describe the scratch resistance of polymers from a material science point of view.

The field of tribology focuses on wear, lubrication and friction. Abrasion is a form of wear and it can be defined as the process of removing material from a surface by another material sliding along the surface under a prescribed load. Abrasion can be categorized as single-pass and multi-pass abrasion. In single-pass, the sliding face encounters the surface of the counterpart only once. In multi-pass, the sliding face encounters the same surface of the counterpart many times [1]. In many situations, scratches can be considered as precursors of wear and abrasion. Therefore, fundamental understanding of the scratch behavior of polymers can offer unambiguous insights about how the abrasion and wear induced damage form and evolve. The scratch resistance of a polymer is described by its ability to resist surface deformation due to the sliding indentation of an asperity subjected to a prescribed normal load. In the view of this definition, a scratch can be considered a single-pass with a single-asperity abrasion.

Numerous devices to assess scratch resistance of materials have been developed over the years. The main limitation of many scratch testing methods is they only provide a qualitative or relative assessment. The scratch resistance is often described in a “pass” or “fail” fashion, which does not explain why a material behaves in a particular way. Some of the scratch testing methods involve the pencil hardness test [2], single-pass pendulum [3-5], pin-on-disc test [6], Taber test scratcher [7] and Ford Lab Test Method (FLTM) scratcher [8]. A more detailed review of these methodologies is presented by Wong et al. [9]. The pencil hardness test is widely used to evaluate the scratch resistance of coatings [10, 11]. It involves a pencil firmly held against the surface of a sample in a pencil hardness kit. The device is designed to apply a load of 7.5 N at an angle of 45°

while it's pushed away from the operator to generate a scratch [12]. The process is repeated down the pencil hardness scale until a pencil that will not produce visible damage on the sample surface is found, which is denoted as the pencil hardness grade. Because of many uncontrolled process variabilities, such as pencil type, the surface finish of the pencil tip, and operator's variability, the reproducibility of the results is usually poor. Since the results are based on visibility of damage, the information provided about the scratch behavior is limited. Moreover, it has been shown that different systems with the same pencil hardness grade may experience different scratch mechanisms, damage features and extent of damage [10, 13]. The other testing methods mentioned above involve mechanically generated scratches on the material surface and are not as sensitive to operator's variability. Although these methods generate scratches in a more reproducible manner, it is still difficult to gain fundamental knowledge about the observed scratch behavior to enable the design of materials with improved scratch resistance.

The establishment of the ASTM D7027/ISO 19252 scratch test standard has led to significant progress in the understanding of the scratch behavior of polymeric systems [14]. This standardized test consists of a linearly increasing normal load, which generates continuous progression of deformation. This allows for the observation of the scratch-induced damage evolution, leading to straightforward analysis and development of structure-property relationship. The onset and extend of scratch-induced deformation features, such as scratch depth and shoulder height, and scratch-induced damage, such as cracking and fish-scale formation, depend largely on the surface characteristics and material constitutive behavior of the polymer [15, 16]. Frictional characteristics, heat dissipation, and geometrical factors are among other important factors that can greatly influence scratch behavior. For compression molded polymers or annealed samples, the evolution of scratch-induced damage features has been correlated with bulk mechanical

properties [15, 17, 18]. Under such a scenario, numerical simulation can be utilized as a tool to understand the stress state in a particular testing scenario, and thus predict the material response when subjected to scratching [18-20].

Another challenging aspect of scratch testing is determining the onset of scratch visibility. Assessing the scratch visibility merely based on human observation is troublesome. Differences between the eyes of human observers and variations in lighting condition add complexity to unambiguously evaluate the scratch visibility of polymers. Several methodologies have been developed over the years to evaluate the scratch visibility [7, 21, 22]. Wong et al. [23] introduced a method to precisely quantify the onset of scratch visibility by using a scratch tester and a digital image analysis software. Quantitative evaluation of scratch resistance requires the elimination of ambiguity and subjectivity. Employing a reliable testing and analysis methodology that is based upon the principles of material science facilitates the fundamental understanding of polymer scratch behavior.

In many applications, the main concern regarding scratch behavior is visibility. Scratch visibility originates from the scattering of incident light differs from the background due to changes in surface roughness and/or other scratched surface features. These surface features include scratch-induced cracks, crazes and localized molecular orientation. The size of this features must be comparable or above the wavelength of visible light to become visible. At low normal loads, the scratch damage is difficult to be detected by the naked eye. With increasing load, the contrast between the damage and undamaged surface will increase, and thus become visible. Since the applied load can be related to the scratch distance, it is possible to quantitatively locate the load at which the scratch becomes visible. The standardized scratch test machine is used in conjunction with a commercially available software package (Surface Visibility Analyze (SVA)

software by Surface Machine Systems®), enabling meaningful quantitative evaluation of the onset of scratch visibility. More recently, the procedure was further refined by employing a custom-built black box to take images of the scratches at a predetermined lighting condition. The captured images are analyzed using the SVA software based on the contrast between the damage and undamaged area [24].

1.2 Research Scope

Polymer surfaces are prone to scratch damage even at low contact loads. The demand for polymers with high scratch resistance polymers is continuously increasing due to new arising applications. Many studies have been conducted to establish a methodology to evaluate the scratch resistance of polymers [5, 8, 9]. It has been shown that scratch-induced deformation using the standardized scratch test can be correlated to mechanical properties of the tested materials to gain fundamental understanding about the scratch behavior of polymers [13, 25, 26]. Poly(methyl methacrylate) (PMMA) is a promising material for automotive, electronic and optical applications because of its light-weight, transparency and weather resistance [27]. However, it exhibits poor impact, scratch and fracture resistance, which is a major disadvantage with respect to other transparent engineering polymers, such as polycarbonate (PC) [28]. Diverse approaches such as functionalization of inorganic fillers [29], organic-inorganic hybrid systems [30], interpenetrating networks [31], plasticizers [32] and carbon nanotubes [33] have been reported to moderately improve scratch resistance of PMMA. Typically, functionalization of the fillers is required to ensure good compatibility between the filler and the polymer matrix, tedious sample preparation procedures are often needed, and the scalability of the processes is challenging. More importantly, improvements in scratch resistance are attributed to an increase in hardness or modulus, which may not be directly correlated to the complex scratch behavior of polymers [13]. Thus,

fundamental understanding about the parameters that govern the scratch behavior of PMMA composites is still needed.

Novel material design concepts are required to develop polymers with superior scratch that can meet demanding applications. Polyrotaxane (PR) is a supramolecule with rings threaded onto a backbone linear chain that is capped by bulky end groups [34]. The cyclic component, cyclodextrin (CD), serves as the ring structure and it is sparsely incorporated in the backbone linear chain. CD is subsequently crosslinked on different PRs to crosslinking junctions that exhibit an exhibit a figure-of-eight shape. The crosslinking junctions can slide upon stressing allowing for stress redistribution. This type of crosslinked networks is known as slide-ring (SR) materials [35]. Due to high elasticity and flexibility, SR elastomers have shown significant self-recovery abilities after scratch-type of damage [34, 35]. Recently, both the scratch resistance and flexibility of organic-inorganic hybrid coatings was improved by employing alkoxysilyl-functionalized polyrotaxane cross-linker [36]. Thus, showing the potential to expand the utilization of SR materials into rigid polymer networks to enhance the scratch resistance.

To successfully design polymers with high scratch resistance, the first step is to fundamentally understand what factors influence the scratch behavior. To do so, a set of well-controlled model systems was employed. Three model epoxy systems with low, medium, and high crosslinking densities were prepared to systematically investigate how the scratch behavior, specifically, the onset of crack formation, might be influenced. Mechanical and scratch tests were performed to correlate the intrinsic material properties to the observed scratch-induced deformation of the epoxy systems. The findings indicate that the resistance against crack formation during scratching can be directly correlated to the mechanical properties of the material. Both the tensile strength and compressive yield stress determine the resistance against scratch damage formation. To investigate

more in-depth how the tensile and compressive properties interplay during scratch damage formation, a set of well-controlled polycarbonate (PC) model systems was utilized. It was shown that the both the tensile strength, tensile and compressive yield stresses play an important role during the scratch process. The yielding behavior of the model PC systems was strongly related to the scratch depth, which in turn strongly affects the friction behavior. Moreover, the tensile strength of the PC model systems was closely related to resistance against cracking. These studies serve to fundamentally understand how material properties relate to scratch resistance, and they will be used as a foundation to investigate how PR influences the scratch behavior of PMMA.

Finally, the mechanical and scratch behaviors of polyrotaxane (PR) modified poly(methyl methacrylate) (PMMA) were investigated. The effect of PR concentration and the effect of CD functionalization were studied. To systematically investigate the effect of CD functionalization on the properties of PMMA, PR with polycaprolactone (PCL) grafted chains on CD, and PR with methacrylate functional groups at the terminal of the PCL grafted chains on CD were chosen for this study. Dielectric relaxation spectroscopy, dynamic mechanical analysis, tensile and compressive true stress-strain tests, in conjunction with ASTM scratch test, were conducted to fundamentally understand how PR influences the mechanical and scratch behaviors of PMMA.

1.3 Layout of the dissertation

The overview of polymer scratch research presented in this chapter provides the groundwork to perform a comprehensive investigation on the scratch behavior of polymers. In Chapter II, performed experiments and testing methods along with the results and discussion are presented to determine the governing material properties that influence the scratch resistance of model epoxy systems. An in-depth investigation about the relationship between yielding behavior and scratch-induced damage on a set of model PC systems is presented in Chapter III. Based on the knowledge

gained in the previous chapters, Chapter IV focuses on developing high scratch resistance PMMA by using polyrotaxane (PR). This chapter will focus on the experimental work conducted to fundamentally understand the scratch behavior of the PMMA/PR systems. Additionally, dielectric relaxation spectroscopy and dynamic mechanical analysis are used to explore what possible molecular mechanisms might be behind the observed improvements in the mechanical and scratch properties of the PMMA/PR systems. Finally, a summary of the research outcome and considerations for future research are given Chapter V, followed by the references cited in this dissertation.

CHAPTER II

SCRATCH BEHAVIOR OF MODEL EPOXY SYSTEMS[1]

In this chapter, the scratch behavior of model epoxy resins with varying degrees of crosslink density was investigated according to the ASTM D7027/ISO 19252 scratch test methodology. Three model epoxy systems with low, medium, and high crosslinking densities were prepared to systematically investigate how the scratch behavior might be influenced. The effect of crosslinking density on the onset of groove, crack and plowing formation during scratching was investigated. Coefficient of friction measurements, uniaxial tensile and compressive stress-strain curves, and dynamic mechanical analyses were conducted to correlate the intrinsic material properties to the observed scratch-induced deformation of the model epoxy systems. The findings indicate that the scratch behavior of epoxy resins can be directly correlated to their material properties. It is found that both the tensile strength and compressive yield stress determine the resistance against damage formation during scratch. Additionally, a comparison between pencil hardness and scratch test is presented to assess the suitability of both methods for evaluating scratch performance of polymers with significantly different mechanical properties.

2.1 Introduction

Polymer products have become essential in many engineering applications due to their versatile properties. Despite their superior processability and low cost, polymers are prone to scratch damage. This limits their application where aesthetics and surface conditions are

[1] Reprinted with permission from Molero, Glendimar, and Hung-Jue Sue. "Scratch behavior of model epoxy resins with different crosslinking densities." *Materials & Design* 182 (2019). Copyright 2019. Elsevier

imperative. Scratch resistance is crucial in many scenarios not only for aesthetic purposes but also for the structural integrity and functionality of the surfaces. For instance, in the case of protective coatings, scratch resistance is key to maintain the functionality of the coating. Many studies have been performed to establish a methodology that quantitatively describe the scratch performance of polymers [9, 15, 37-39]. The ASTM D7027/ISO 19252 standardized scratch test, which consist of a linearly increasing normal load, is widely implemented to evaluate the scratch performance of different polymeric systems [14]. This methodology allows for the identification of the onset of different damage types induced by scratching, such as groove, cracking, and plowing formation. The correlation of the scratch normal load with the onset of damage transitions during scratching can be used to gain fundamental knowledge of scratch behavior in polymers. Several fundamental studies have been conducted to establish a structure-property relationship for different polymeric systems [8, 9, 15, 25, 37-40].

Correlations between material properties have been experimentally established in the past for different types of systems. Browning et al. [17] and Liang et al. [26] investigated the scratch behavior of styrenic copolymers and showed that the resistance against crack formation can be improved by increasing the tensile strength. Xiao et al. [25, 41] showed that the compressive yield stress, tensile strength and coefficient of friction (COF) influence the onset of damage transitions during scratching in polyurethane (PU) elastomers. Moreover, quantitative correlations between material properties and scratch behavior have been established numerically *via* finite element methods (FEM) modeling. Jiang et al. [15] found that during the scratch process, as the normal load is increased, the material underneath the tip experiences a tensile stress that quickly transforms into a compressive stress during scratching. Subsequently, Hossain et al. [16, 42-45] found that the tensile strength correlates well with the onset of crack formation and that the COF

plays an important role during scratch process, especially in the onset of groove and crack formation. It was also shown that the yield stress, strain at recovery, and strain hardening slope under compression influence the scratch depth and shoulder height during scratch. An effort has been made by Brostow et al. [46] to learn about the fundamental molecular mechanisms during the scratching of polymeric materials using molecular dynamics by adopting the concept of statistical chain segment in the simulation of scratch testing.

Owing to their superior processability and high strength-to-weight ratio, thermosetting polymers, such as epoxy resins, have a wide range of applications where scratch is of extreme importance, such as protective coatings and composites, in the aerospace and automotive industries [47-51]. High crosslinking density and the nature of interchain bonding make epoxies excellent candidates for other applications like corrosion protection, electronic encapsulants and flooring [52]. The crosslinking density is well known for influencing the resulting physical and mechanical properties of cured epoxy-based systems [38, 47, 48, 53-55]. Two important curing states regarding epoxy curing reactions are gelation and vitrification. Gelation is the point where the infinite molecular weight is obtained, which means that the all the monomers are connected to the network. On the other hand, vitrification refers to the point where the material transitions from a rubbery to a glassy state [56]. The distinction between these two points is relevant for the optimization of industrial processing of epoxy-based composites [56, 57].

Wong et al. [38] investigated the scratch-induced surface damage of epoxy resins with varying degrees of crosslinking density under constant loading and scratch rate at the nanoscale. The study suggests that mechanical properties, such as ductility of the epoxy networks influence damage patterns and mechanisms near the surface. Jiang et al. [15] explored the scratch behavior on four categories of polymers with the objective of correlating material parameters with different scratch

mechanics and damage evolution. It was reported that for epoxy, scratch damage is undetectable until a sufficiently high normal load is applied. After the scratching load reaches a certain magnitude, parabolic cracks start to form and become the dominant damage mode. These parabolic cracks point opposite to the scratch direction and propagate in a brittle manner and become more regular as the scratch normal load increases. As the scratch load continues to increase, the transition from crack formation to the material removal zone, i.e., plowing, will occur. To our knowledge, no correlation has been established between material properties and scratch resistance of neat bulk epoxy resins with different crosslinking densities.

As mentioned earlier, epoxy resins have a wide variety of applications as the base material for coatings, adhesives and composites. The scratch behavior of polymers has become a matter of interest due the susceptibility of polymers to surface damage, which may compromise the functionality and aesthetics of a coating. The pencil hardness test [58] has been a common practice in the industry for many years to determine the resistance of the coating against scratch and mar "in a practical and low-cost manner. The test consists of placing a sample on a level and horizontal substrate. As the pencil is firmly held against the film, the pencil hardness testing kit is pushed away from the operator. With a smooth and chip-free tip of pencil, the tester is designed to apply a load of 7.5 N load over a stroke distance of 6.5 mm at an angle of 45°. The process is repeated down the pencil hardness scale until a pencil that will not produce visible damage on the sample surface is found, which is denoted as the pencil hardness grade.

The above procedure has been utilized in several studies to compare the pencil hardness of different coatings basing merely on damage visibility [10, 11, 59]. Because of many testing variations, such as pencil type, the surface finish of the tip, and operator's variability, the reproducibility of the results is usually poor. Moreover, since the results are based on visibility of

damage, the information provided about the scratch behavior is limited. In fact, it has been shown that different systems with the same pencil hardness grade may experience different scratch mechanisms, scratch features and extend of damage [10].

The objective of this study is to gain fundamental understanding of the scratch behavior of epoxy resins and their structure-property relationship by investigating a set of model epoxy systems with varying degrees of crosslinking density, i.e., the molecular weight between crosslinks (M_c). Several mechanical tests were conducted to correlate the effect of crosslinking density upon scratch damage. Special attention is given to how material properties correlate to scratch-induced damage with the purpose of understanding and improving the scratch-resistant of epoxy-based systems. Additionally, a pencil hardness test analysis is presented to evaluate the usefulness of the procedure to evaluate scratch performance.

2.2 Materials & Methods

2.2.1 Materials and Sample Preparation

Epoxy resins based on diglycidyl ether of bisphenol A (DGEBA) from Olin Corporation, consisting of three different epoxide monomer molecular weights (low, medium, and high) were used in this study. The resins were D.E.R. 332 (E_L), D.E.R. 661 (E_M) and D.E.R. 667 (E_H) with their epoxide equivalent weights of 173, 542 and 1,666 g/eq, respectively. E_M and E_H, which come in a solid form, were heated to 160 °C until the viscosity of the resins was low enough to be properly mixed with hardener. A stoichiometry amount of the curing agent diamino diphenyl sulfone (DDS) from Sigma-Aldrich was added to the epoxies. The mixture was heated to 130°C until the DDS was dissolved. The mixtures were poured into a preheated glass mold coated with a polytetrafluoroethylene (PTFE) mold release agent from Miller-Stephenson Chemical. The mixed

epoxy was cured in an oven at 180°C for 2 hours followed by 220°C for 2 hours, and then slowly cooled to room temperature. The samples were polished to remove residual of the mold release agent from the surface of the epoxy resins by going from coarse to fine polishing paper (180-, 800-, 1200-, and 2400-grit polishing paper) before any surface measurement. The model systems were dried in a vacuum oven in between two smooth glass plates at 80°C for at least 6 hours before any mechanical testing.

2.2.2 Dynamic Mechanical Analysis (DMA)

DMA was performed using a TA Instruments ARES G2 Rheometer in torsional mode to compare the T_g and crosslinking densities of the epoxy resins. The T_g of the model systems was defined as the peak point of the tan (δ) curve. The temperature range used was 30-285°C at a constant ramp rate of 5 °C/min and at a strain amplitude of 0.05%. The frequency of the test was set at 1 Hz. The specimens were cut to 3 mm in thickness, 8 mm in width and 25 mm in length for DMA testing.

2.2.3 Coefficient of Friction (COF) and Surface Roughness (Rq)

A commercial scratch machine (Scratch 5, Surface Machine Systems, LLC) built according to the ASTM D7027/ISO 19252 standard (6) was used to measure the COF of the epoxy resins. The COF is also known as dynamic friction and it refers to ratio between the force required to maintain motion at a prescribed scratch speed and the force pressing the surface [60]. A flat stainless steel (10 mm x 10 mm) tip was utilized. The tests were performed at a 5 N constant normal load and the speed was 10 mm/s. The tip and the surface of the sample were cleaned using compressed air before taking the measurement. Three tests were performed on each sample. The surface roughness (R_q) was measured by Keyence® VK9700 violet laser scanning confocal

microscope (LSCM) using a sampling area of 675 μm x 506 μm. Ten measurements were taken on each sample.

2.2.4 Uniaxial Tensile Stress-Strain Curves

Engineering stress-strain curves were obtained for E_L and E_M model systems, which were expected to fail in a brittle fashion under tension. Uniaxial tensile stress tests were performed using a MTS Insight® universal testing machine at a crosshead speed of 5 mm/min. The tensile specimens were shaped with a router into a dog-bone shape with 42 mm gauge length, 5 mm width and 3 mm thickness. In the case of E_H, which was expected to behave in a ductile manner, a true stress-strain curve was generated by measuring instantaneous cross-sectional area using digital image correlation (DIC) video setup. A black ink marker was used to generate a random speckle pattern on the gauge section of the samples. A single Canon EOS 5D Mark II DSLR camera and VIC-2D™ DIC software were used to track the deformation of the random speckle pattern on the tensile specimens during the test. This allowed for the acquisition of the true strains in tensile direction (e_{yy}) and lateral directions (e_{xx}). The true stress was obtained by dividing the applied load by the instantaneous cross-sectional area. Three tests were performed on each model system.

2.2.5 Uniaxial Compressive True Stress-Strain Curves

Uniaxial compression tests were conducted using a MTS Insight® universal testing machine at a crosshead speed of 3 mm/min according to the ASTM D695-10 standard [61]. The specimens were cut with a diamond saw blade to the nominal dimensions of 10 mm x 5 mm x 5 mm. Polishing paper with 2400 grit was used to ensure the surfaces were flat and parallel to each other. Lubricant was applied on the compression fixture to minimize friction during the test. Epoxies will undergo severe deformation under compressive loading with significant changes in cross-sectional area. A Canon EOS 5d Mark II DSLR video camera was used to record the

compression test. The images in the video were analyzed to obtain the true strains in the compression direction (e_{yy}) and lateral direction (e_{xx}). Since model systems are considered to be isotropic, the strain in the thickness direction (e_{zz}) is assumed to be equal to e_{xx}. Since only the compressive yield stress is of interest to the present study, the test was terminated soon after the yielding stress was detected. Three tests were performed on each model system.

2.2.6 Scratch Test

The scratch test was conducted according to the ASTM D7027/ISO 19252 methodology. A linearly increasing normal load of 1-200 N was applied. The scratch speed and length were 10 mm/s and 80 mm, respectively. A 1-mm diameter spherical stainless-steel tip was used to conduct the scratch tests. The surface of the samples was cleaned using compressed air before scratching. Three scratches were generated on each model system. The onset of groove, crack and plowing formation and their corresponding damage features were identified using LSCM. The onset loads for the previously mentioned damage transitions were obtained from the scratch test data by identifying the normal load corresponding to the location of the transition of interest. The LSCM was also used to measure the scratch depth, which refers to the residual scratch depth in this study. The scratch coefficient of friction (SCOF) curve was obtained by taking the ratio of the tangential load and the normal load during the scratch test.

2.2.7 Pencil Hardness Test

Pencil hardness test were conducted using an Elcometer 501 tester. This device is designed to apply a load of 7.5 N during scratching. Faber-Castell pencil brand was used. The samples were fixed to a flat horizonal surface and their surfaces were cleaned using compressed air before testing. Scratches of at least 6.5 mm were performed going from the hardest to lowest pencil grade.

The pencil tip was polished before each test to ensure a smooth chip-free surface. The pencil hardness was determined by direct visualization and the pencil scratch depth was measured using LSCM.

2.3 Results

2.3.1. DMA: T_g and Molecular Weight between Crosslinks (M_c)

The M_c of highly crosslinked polymers can be estimated using the following equation:

$$log_{10}G_e = 6.0 + \frac{293\rho}{M_c},$$

where G_e is the storage modulus (Pa) in the rubbery state, ρ is the density of the material, which is 1.16, 1.18 and 1.19 g/cm^3 for E_L, E_M and E_H, respectively. In the case of lightly crosslinked epoxies, M_c can be estimated by:

$$M_c = \frac{\rho RT}{G_e},$$

where R and T are the ideal gas constant and temperature in °K, respectively. F shows the storage modulus and tan δ curves for the three model systems from DMA. The estimated M_c values are 250, 500, and 2,000 g/mol for E_L, E_M and E_H, respectively. Figure 1 serves to visualize the effect of M_c on the polymer network of the model systems. The T_g, G_e and M_c values obtained from DMA for the three resins are summarized in Table 1.

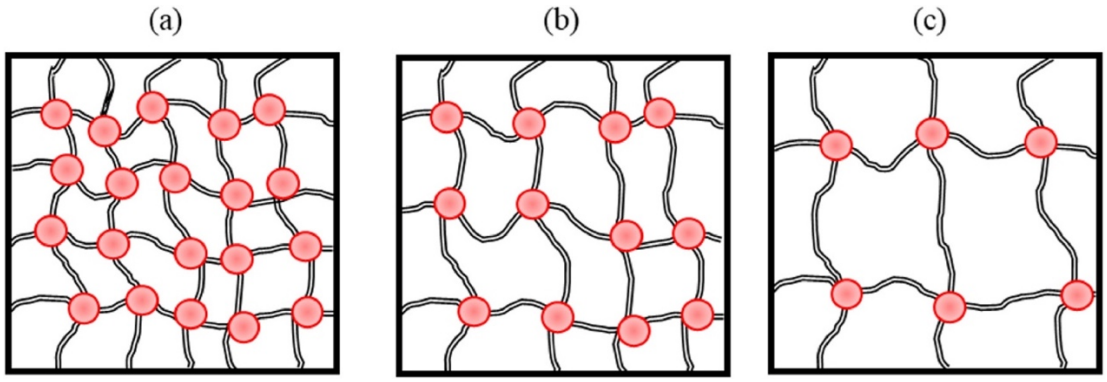

Figure 1. Simplified schematic of network structure in the epoxy model systems: (a) E_L, (b) E_M, and (c) E_H. Reprinted with permission from Materials & Design 182 (2019). Copyright 2019. Elsevier.

Table 1. T_g, M_c and G_e values of the epoxy model systems obtained from dynamic mechanical analysis. Reprinted with permission from Materials & Design 182 (2019). Copyright 2019. Elsevier.

Sample	**T_g (°C)**	**G_e (MPa)**	**M_c (g/mol)**
E_L	235	23.5	250
E_M	133	4.9	500
E_H	113	1.3	2,000

2.3.2 Surface Roughness (R_q) and Coefficient of Friction (COF) Measurements

The surface roughness and COF results are depicted in Figure 2. As shown, there is not a significant difference in the R_q for the three model systems after the samples were prepared. Furthermore, external factors like surface conditions of the samples and the tip can influence the COF measurement. In this case, the applied constant normal load was 5 N to minimize material deformation. The small surface roughness differences among the systems, which is not pronounced, suggests that slight changes in COF are likely due to material property differences instead of surface roughness effects. From Figure 2, it is observed that the COF increases as the

M_c increases, which is possibly due to the lower compressive modulus, which increases the contact area between the sample surface and the tip.

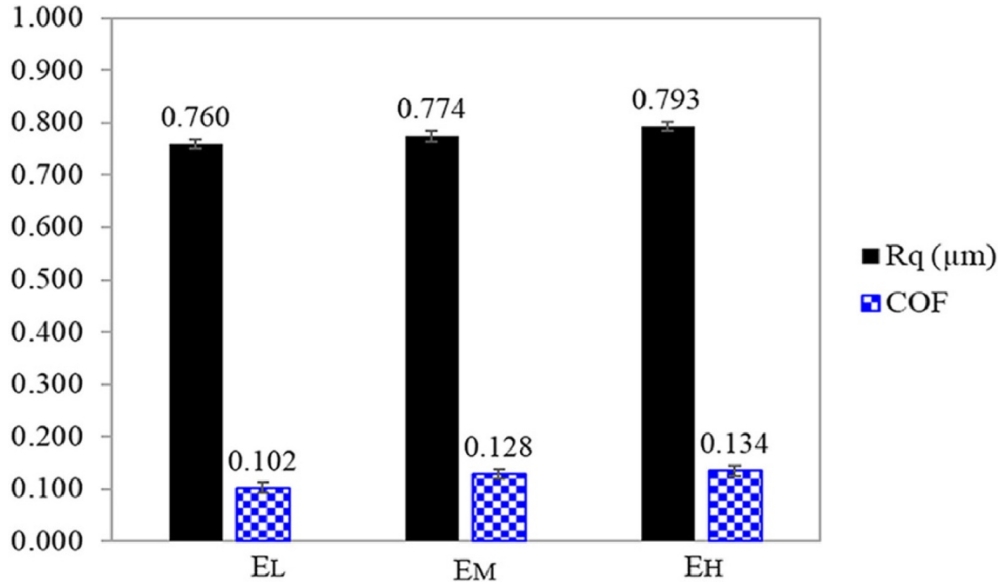

Figure 2. Surface roughness (R_q) and COF measurements for E_L, E_M and E_H. Reprinted with permission from Materials & Design 182 (2019). Copyright 2019. Elsevier.

2.3.3 Uniaxial Tensile Stress-Strain Curves

Table 2 summarizes the results of the tensile test. Although epoxies are expected to fail in a brittle manner, lightly crosslinked epoxies can show significant plastic deformation. It is observed that differences in M_c, i.e., crosslinking densities, significantly alter the tensile stress-strain behavior of the three resins. As shown, the three systems have a similar tensile modulus close to 3 GPa. However, E_H is lightly crosslinked, which implies that it is less rigid than the other systems, explaining why a slightly lower tensile modulus is obtained. It is evident that increasing the M_c produces an increase in the tensile strength, suggesting that a polymer with a more flexible network (E_H) is more tolerant to pre-existing defect and can undergo more plastic deformation before breaking.

Table 2. Tensile properties of the epoxy model systems. Reprinted with permission from Materials & Design 182 (2019). Copyright 2019. Elsevier.

Sample	Tensile Strength (MPa)	Tensile Modulus (GPa)	Elongation at break (%)
E_L	75 ± 2	3 ± 0.4	4 ± 0.4
E_M	83 ± 1	3 ± 0.1	7 ± 0.8
E_H	96 ± 3	2.6 ± 0.1	78 ± 12

2.3.4 Uniaxial Compression True Stress-Strain Curves

Epoxies are well-known for behaving differently when being loaded under compression instead on tension. Since both tensile and compressive stresses are developed near the scratch tip during the scratch test, the compressive behavior, specifically the compressive yield stress, of the model systems becomes critical for understanding the damage process during scratching.

Uniaxial compressive true stress-strain curves were generated to determine the yield point for the three model systems. As expected, changes in the M_c of the model systems are reflected on the compressive behavior of the samples, which is different from their tensile behaviors. It is observed that a lower M_c (higher crosslinking density) produces a significantly higher yield stress. A slight decrease in modulus with an increase in M_c is also found in the compressive behavior of the systems. As expected, the compressive modulus is higher than the tensile modulus. It can be observed in Table 3 that the E_L sample exhibits the highest yield stress of ~120 MPa, suggesting that an epoxy with such a highly crosslinked network can withstand higher stress before yielding under compression. In the systems with E_M and E_H, the yield stress decreases due to their flexible network. The above findings are in accordance with previous studies in epoxy resins [48], in which the yield stress increased when the level of crosslinking was raised without altering chemical

composition. Knowledge about the compressive and tensile behaviors of the epoxies can help to understand the scratch-induced damage, as will be discussed in the subsequent sections.

Table 3. Compressive properties of the epoxy model systems. Reprinted with permission from Materials & Design 182 (2019). Copyright 2019. Elsevier.

Sample	Yield Stress (MPa)	Compressive Modulus (GPa)
E_L	121 ± 2.9	3.7 ± 0.1
E_M	92 ± 2.2	3.2 ± 0.1
E_H	72 ± 3.2	3.0 ± 0.1

2.3.5 Scratch Behavior

The load range, scratch speed and scratch length were set at 1-200 N, 10 mm/s, and 80 mm, respectively. Three transitions are noted during the scratch process: (1) groove formation, (2) crack formation, and (3) material removal (plowing). The onsets of the damage transitions are shown in Figure 3. The groove formation is identified from the height of the surface profile of the samples *via* LSCM. Cracking and plowing were determined by direct visualization and were further confirmed *via* LSCM. Figure 4 shows the LSCM images at the onset of cracking and material removal of the model systems. The onset of cracking is depicted by a dashed line. The three resins exhibit a clear onset of damage. All the systems exhibit periodic cracks until plowing takes place. Based on the findings, it is apparent that changes in the crosslinking density of epoxy systems dramatically affects the onset load for different damage types to occur. It is shown that a higher M_c leads to an earlier onset of groove, crack and plowing formation (Figure 3). The E_L sample shows the best scratch performance among the systems.

The results from the scratch test suggest that systems that exhibit high compressive yield stress require higher loads to induce different scratch damage. As mentioned earlier, E_L exhibits

the lowest tensile strength among the samples but shows a higher resistance against crack formation during scratching. These findings contradict previous studies, showing that an increase in tensile strength can enhance the scratch resistance [15-17, 25]. Based on the numerical studies [16, 44], it has been observed that the material located behind the scratch tip will experience a high tensile stress during scratching and that the stress state along the scratch direction near the surface is dominated by uniaxial tension. To explain the onset of crack formation in polyurethane (PU) elastomers, Xiao et al. [25] proposed that as the normal scratching load increases, the magnitude of the tensile stress behind the tip will increase until it exceeds the tensile strength of the material, which leads to crack formation. It must be noted these PU elastomers have a similar compressive yield stress. Contrarily, the epoxy model systems used in the current study exhibit substantially different compressive behaviors, suggesting that both tensile strength and compressive yield stress will play a role on the onset of crack formation.

Figure 5(a) shows the SCOF curves of the three resins. As it can be observed, changes in M_c give rise to significant changes in SCOF behaviors. In fact, a higher M_c will lead to a higher SCOF, especially when the penetration of the scratch tip takes place due to yielding of the epoxy matrix. The earlier onset of crack formation in the E_H system is mainly attributed to its low compressive yield stress. Because of its low yield stress that causes higher frictional forces during scratching, the SCOF of E_H increases much higher and faster even though it possesses a higher tensile strength. This, in turn, leads to an earlier onset of crack formation. The above argument is further supported by Figure 5(b), which shows that E_H has indeed formed a significantly higher residual scratch depth at an early stage of the scratch when compared against E_L and E_M. Therefore, tensile strength alone is insufficient to account for crack formation. The compressive yield stress of the samples must be considered, as well, which have a significant impact in SCOF.

It should be mentioned that the onsets of scratch-induced damage may change if the test is performed under different conditions, such as using a different tip material or scratch speed. Surface impurities such as residual mold release can also have an effect. The scratch test was also conducted in uncleaned surfaces. Residual mold release agent used for sample preparation were found on the surface of the samples. This has resulted in significantly higher onset loads for cracking and plowing formation during scratching, suggesting that the mold release agent can act as a lubricant during the scratching process, thus delaying damage formation.

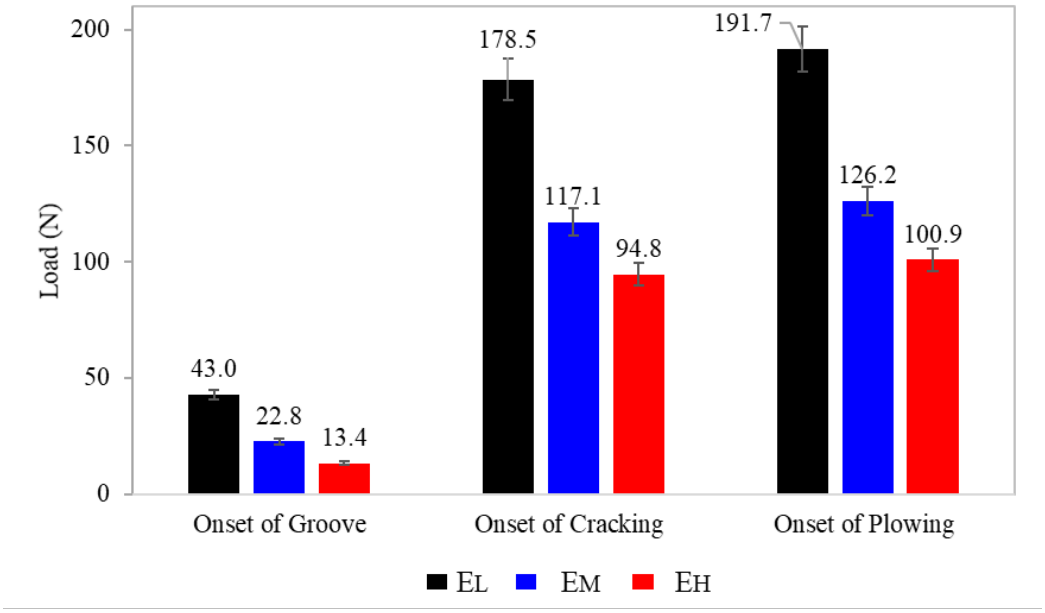

Figure 3. Onset of groove, cracking and plowing of E_L, E_M and E_H. Reprinted with permission from Materials & Design 182 (2019). Copyright 2019. Elsevier.

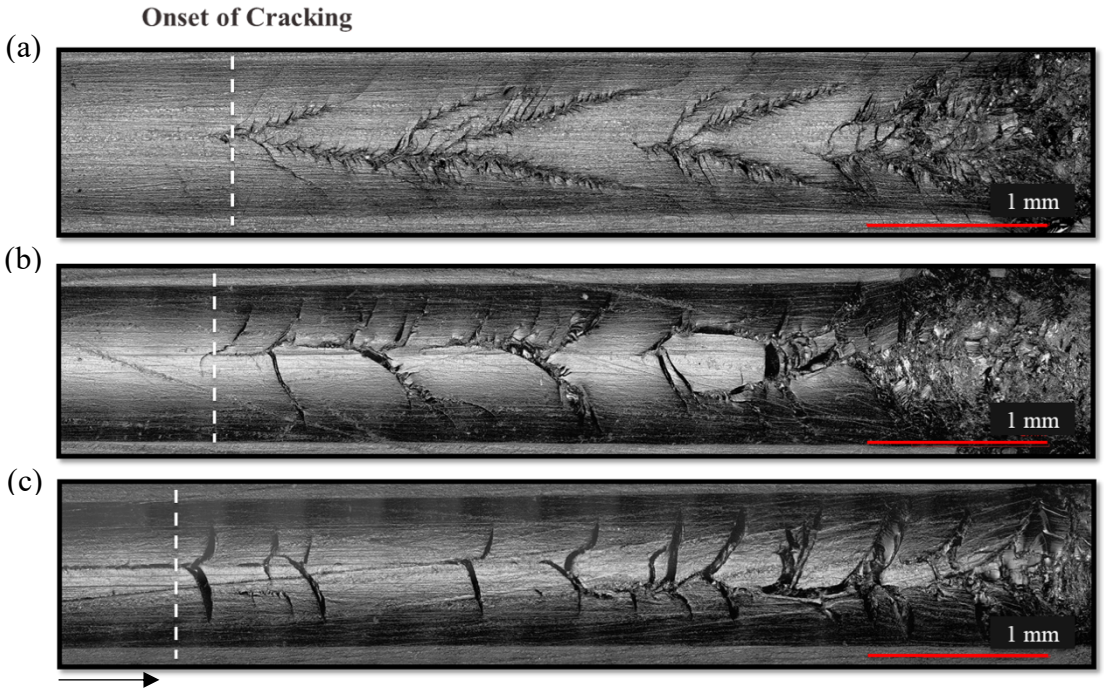

Figure 4. Onset of cracking and plowing of (a) E_L, (b) E_M, and (c) E_H. The black arrow depicts the scratch direction. Reprinted with permission from Materials & Design 182 (2019). Copyright 2019. Elsevier.

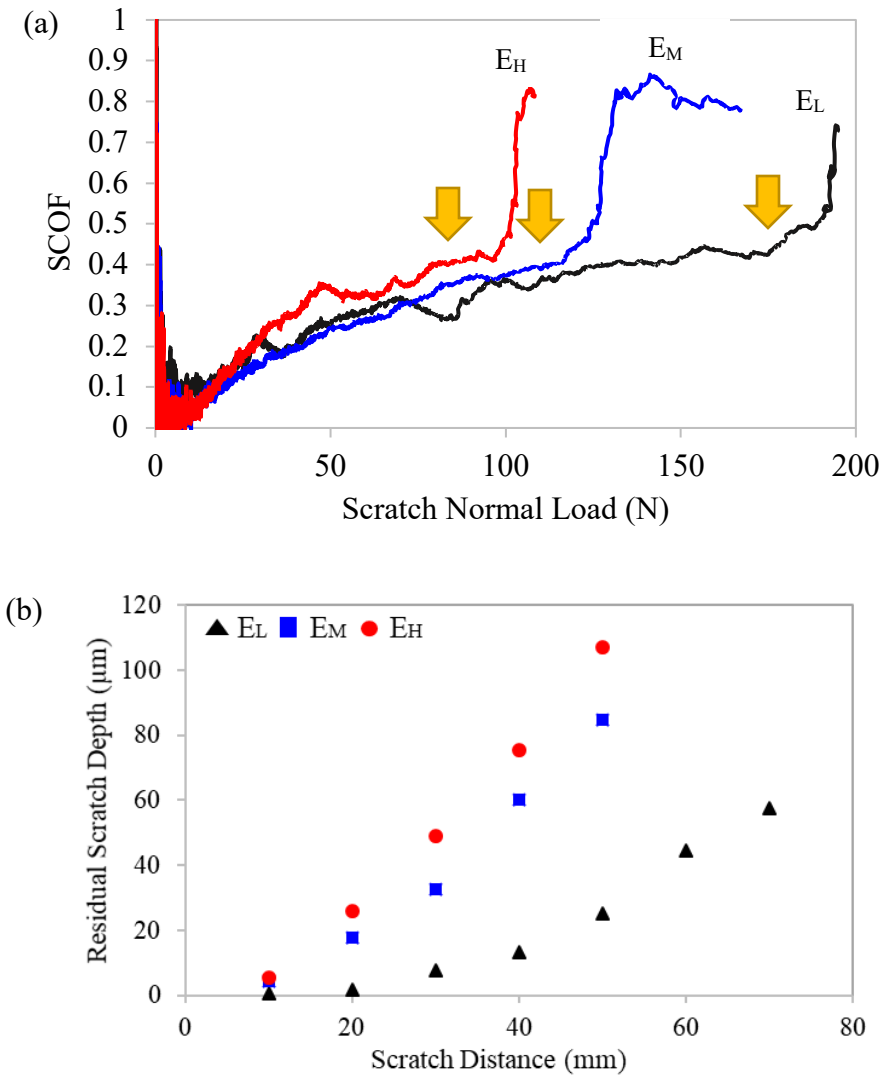

Figure 5. (a) SCOF plots and (b) the residual scratch depth measured *via* LSCM. The yellow arrows depict the onset of crack formation. Reprinted with permission from Materials & Design 182 (2019). Copyright 2019. Elsevier.

2.3.6 Pencil Hardness

Pencil hardness test was performed on the three model systems. As mentioned earlier, the pencil hardness test has been implemented in the past because of the convenience it offers to quickly assess the scratch performance among samples at low cost. However, the definition of pencil hardness might vary depending on the application. For instance, in coatings, pencil hardness is defined by the pencil grade that produced visible delamination from the substrate. In other cases,

pencil hardness is defined by the pencil grade that does not induce visible damage. The pencil hardness of E_L, E_M and E_H was difficult to determine by direct visualization due to the transparency of the epoxy samples and the deposit of the residual of pencil graphite on the scratch path after scratching, which can render misleading pencil hardness results. Therefore, after each scratch, an eraser was used to remove excess of graphite residues on the sample, then the pencil hardness grade was determined. The results for pencil hardness based merely on visibility of damage are reported in Figure 6, in which the pencil hardness grade for each model system is depicted by a yellow square. It is observed that although E_L and E_M systems have a noticeably different network structure that causes the three systems to have different T_g, tensile strength and yield stress, the pencil hardness results are the same for both systems.

To further analyze pencil scratch induced damage, the scratch depth was measured *via* LSCM. Figure 7 shows the area where three depth measurements were taken for each system. The average of the three measurements of each pencil grade for the three model systems is shown in Figure 6(a-c). The depth results are shown for pencils before and after no visible damage is observed to gain insights about the transition of damage visibility. It can be observed that samples with low M_c exhibit low pencil scratching depths, which decreases as the pencil grade goes down in the hardness scale.

It is noted that for more ductile materials, like E_M and E_H, the pencil scratch depth with respect to the pencil grade results shows more variation. For instance, in Figure 6(c), the pencil scratching depth for the E_H system is lower for pencil grade 6H than 5H, which can be considered counterintuitive since 6H is harder than 5H and it should induce a deeper groove than 5H. These findings suggest that the accuracy of the pencil hardness test could be compromised by many factors. The anomaly in the trend for the softer systems is possibly due to undesired variations

during the test, e.g., variation in the pencil tip surface finish before each scratch and the effect that the sample surface has on the deformation of the pencil tip as it scratches the sample.

A more ductile material will impose more deformation to surface of the pencil, causing significant variations in the stress state during scratching. The inset images in Figure 6(a-c) show the scratch features of the pencil grade that did not leave a mark on the sample surface. It is observed that the scratch features and the extent of damage are significantly different for the three systems, and even though the damage is not detectable by our naked eyes, there are still significant depth variations in the surface profile that can be captured *via* LSCM. It observed that in the visibility transition, the pencil scratching depth is decreased as the pencil grade goes down in the hardness scale. Furthermore, although soft pencils can lead to misleading results because of graphite residues, they do not induce substantial surface damage. Instead, the scratching depth will approach the surface roughness of the material making the damage undetectable by our naked eyes.

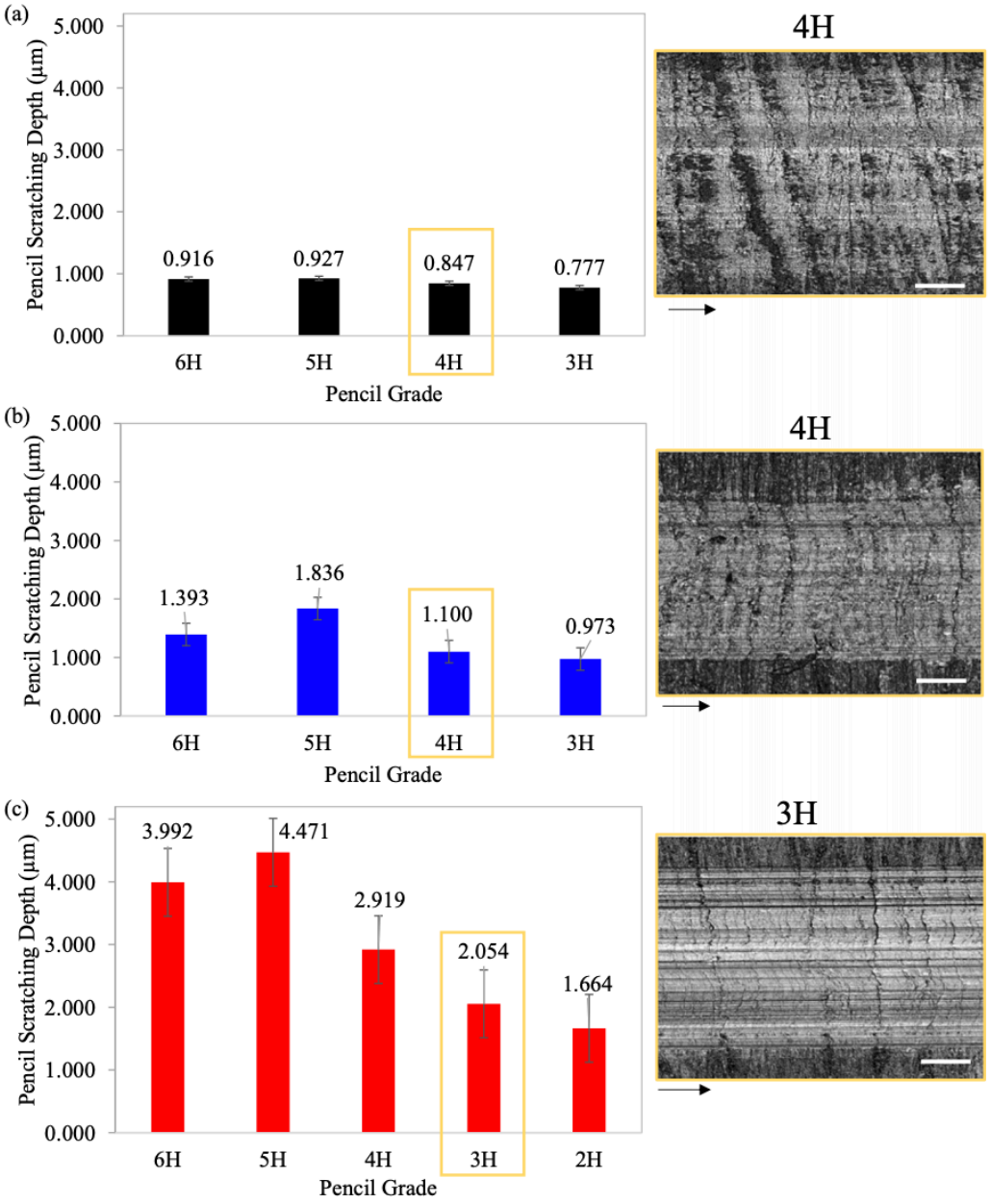

Figure 6. Pencil scratching depth of (a) E_L, (b) E_M, and (c) E_H using different pencil grades. The yellow box denotes pencil hardness of each systems, i.e., no visible damage. Inset image in each figure shows pencil-induced scratch features *via* LSCM. The black arrow represents the scratch direction. The scale bar is 100 μm. Reprinted with permission from Materials & Design 182 (2019). Copyright 2019. Elsevier.

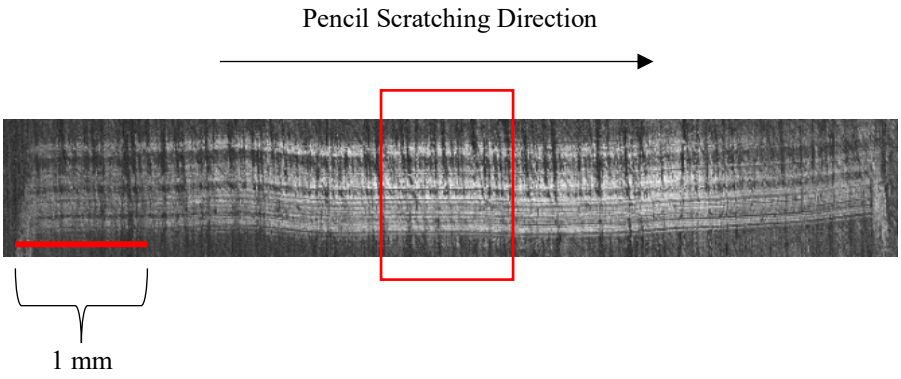

Figure 7. LSCM view of the full length of pencil scratching in E_M. The region where the pencil scratching depth measurements were taken is represented by the red box. Reprinted with permission from Materials & Design 182 (2019). Copyright 2019. Elsevier.

2.4 Discussion

Based on the current study, it is found that differences in crosslinking density dramatically affect the mechanical behavior of the model epoxy resins. Even though the tensile and compressive moduli are less affected by M_c, other properties like tensile strength and compressive yield stress are dictated by M_c. It is shown that epoxies with lower M_c, exhibit a higher glass transition temperature, fail in a brittle manner under tension, and exhibit a high yield stress under compression. It is also found that the compressive yield stress increases as the M_c decreases. However, the relationship between yield stress and crosslinking has rendered contradictory results in the literature. A previous study showed that the yield stress of a set of amine-cured resins was independent of crosslinking density unless large deviations from the amine/epoxy ratio were used [62], some have shown that the yield stress decreased as the amine/epoxy ratio was increased [63, 64]. Similar to our results, other studies have shown that increased crosslinking raised the yield stress [48, 65]. These discrepancies are likely due to the changes in chemical composition that accompanied changes in crosslinking density and molecular mobility. Mayr et al. [48] showed that

when the chemical composition is unchanged, increasing the crosslinking density will cause an increase in the yield stress because more crosslinks are involved in the yielding process in the systems with higher crosslinking densities. As a result, the stress required to slide a molecular unit over other segments will be larger. In other words, in the systems with higher crosslinking density, a larger activation energy is required for the yielding process.

The tensile and compressive behavior of polymers are closely associated with scratch performance. It has been shown in previous numerical studies that groove formation is dominated by the compressive yield stress of a polymer, which is also associated with its COF [15, 16, 43, 44]. It was also shown experimentally and numerically that a higher yield stress and a lower COF can delay the development of the groove during scratching [25, 43]. It should be pointed out that a polymer experiences a multi-axial compressive stress beneath the tip during scratching. The use of uniaxial compressive properties to understand groove formation in the model systems might be oversimplified, especially in the case of E_H since it has a more mobile structure that allows for severe scratch-induces damage. Furthermore, cracking has been correlated to the high magnitude tensile stress that exists behind the scratch tip during scratching [15, 44]. The tensile stress direction is the same with the scratch direction and is parallel to the surface of the sample. As a result, the stress state is dominated by uniaxial tension along the scratch direction on the surface of the sample. However, in our model systems increasing the compressive yield stress, like in the case of E_L, result in the delay of the onset of groove, crack formation, and plowing during the scratch test. Although both E_M and E_H have higher tensile strengths than that of E_L, they both exhibit lower yield stresses, higher scratching depths, and higher SCOF that lead to lower onsets loads for crack formation. The findings suggest that considering tensile strength alone is insufficient to explain resistance to crack formation during scratch. A material with a low tensile

strength but with a high compressive yield stress can show better resistance against crack formation. It should be noted that the scratch process is very complex and the results depend on many other factors, such as surface roughness, COF and others. To gain fundamental knowledge about structure-property relationships, the surface conditions of the tested samples must be the same.

It was shown in the pencil hardness analysis that more rigid surfaces, like that of E_L, will exhibit lower pencil scratching depths. It was also noted that when systems with softer surfaces are tested, many factors, such as the pencil tip deformation during the scratching, can cause variations in the trend of the pencil scratching depth with respect to the pencil grade. Our findings suggest that the results from pencil hardness test are more reliable for samples with rigid surfaces. However, when more deformable surfaces are tested, the accuracy of the test is compromised. When more ductile samples were tested, such as E_H, more discrepancies in the depth measurement were found. Even though the pencil tester is designed to apply a constant load, the stress state during scratching might vary due to changes in contact area provoked by the deformation of the tip of the pencil. Based merely on direct visualization, E_L and E_M would exhibit the same pencil hardness value while showing markedly different pencil scratching features and extent of damage. Even though the three resins have a significantly different network structure and mechanical properties, the pencil hardness results are only one or two pencil grades from each other. The pencil hardness results are unable to adequately reflect the significant differences in mechanical properties of these resins and no fundamental knowledge can be deduced about the scratch performance and their intrinsic material characteristics. Based on the above results, it is concluded that the ASTM/ISO scratch test is a more comprehensive methodology that allows to correlate the scratch-induced damage transitions with the mechanical properties of materials.

The present study provides fundamental understanding of the scratch behavior of thermosets with varying crosslinking densities. The scratch-induced damage in the model systems is explained through tensile and compressive behaviors, which allows for correlation between material properties and different scratch behaviors. Future work in this area will encompass the incorporation of the gained structure-property relationships in the development of scratch resistance coatings and possibly in the design of reinforced nanocomposites.

2.5 Conclusion

Fundamental structure-property relationships have been established by investigating three model epoxy resins with low, medium, and high M_c. A correlation between material properties and scratch-induced damage has been quantitatively assessed and it was found that the tensile strength alone is insufficient to determine the resistance against crack formation. Both tensile strength and compressive yield stress play important roles in damage formation during scratching. Increasing the compressive yield stress can improve the scratch resistance of polymers by delaying the onset of crack formation. Moreover, pencil hardness is a quick method to assess the scratch resistance of polymeric systems. However, pencil hardness results do not correlate with the intrinsic material properties of the model systems. The pencil hardness results can be influenced by many external factors, such as operator, surface characteristics of the sample and the surface finish of the pencil tip.

CHAPTER III

EFFECT OF TENSILE AND COMPRESSIVE YIELD STRESSES ON THE SCRATCH BEHAVIOR OF INJECTION MOLDED POLYCARBONATE

In this chapter, the scratch behavior of injection-molded model polycarbonate (PC) systems was investigated according to the ASTM scratch test methodology. Four model PC systems with different tensile and compressive yield stresses were used to investigate how the scratch behavior might be influenced. The effect of mechanical properties on the onset of scratch visibility and the onset of scratch-induced cracking was investigated. Coefficient of friction (COF) measurements, uniaxial tensile and compressive stress-strain curves, and dynamic mechanical analyses were conducted to correlate the intrinsic material properties to the observed scratch-induced deformation of the model PC systems. Special attention is given to how geometric scratch groove parameters, such as scratch depth and shoulder height, correlate with the mechanical properties and the scratch visibility of the model PC systems. It is found that both the tensile yield and compressive yield stresses and surface characteristics, specifically, the COF, interplay during the scratch deformation process.

3.1 Research Motivation

Polymeric systems are widely used for numerous engineering applications in the microelectronic packaging, coatings, aerospace, automotive, food packaging and biomedical industry due to their strength, lightweight, low cost and versatile properties [66]. Typically, polymer products are subjected to wear or scratching during shipping, handling, installation and use. Polycarbonate (PC) is used in automotive and ophthalmology applications due to its high toughness and transparency. Similar to most polymers, PC-based products are susceptible to

surface damage, which deteriorates the perceived value, optical, aesthetic, and mechanical properties.

The ultimate goal of this dissertation is to design polymers with superior scratch-proof properties. To accomplish that goal, a fundamental understanding of the scratch behavior of ductile polymers is needed. Specifically, it is important to determine what parameters govern the scratch visibility resistance and the scratch-induced cracking resistance. Several routes like gas-phase, vacuum deposition and sol-gel methods, have been pursued to develop protective coatings to improve the scratch resistance of PC [67-70]. The sol-gel method is a common approach to develop organic-inorganic coatings to combine the attributes of organic polymers with the characteristics of inorganic oxides [71, 72]. Fabbri et al. [73] employed organic-inorganic hybrids prepared *via* sol-gel process with alkoxysilane-terminated polymer chains as the organic phase and tetraethoxysilane as the inorganic network precursor. A high degree of crosslinking between the two phases led to improvements in the scratch resistance and photodegradation of the coated PC. Fabbri et al. [74] employed organic-inorganic hybrid coatings based on poly(ethylene oxide) and silica to improve the scratch resistance of bisphenol-A PC sheets. Le Bail et al. [75] utilized hybrid organic-inorganic films by sol-gel based on 3-glycidoxypropyltrimethoxysilane, tetraethoxysilane and zirconium (IV) propoxide (ZTP) to improve the scratch resistance of PC. Sowntharya et al. [76] deposited hybrid nanocomposites coatings using titanium tetraisopropoxide and epoxy or acrylic modified silanes on PC by dip coating to improve the abrasion and scratch resistance. Boentoro et al. [77] investigated the effect of silicon oxide film and film thickness on the scratch resistance of PC. Seong et al. [78] employed blends of poly(methyl methacrylate-co-phenyl methacrylate) and PC to improve the scratch resistance of pure PC.

One challenging aspect of developing high-scratch resistance PC products is the lack of understanding of the complex scratch behavior of polymers. In many cases, the scratch resistance of PC systems is assessed using pencil hardness testing [10, 11, 76], which only provides a relative assessment of the scratch resistance and can be easily influenced by external factors, such as the operator and the surface finish of the pencil tip. Moreover, the relationship between material properties and pencil hardness is unclear. It has been shown that polymers with the same pencil hardness can exhibit completely different scratch features and extent of damage [10, 13]. The ASTM D7027/ISO 19252 standardized scratch test, which consist of a linearly increasing normal load, is widely implemented to evaluate the scratch performance of different polymeric systems [14]. This methodology allows for the identification of the onset of different damage types induced by scratching, allowing for more comprehensive understanding of the polymer scratch behavior. Several fundamental studies have been conducted to establish a structure-property relationship for different polymeric systems [8, 9, 15, 25, 37-40].

3.2 Scratch Behavior of PC

3.2.1 Scratch-induced Damage

Several scratch-induced deformation modes have been observed in polymers. Scratch-induced damage starts with the initial viscoelastic deformation, followed by possible plastic groove formation, then by fish-scale, microcracking or a combination of both, followed by the material removal zone. In the initial viscoelastic deformation zone, the applied load is low, resulting in only a small amount of deformation, if any. This zone involves fully recoverable viscoelastic deformation and may include a small amount of non-recoverable plastic deformation originating from compressive indentation. The initial damage zone can be followed by either a fish-scale or a microcracking/cracking zone. Jiang et al. [15] show that in polymers with relatively high modulus

and high yield stress like PC, the scratch depth is initially low. When the tip penetration is low, the resistance coming from the pile-up material in front of the tip is also low, leading to a lower frictional force during the scratching process. The frictional behavior is key to understand scratch-induced damage formation and it can be considered a manifestation of the material properties. Hossain et al. [42] showed experimentally and numerically that in polymers like PC, the scratch groove formation comes from both the elastic recovery and the material displacement from the front of the scratch tip toward the side or edge of the scratch path. The displaced material is added to the shoulder height of the scratch path. An increase in surface roughness with increasing normal load was also observed in PC.

The relationship between the polymer structure and scratch deformation started to be explored nearly 20 years ago. Briscoe et al. [79, 80] employed the scratch hardness method to provide an evaluation of the relative scratch resistance of polymers. It was shown that PC undergoes significant plastic deformation during scratching. The observed scratch behavior of PC was closely linked to the bulk yield stress, which is a function of strain, strain rate and temperature. It was pointed out that frictional heating during scratching can significantly influence the scratch deformation processes and damage features. Bucaille et al. [66] showed that the scratch behavior of PC is characterized by significant plastic deformation and the formation of pile-ups in-front of the indenter and on the sides of the residual scratch groove. It was also shown that polymers can exhibit significant viscoelastic recovery after scratching close to 90%. More recently, Zhang et al. [81] investigated the scratch behavior of injection molded PC and showed that the dominant scratch damage mode is different from the parabolic ductile tearing cracks observed for PC in other studies [15]. It was shown that PC exhibits smooth groove formation, followed by a periodic zig-zag shaped damage formation, similar to reported damage features in injection-molded ethylene-

propylene systems [82]. It was also shown that due the extensive plastic deformation of PC during scratching, the temperature rise is significant on the scratched specimen. As a result, the microstructure of PC near the surface is altered by the heat generation during scratch.

3.2.2 Scratch visibility

There are many applications in which surface appearance is the primary concern. In the case of eyeglasses, scratches are highly undesirable, and the scratch visibility resistance is one of the most important property requirements. Thus, a correlation between scratch visibility resistance and scratch-induced deformation features, which can be correlated to material properties, would facilitate tailoring the scratch visibility resistance polymers.

Assessing the scratch visibility merely based on human observation is troublesome due to the variations in lighting condition and natural differences between the eyes of human observers. Several methodologies to evaluate the scratch visibility have been developed over the years [7, 21, 22]. Wong et al. [23] introduced a method to precisely quantify the onset of scratch visibility by using a scratch tester and a digital image analysis software. Quantitative evaluation of scratch resistance requires the elimination of ambiguity and subjectivity. Employing a reliable testing and analysis methodology that is based upon the principles of material science facilitates the fundamental understanding of polymer scratch behavior. Scratch visibility originates when the scattering of incident light differs from the background due to changes in surface roughness and/or other surface features. These surface features include scratch-induced cracks, crazes and localized molecular orientation. The size of this features must be comparable or above the wavelength of visible light to become visible. At low normal loads, the scratch damage is difficult to be detected by the naked eye. With increasing load, the contrast between the damage and the undamaged surface will increase, and thus the scratch becomes visible. Since the applied load can be related

to the scratch distance, it is possible to quantitatively locate the load at which the scratch becomes visible. The software has the ability to locate the onset of scratch visibility by removing the influence of the common sources of biases, such as sample color, light source and scanner exposure algorithm [39, 83]. The standardized scratch test machine is used in conjunction with a commercially available software package (Surface Visibility Analyzer (SVA) software by Surface Machine Systems®), enabling meaningful quantitative evaluation of the onset of scratch visibility. More recently, the procedure was further refined by employing a custom-built black box to take images of the scratches at a predetermined lighting condition. As depicted in Figure 8, Angle 1 represents the angle between the camera and the sample surface. Angle 2 is the angle between the camera and the light source. Subsequently, the captured images are analyzed using the SVA software based on the contrast between the damage and undamaged area [24].

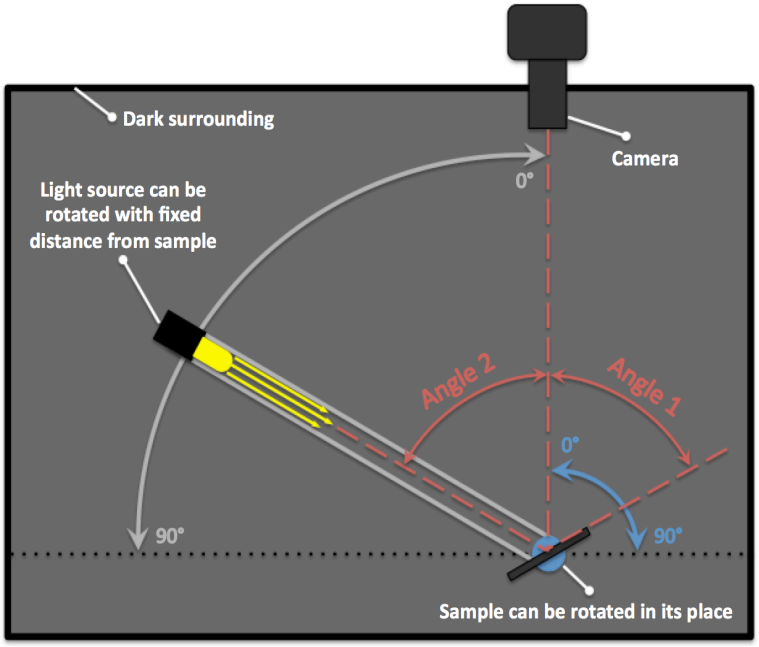

Figure 8. Black-box set up for scratch visibility assessment. Reproduced with permission from Polymer Testing (2018) 69. Copyright 2018. Elsevier [24].

Hossain et al. [44] showed experimentally and numerically that the scratch visibility resistance is closely related to geometrical scratch groove parameters, namely, scratch depth and shoulder height. The study indicated that a higher yield stress leads to lower scratch depth and shoulder height, resulting in better scratch visibility resistance. Plastic deformation is a result of yielding and it occurs due to the flow of molecular chains under applied stresses, suggesting that by modifying the molecular structure of the polymer, the yield stress can be altered, which will impact the scratch resistance of the polymer. Several studies have shown that the yield stress can be altered by physical aging [84], crystallinity [85], and molecular weight [86, 87]. Moreover, the post-yield behavior, namely, strain softening and strain hardening, has been also been associated with the scratch resistance, and can be altered by modifying the molecular structure of the polymer. For instance, the increasing the molecular weight can lead to a stiffer strain hardening slope, or can also lead to the polymer chains orienting in the loading direction, resulting in orientation hardening [88].

Hossain et al. [16] also indicated that tensile and compressive properties play different roles during scratch deformation of PC. It was shown that the higher compressive yield stress induces lower shoulder height and shallower scratch depth while the tensile yield stress has a minor effect on these two parameters. The formation of the scratch depth and shoulder height originates from the material being compressed in front of the scratch tip and displaced to the sides. Since the material in front of the tip is in compression, the groove formation and the groove geometrical parameters are closely related to the compressive behavior rather than the tensile behavior. It was proposed that the compressive yield stress, strain at recovery and strain hardening slope beyond the strain at stress recovery determine the scratch depth and shoulder height. On the other hand, the tensile properties have a minor influence on the scratch visibility resistance of ductile polymers.

However, if brittle-like features such as crazing and cracking occur, the tensile properties become important. While the compressive yielding and post-yielding behavior govern the formation of scratch depth and shoulder height, the surface roughness within the scratch groove can increase due to the formation damage features. Thus, the tensile constitutive behavior becomes critical as it influences the surface characteristics inside the scratch groove, which in turn affects the scratch visibility. It should be noted that several studies have shown that modulus have a minimal effect on scratch depth if is greater than 1.5 GPa under the ASTM scratch standard [13, 14, 89].

The frictional behavior is another parameter that affects the scratch behavior of polymers. Changes in the coefficient of friction (COF) affects the stress state near the surface. It has been shown that the stress field shifts and localizes toward the surface as the COF increases [90, 91], which in turn will directly impact scratch-induced deformation. Therefore, both the surface friction coefficient and the constitutive behavior must be considered to understand scratch-induced deformation. In the case of PC, it was shown that that the onset of groove formation is not only affected by the yield stress but also by the COF [43].

In order to design high scratch resistant polymers for numerous engineering applications, fundamental understanding of the scratch behavior of ductile polymers is needed. The objective of this work is to understand how the tensile and compressive yield stresses influence the scratch deformation of a set of model PC systems. The model systems were injection molded and exhibit significantly different mechanical properties that originate from having different molecular structures. Tensile, compressive, scratch, COF and dynamic mechanical tests and analyses were conducted to determine the effect of frictional, tensile and compressive constitutive behavior upon scratch damage with the purpose of understanding and improving the scratch-resistant of injection molded PC-based systems.

3.3 Materials & Methods

3.3.1 Materials and Sample Preparation

Model polycarbonate (PC) systems were provided by Sabic. A bisphenol-A PC homopolymer as a control system (PC), two PC copolymers (PC-cp1 and PC-cp2), and a blend of acrylonitrile styrene acrylate (ASA) and PC (PC blend) were investigated. The samples were injection molded and were tested as received.

3.3.2 Dynamic Mechanical Analysis (DMA)

DMA was performed using a TA Instruments ARES G2 Rheometer in torsional mode. The T_g of the model systems was defined as the peak point of the tan (δ) curve. The temperature range used was 30-190°C at a constant ramp rate of 5°C/min and at a strain amplitude of 0.05%. The frequency of the test was set at 1 Hz. The specimens were 3 mm in thickness, 8 mm in width and 30 mm in length for DMA testing.

3.3.3 Coefficient of Friction (COF) and Surface Roughness (R_q)

A commercial scratch machine (Scratch 5, Surface Machine Systems, LLC) built according to the ASTM D7027/ISO 19252 standard was used to measure the COF of the model PC systems. The COF is defined as the ratio between the force required to maintain motion at a prescribed scratch speed and the force pressing the surface [60]. A flat self-aligning stainless steel (10 mm x 10 mm) tip was utilized. The tests were performed at a 5 N constant normal load and the speed was 10 mm/s. The tip and the surface of the sample were cleaned using compressed air before taking the measurement. At least three tests were performed on each sample. The surface roughness (R_q) was measured by Keyence® VK9700 violet laser scanning confocal microscope

(LSCM) using a sampling area of 675 μm x 506 μm. Three measurements were taken on each sample.

3.3.4 Uniaxial Tensile and Compressive Stress-Strain Curves

Uniaxial tensile stress tests were performed using a MTS Insight® universal testing machine at a crosshead speed of 5 mm/min. The injection-molded and dog-bone shaped tensile specimens were 3 mm thickness and 12 mm in width. True stress-strain curve was generated by measuring instantaneous cross-sectional area using digital image correlation (DIC) video setup. A black ink marker was used to generate a random speckle pattern on the gauge section of the samples. A single Canon EOS 5D Mark II DSLR camera and VIC-2DTM DIC software were used to track the deformation of the random speckle pattern on the tensile specimens during the test. The true strains in tensile direction (e_{yy}) and lateral directions (e_{xx}) were obtained. The true stress was obtained by dividing the applied load by the instantaneous cross-sectional area. Three tests were performed on each model system.

Uniaxial compression tests were conducted using a MTS Insight® universal testing machine at a crosshead speed of 5 mm/min according to the ASTM D695-10 standard [61]. The specimens were cut with a diamond saw blade to the nominal dimensions of 12 mm x 6 mm x 6 mm. Polishing paper with 2400 grit was used to make the surfaces flat and parallel to each other. Lubricant was applied on the compression fixture to minimize friction during the test. A Canon EOS 5d Mark II DSLR video camera was used to record the compression test. The images in the video were analyzed to obtain the true strains in the compression direction (e_{yy}) and lateral direction (e_{xx}). Since model systems are considered to be isotropic, the strain in the thickness direction (e_{zz}) is assumed to be equal to e_{xx}. Only the compressive yield stress is of interest to the

present study, the test was terminated soon after the yielding stress was detected. Two tests were performed on each model system.

3.3.5 Scratch test

The scratch test was conducted according to the ASTM D7027/ISO 19252 methodology. A linearly increasing normal load of 1-80 N was applied. The scratch speed and length were 100 mm/s and 100 mm, respectively. A 1-mm diameter spherical stainless-steel tip was used to conduct the scratch tests. The surface of the samples was cleaned using compressed air before scratching. Three scratches were generated on each model system. The scratch coefficient of friction (SCOF) curve was obtained by taking the ratio of the tangential load and the normal load during the scratch test. The onset of microcracking formation and their corresponding damage features were identified using LSCM. The onset loads for the previously mentioned damage transitions were obtained from the scratch test data by identifying the normal load corresponding to the location of the transition of interest. The LSCM was also used to measure the residual scratch depth, shoulder height, and roughening withing the scratch groove. The onset of visibility was determined by a commercially available software package (Surface Visibility Analyzer (SVA) software by Surface Machine Systems®). A detailed explanation on how the software determines the onset of scratch visibility can be found elsewhere [24].

3.4 Results

3.4.1 Dynamic Mechanical Analysis (DMA)

The model PC systems were investigated under dynamic mechanical analysis. The model systems exhibit slight differences in the storage modulus near room temperature (Figure 9a). There is a noticeable decrease in the T_g of the model systems in comparison to the PC homopolymer

(Figure 9b). The T_g of the model systems was are shown in Table 4. All model systems exhibit one T_g with the exception of the PC blend, which shows two distinct peaks.

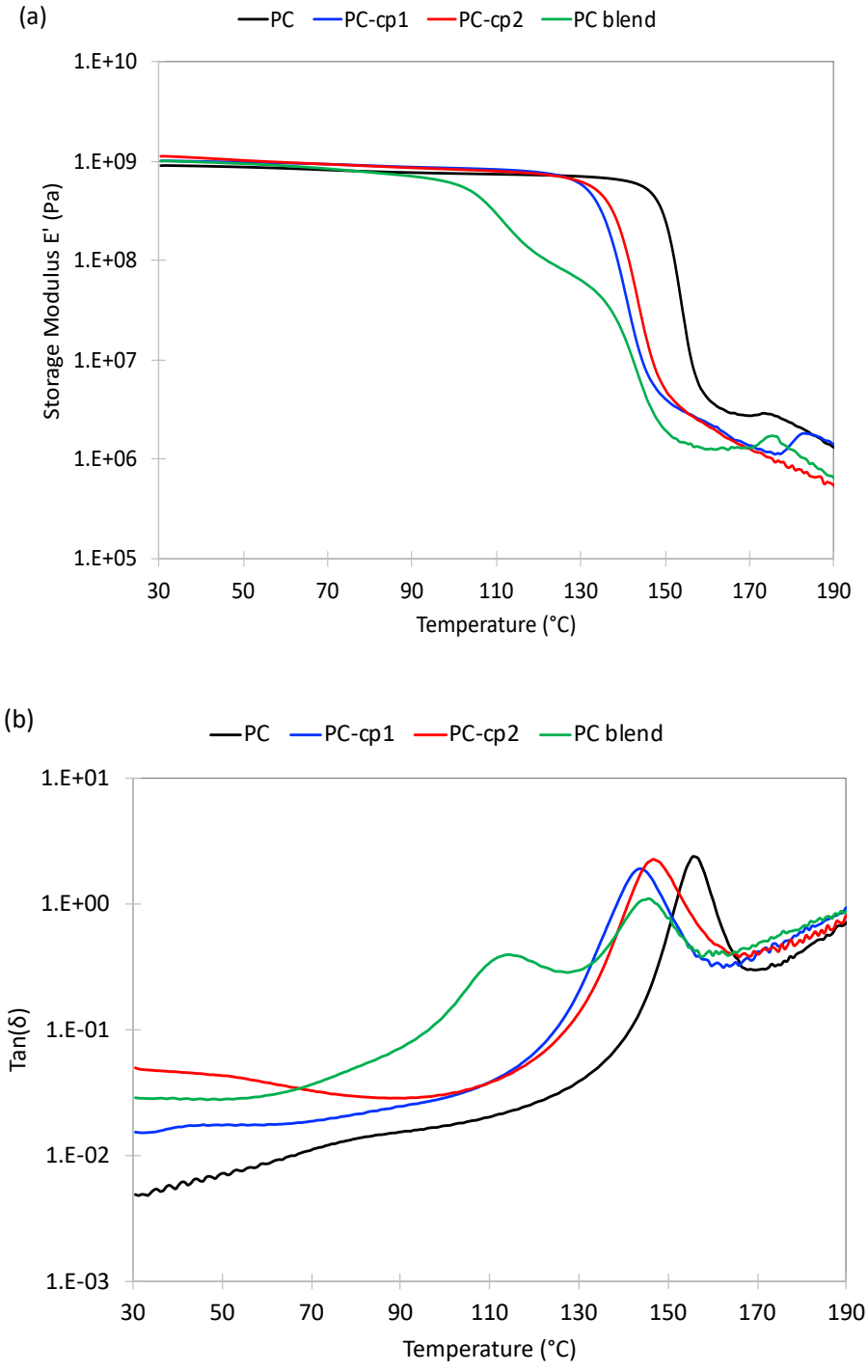

Figure 9. (a) Storage modulus and (b) tan(δ) curves for the model PC systems.

Table 4. Glass transition temperature (T_g) of the model PC systems.

Sample	T_g (°C)
PC	157
PC-cp1	145
PC-cp2	147
PC blend	115, 145

3.4.2 Surface Roughness (R_q) and Coefficient of Friction (COF) Measurements

The surface roughness and COF results are depicted in (Figure 10a). The surface roughness of PC is slightly lower than the rest of the samples, PC-cp1 and PC-cp2 exhibit a similar surface roughness while the PC blend shows the roughest surface among all. A constant normal load of 5 N was used to determine the COF of the model systems. PC shows the highest COF among all the model systems (Figure 10b). Changes in COF can be attributed to differences in material properties. For instance, a higher COF could possibly be due to the lower compressive modulus, which can increase the contact area between the sample surface and the tip, resulting in an increase in COF. The results indicate that the surface characteristics of these model systems are different and must be considered to understand scratch-induced deformation.

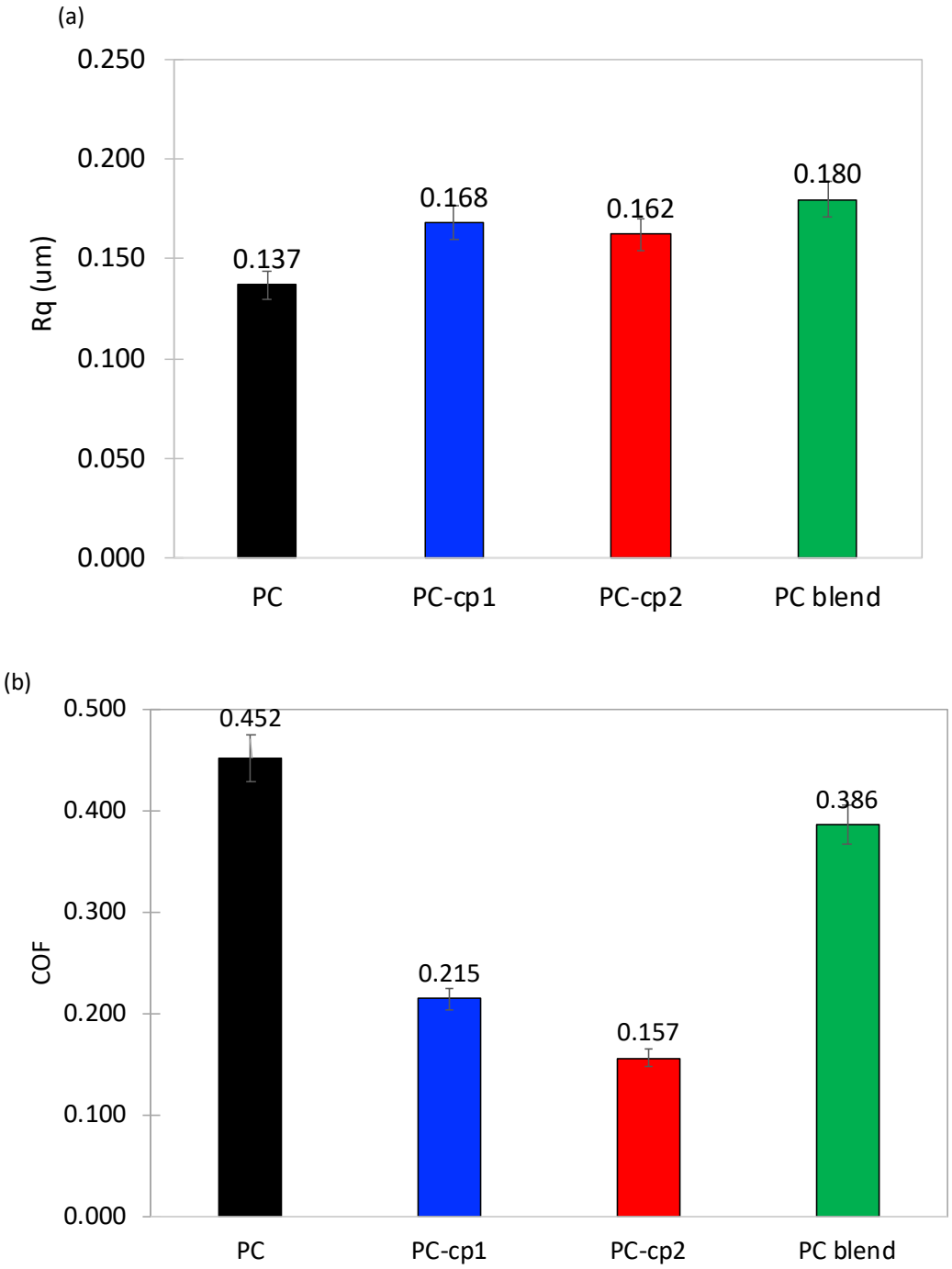

Figure 10. (a) Surface roughness (R_q) and (b) coefficient of friction (COF) of the model PC systems.

3.4.3 Uniaxial Tensile and Compressive Stress-Strain Curves

Table 5 summarizes the tensile test results. All the model PC systems exhibit high ductility except for PC-cp2, which fails in a brittle manner. As shown in Figure 11, the model systems exhibit clear differences in the tensile yield stress and tensile strength. The PC blend shows the lowest and PC-cp2 shows the highest tensile yield stress, while PC and PC-cp1 lie somewhere in between. Polymers are known to behave differently under compression instead of tension. Both tensile and compressive stresses are developed near the scratch tip during the scratch test. Thus, the compressive behavior is critical for understanding the damage process during scratching. Table 6 summarizes the results for the compression test. As shown in Figure 12, and similar to the tensile test results, the PC blend shows the lowest compressive yield stress, PC-cp2 shows the highest, and PC and PC-cp1 lie in between. Knowledge about the compressive and tensile behaviors of the model PC systems can help to understand the scratch-induced damage, as will be discussed in the subsequent sections.

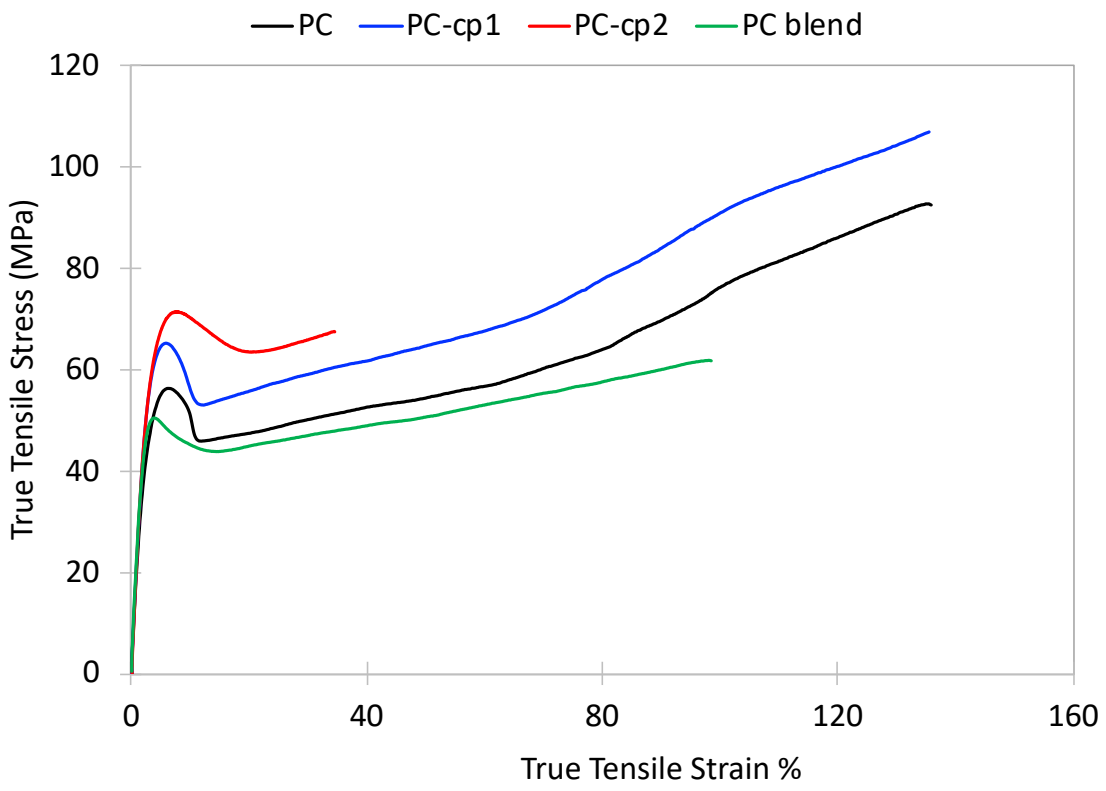

Figure 11. True tensile stress-strain curves of the model PC systems.

Table 5. Tensile yield stress, tensile strength, elongation at break (ε_B) and tensile modulus of the model PC systems.

Sample	Tensile Yield Stress (MPa)	Tensile Strength (MPa)	ε_B (%)	Tensile Modulus (GPa)
PC	58 ± 2	92 ± 2	139 ± 3	2.1 ± 0.1
PC-cp1	66 ± 3	116 ± 3	142 ± 3	2.7 ± 0.2
PC-cp2	73 ± 2	67 ± 2	31 ± 4	2.7 ± 0.1
PC blend	51 ± 2	64 ± 13	97 ± 50	2.2 ± 0.1

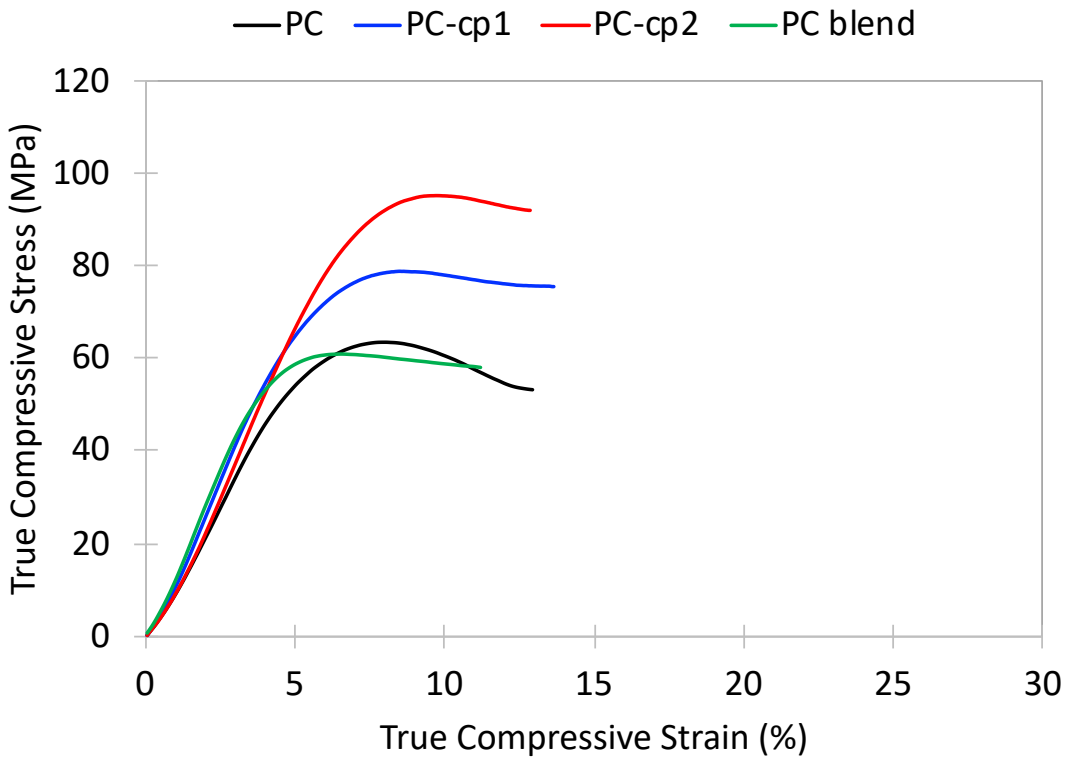

Figure 12. True compressive stress-strain curves of the model PC systems. Results shown up to yield point.

Table 6. Compressive yield stress and compressive modulus of the model PC systems.

Sample	Compressive Yield Stress (MPa)	Compressive Modulus (GPa)
PC	62 ± 1.2	2.8 ± 0.5
PC-cp1	80 ± 1.5	2.5 ± 0.4
PC-cp2	92 ± 2.2	3.0 ± 0.2
PC blend	57 ± 1.4	2.5 ± 0.1

3.4.4 Scratch Behavior

The onset of visibility of the model systems is shown in Figure 13. PC shows the lowest onset of visibility, followed by the PC blend, PC-cp1, and then PC-cp2. The onset of damage

transition, specifically, cracking, was determined using LSCM. As shown in Figure 14, the onset of microcracking occurs earlier for the PC blend, followed by PC, while PC-cp1 and PC-cp2 have a similar onset of scratch damage. The observed differences in the scratch visibility resistance and resistance against scratch-induced cracking are related to differences among the constitutive behavior of the model systems. The SCOF takes into account the resistance the tip experiences while it moves forward. PC shows a higher SCOF (Figure 15), suggesting there is significant amount of material being compressed in front of the tip and displaced to the sides. Post-mortem analysis of the scratch groove reveals that the scratch depth and shoulder height is significantly higher for PC and the PC blend. On the other hand, PC-cp2, which shows the highest scratch visibility resistance, exhibits the lowest scratch depth and shoulder height. The results suggest that these two geometrical parameters govern the onset of scratch visibility of the model PC systems, and these two are closely linked to the compressive constitutive behavior of the model systems. The higher compressive yield stress of PC-cp2 is responsible for its low SCOF, low scratch depth and shoulder height, and account for the significant improvement in scratch performance. Having higher compressive yield stress require higher loads for scratch tip to move deeper into the material during scratching. Previous experimental and numerical studies have shown that, when the compressive behavior between two materials is similar, increasing the tensile strength usually increases the scratch resistance [16, 17, 25, 44]. However, when the compressive behaviors between two materials are substantially different, as it is the case in this study, the material with lower compressive yield stress can significantly exert high SCOF at a low scratching load and cause early crack formation process during the scratch test [13]. A low yield stress allows for the scratch tip to penetrate much deeper upon compressive yielding, which the generates much higher SCOF and promote early crack formation. This phenomenon is supported Figure 15 and Figure

16, which shows that PC indeed exhibits much higher SCOFs, residual scratch depth and shoulder height, which result in an early onset of scratch visibility.

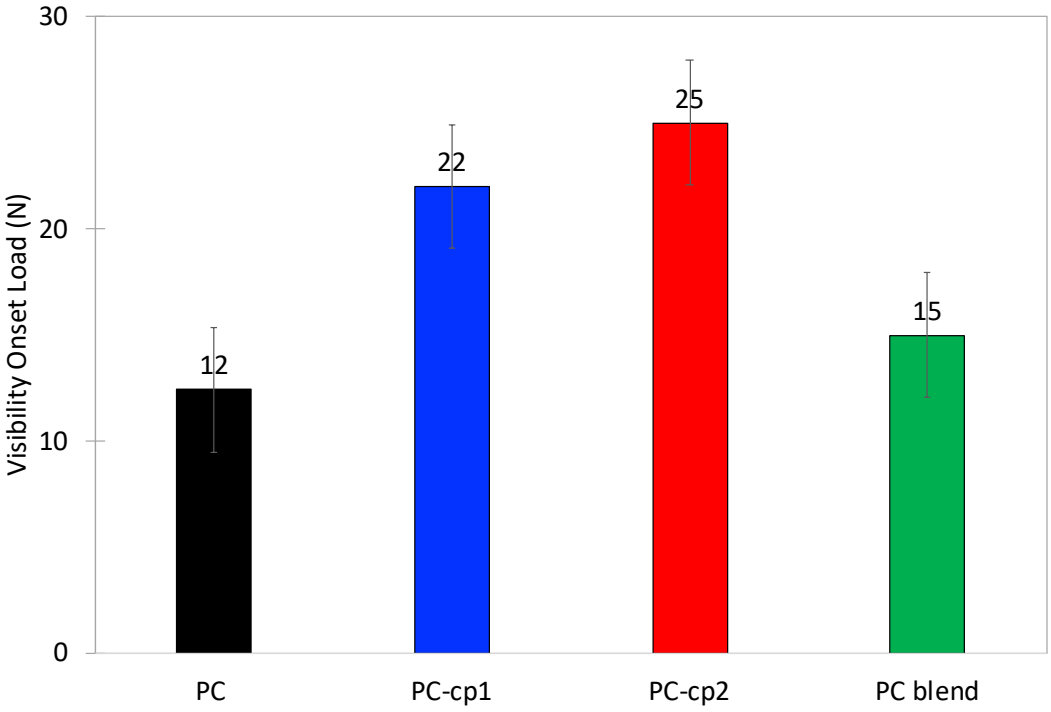

Figure 13. Onset of scratch visibility of the model PC systems.

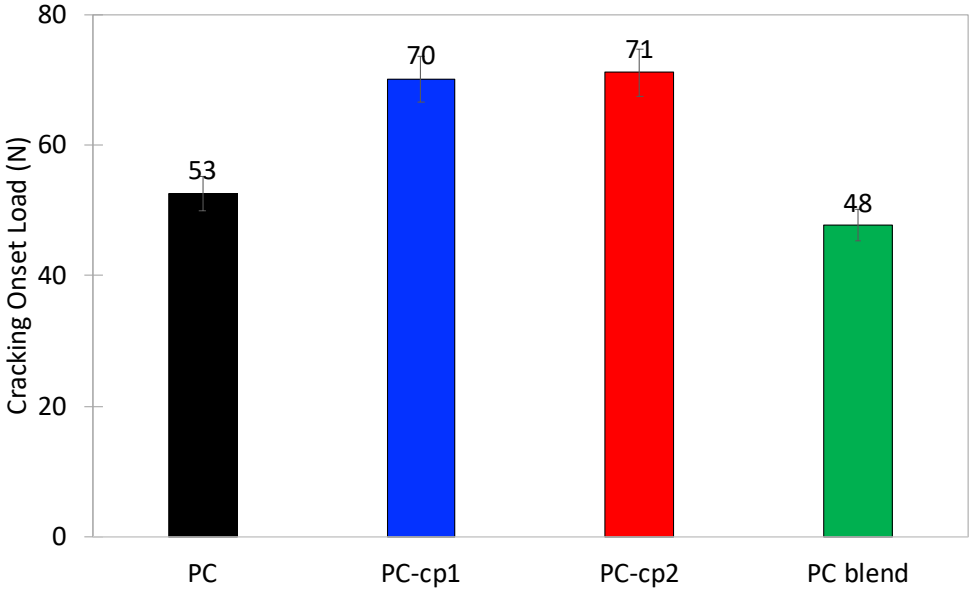

Figure 14. Onset of scratch-induced cracking of the model PC systems.

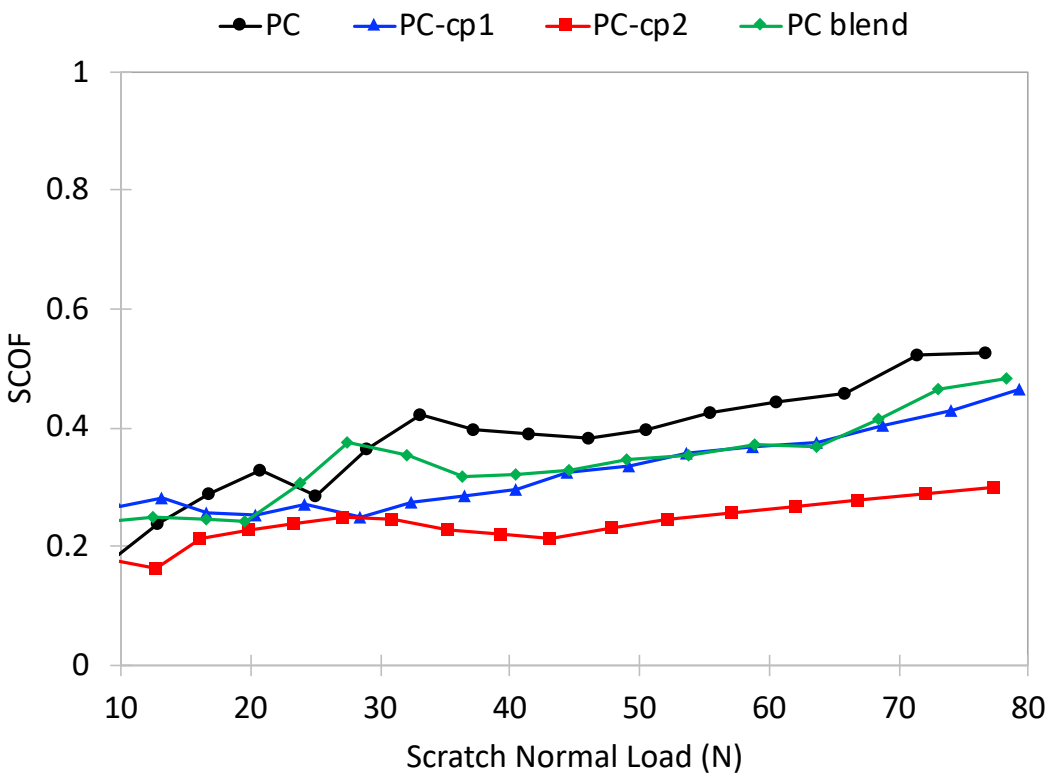

Figure 15. Scratch coefficient of friction (SCOF) of the model PC systems.

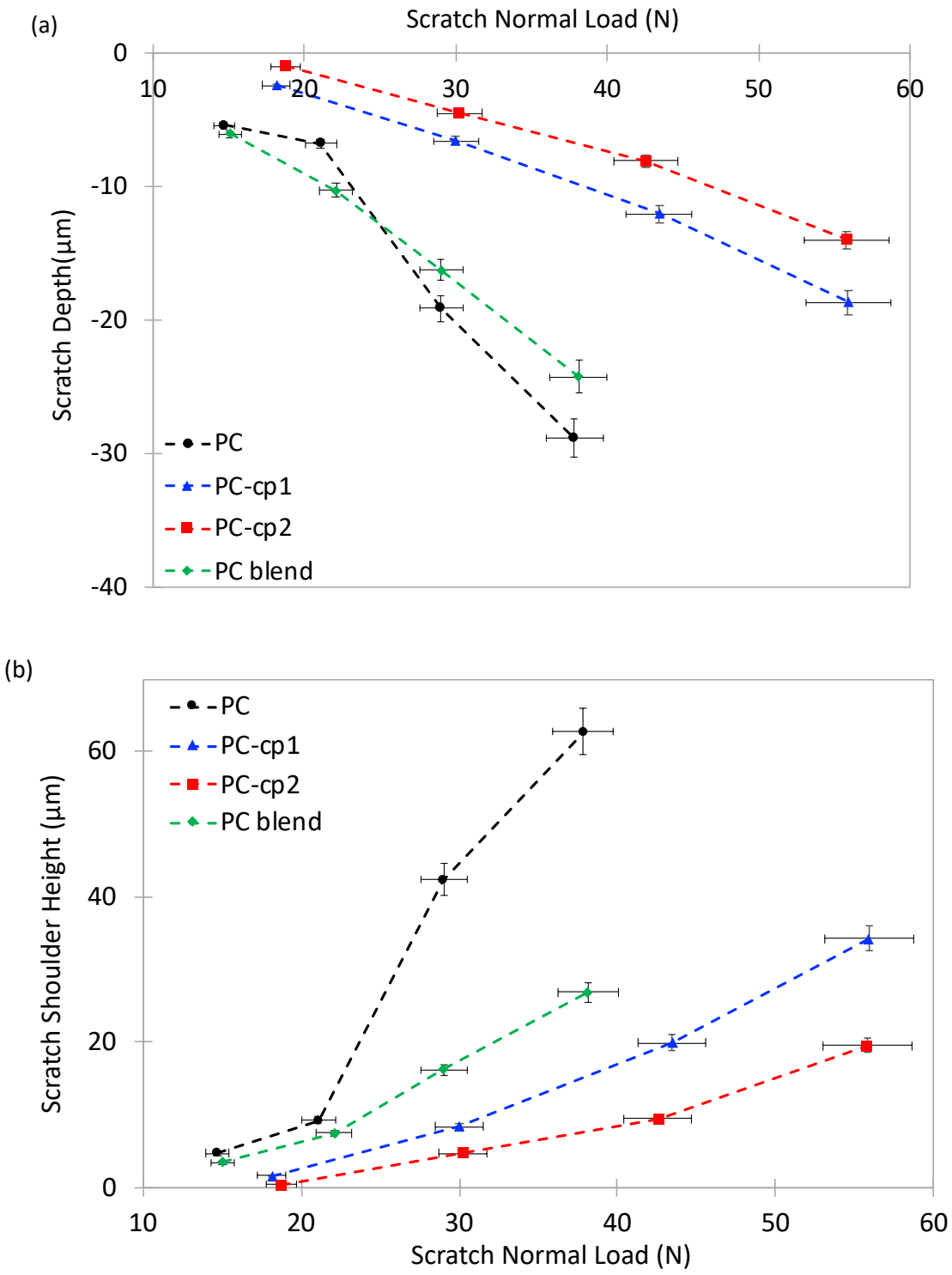

Figure 16. (a) Scratch depth and (b) shoulder height as a function of scratch normal load.

The increase in roughness inside the scratch groove can also affect the scratch visibility resistance. A scratch becomes visibility because the scattering of incident light differs from the background due to changes in surface roughness. Moreover, the change in roughness (ΔR_q), is defined follows:

$$\Delta R_q\,\% = \frac{R_q\,(Scratched) - R_{q0}(Virgin)}{R_{q0}(Virgin)} x100$$

where R_q is the roughness within the scratch groove and R_{q0} is the roughness of the virgin area of the sample, affects the scratch visibility. The ΔR_qtakes into account the roughening against the undamaged part of the sample of the sample while the R_q of the scratched region is the roughness within the scratch groove. As shown in Figure 17a, the scratch roughening, R_q, is significantly higher for PC and the PC blend. By considering the ΔR_q shown in Figure 17b, it can be observed that PC shows a much higher ΔR_q. Even though the scratch roughening of PC and the PC blend is similar, the change in roughness compared against the background material is higher for PC, causing the scratch to be visible earlier in PC than in the PC blend.

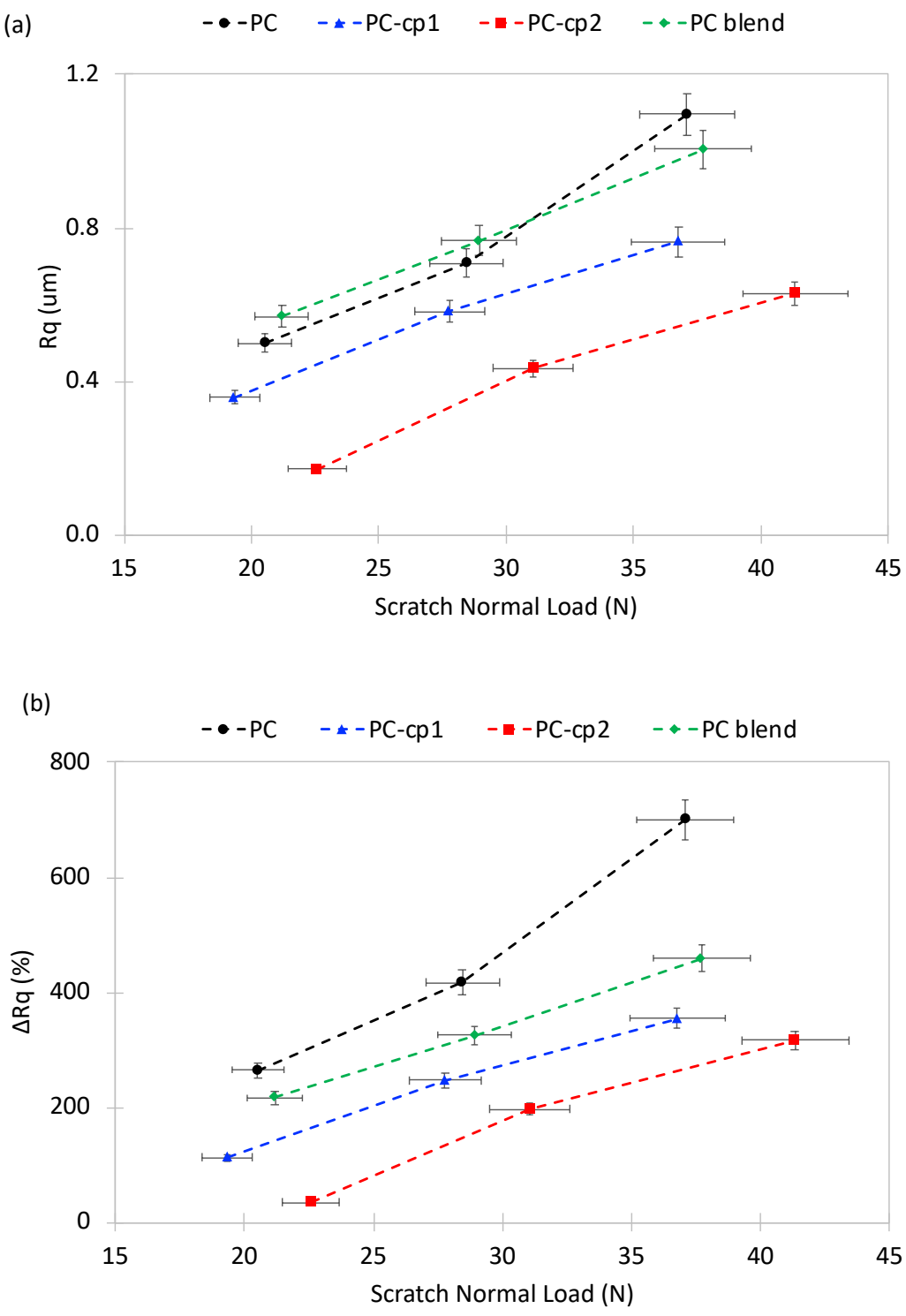

Figure 17. (a) Surface roughness (R_q) and (b) surface roughness change (ΔR_q).

3.5 Discussion

This study indicates that the constitutive behavior affects the scratch deformation of polymers. The onset of scratch visibility and the onset of scratch-induced damage originate from different surface parameters and mechanical properties. The scratch visibility resistance can be addressed in terms of geometrical scratch groove parameters such as scratch depth and shoulder height. The magnitude of these parameters originates from the mechanical properties of the model PC systems. Previous numerical studies have shown that groove formation is dominated by the compressive yield stress of a polymer, which is also associated with its COF [15, 16, 43, 44]. It was also shown experimentally and numerically that a higher yield stress and a lower COF can delay the development of the groove during scratching [25, 43]. This can be explained by considering that a polymer with a higher yield stress can induce shallower scratch depth and shoulder height, which implies that a polymer with a higher yield stress is expected to have better scratch visibility resistance.

Our findings indicate that the tensile and compressive properties of the model PC systems play different roles during scratch deformation. The compressive yield stress strongly influences the scratch depth and shoulder height formation, which originate from the material being compressed in front of the scratch tip and displaced to the sides. Since the material in front of the tip is in compression, the groove formation and the groove geometrical parameters are closely linked to the compressive behavior rather than the tensile behavior. On the other hand, the tensile properties have a minor influence on the scratch visibility resistance of ductile polymers unless brittle-like features such as crazing and cracking occur, which will increase the roughening along the scratch path, leading to an early scratch visibility onset. In a word, while the compressive yielding and post-yielding behavior govern the formation of scratch depth and shoulder height, the

tensile constitutive behavior is important as it influences the surface roughness inside the scratch groove, which affects the scratch visibility. Moreover, the frictional behavior also has a significant influence on scratch deformation. A lower COF can delay the onset of groove formation, which in turn delays the onset of visibility [43]. The ΔRq takes into account the roughening against the unscratched part of the sample of the sample. PC shows a much higher ΔRq, scratch depth and shoulder height, explaining why it shows the worst scratch visibility resistance.

Scratch-induced cracking has been correlated to the high magnitude tensile stress that exists behind the scratch tip during scratching [15, 44]. However, in the case of PC-cp2, even though it has a lower tensile strength in comparison to PC and PC-cp1, it shows the highest scratch resistance due to its significantly higher compressive yield stress. The findings suggest that in ductile polymers the compressive yield stress also plays a role in the onset of cracking formation. PC-cp1 has a lower compressive yield stress than PC-cp2 but its tensile strength is significantly higher, resulting in a similar onset of scratch cracking but a lower onset of scratch visibility. A material with a low tensile strength but with a high compressive yield stress can show better resistance against crack formation because it will exhibit a lower scratch depth, which results in a lower SCOF, delaying the onset of cracking. The PC blend shows a lower tensile strength, tensile and compressive yield stresses than PC, resulting in an earlier onset of scratch-induced cracking. However, the COF of PC is higher than that of the PC blend, as well as the scratch depth and shoulder height, resulting in an earlier onset of visibility.

The scratch process is very complex, and as it has been clearly shown throughout this study, the results depend on many factors. As shown in Figure 18 and Figure 19, the mechanical properties of the injection molded PC systems can be correlated with the scratch visibility resistance and scratch cracking resistance.

It is concluded that both the tensile yield stress and the compressive yield stress play a critical role in the onset of cracking formation (Figure 18). Although tensile strength has been shown to be important to determine crack formation, a higher compressive yield stress will alleviate the stresses during scratch deformation, resulting in a lower scratch depth and SCOF, and delaying the onset of scratch damage formation. Both tensile yield and compressive yield stress show a very good correlation with the onset of scratch-induced cracking. Moreover, the compressive properties show a better correlation with the onset of scratch visibility in comparison to the tensile properties Figure 19a. The compressive yield stress dictates the residual scratch depth and shoulder height, which directly impact the scratch visibility resistance. It is also concluded that the shoulder height has a stronger influence in determining the scratch visibility resistance (Figure 19b). Tensile properties become important if there are damage features in the groove that can increase the ΔRq, which will also affect the scratch visibility.

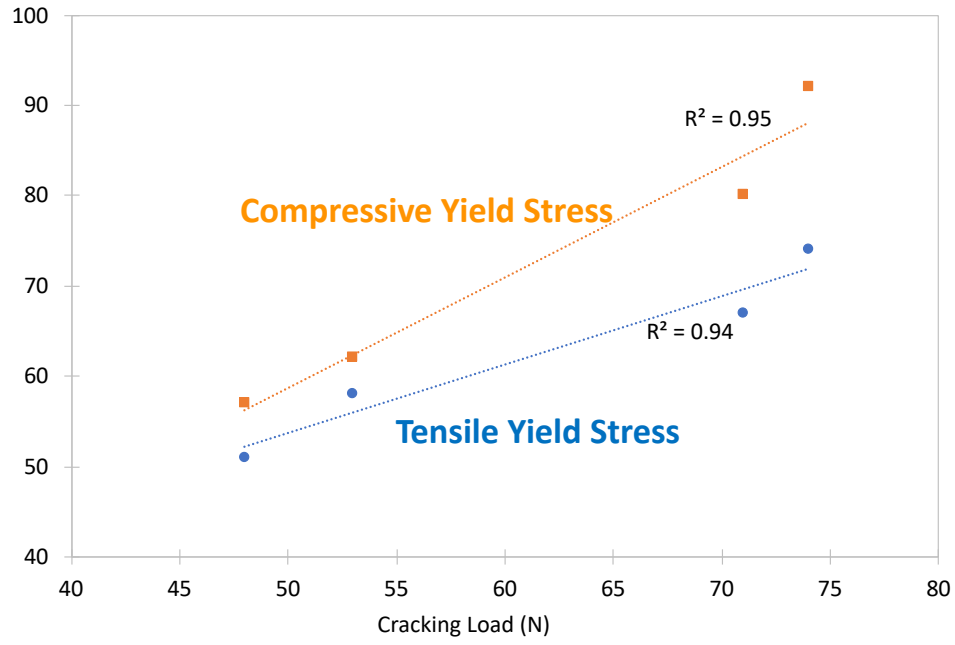

Figure 18. Relationship of tensile and compressive yield stresses with the scratch-induced cracking.

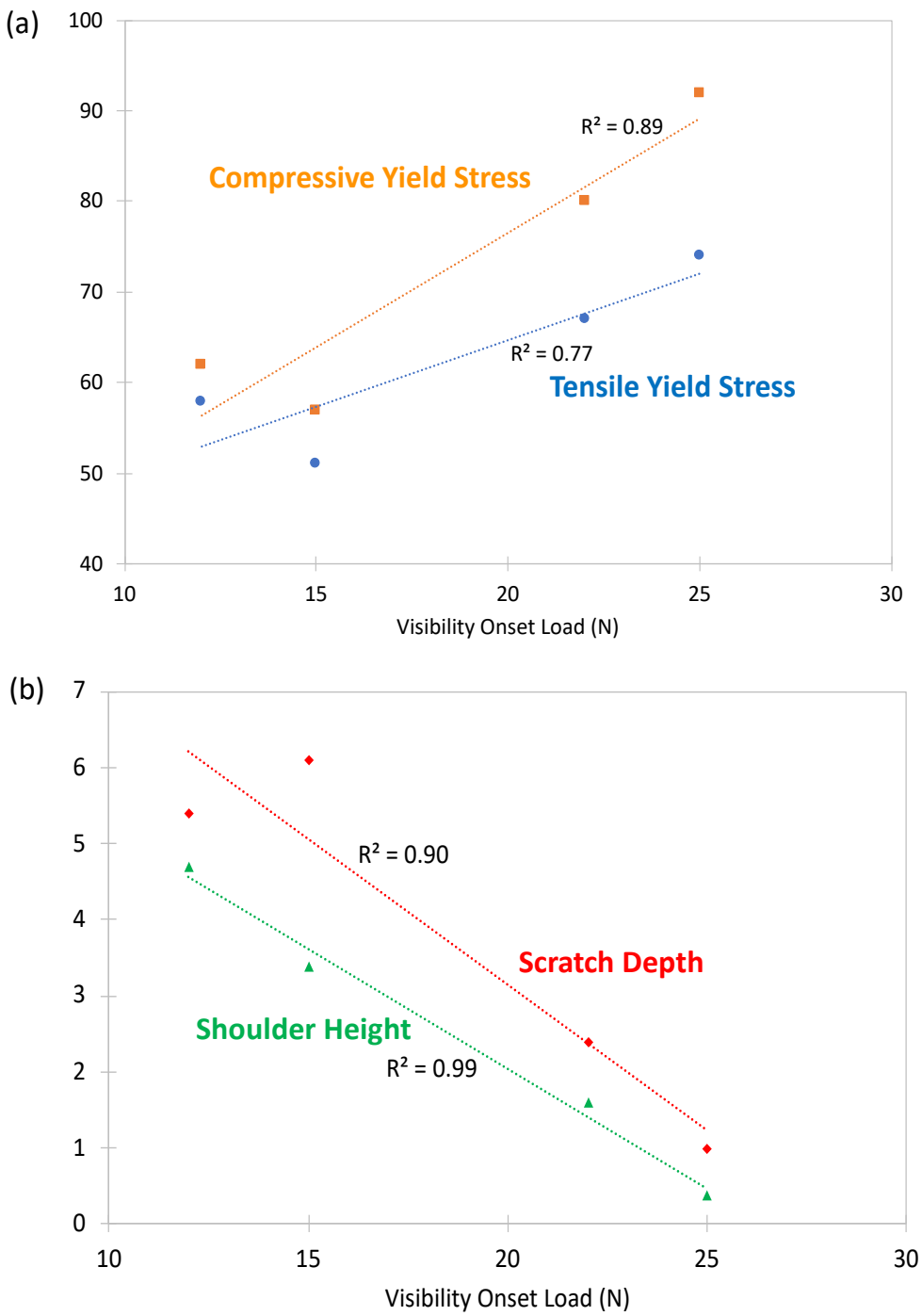

Figure 19. Relationship of tensile and compressive yield stresses with the scratch visibility resistance. (a) Mechanical properties and (b) scratch depth and shoulder height vs. onset of scratch visibility.

3.6 Conclusion

The tensile and compressive constitutive behavior affect the scratch deformation of polymers. The scratch visibility can be addressed by considering two geometrical parameters of the scratch groove: shoulder height and scratch depth, which are closely related to the yielding behavior of the polymer. Our findings indicate that the tensile properties affect the damage features in the scratch groove while the compressive constitutive behavior affects the scratch groove geometrical parameters. The frictional behavior also plays a critical role in an early stage of the scratch deformation process. A lower COF delays the onset of groove formation, which in turn delays onset of scratch visibility. Scratching is a complex process and many factors have to be considered such as constitutive behavior of the material, surface roughness, COF, and processing-induced anisotropy. In this particular case, the superior scratch performance of PC-cp2 is attributed to its low COF, and high tensile and compressive yield stress. Knowledge on what parameters govern the scratch resistance of polymers and how they are linked to material properties can enable the design of high scratch resistant PC-based systems for numerous engineering applications.

CHAPTER IV

SCRATCH BEHAVIORS OF POLYROTAXANE-MODIFIED POLY(METHYL METHACRYLATE)

In this chapter, the mechanical and scratch behaviors of polyrotaxane (PR) modified poly(methyl methacrylate) (PMMA) were investigated. PR is a necklace-like supramolecule with rings threaded onto a linear backbone chain that is capped by bulky end groups. Cyclodextrin (CD) serves as the ring structure and can be functionalized to induce specific interactions with the hosting polymer matrix. The effect of PR on the scratch resistance of PMMA was investigated by varying the PR concentration. The findings suggest that the methacrylate functional group in PR enhances the compatibility with PMMA, leading to an increase in tensile strength and reduction in scratch coefficient of friction, which accounts for an improvement in scratch resistance by over 100%. To systematically investigate the effect of CD functionalization on the properties of PMMA, PR with polycaprolactone (PCL) grafted chains on CD, and PR with methacrylate functional groups at the terminal of the PCL grafted chains on CD were chosen for this study. Dielectric relaxation spectroscopy, dynamic mechanical analyses, tensile and compressive true stress-strain tests, ASTM scratch test, and coefficient of friction measurements were conducted to fundamentally understand how PR influences the mechanical and scratch behaviors of PMMA.

4.1 Introduction

Polymeric materials play an important role in many engineering applications due to their versatile properties. Despite their superior processability and low cost, most polymers are susceptible to surface damage, limiting their durable usage in applications where both aesthetics and functionality are crucial. Due to its light-weight, transparency and weather resistance,

poly(methyl methacrylate) (PMMA) is a commonly-used material for automotive, electronics and optics applications [27, 28]. In some applications, especially window glazing and vehicle indicator lenses, the base polymer has inadequate scratch resistance.

Utilizing inorganic fillers is a common approach to improve the scratch resistance of PMMA. It has been shown that modifying the surface of silica (SiO_2) nanoparticles with amine functional groups can enhance nanoparticle-polymer interactions and reduce the volume of material removed per unit scratch length [29]. Hybrid PMMA-SiO_2 networks have been combined with polycarbonate in interpenetrating polymer networks to increase the scratch resistance of PMMA [31]. Organic-inorganic hybrid coatings, such as PMMA-siloxane-silica films, have also shown the potential to enhance barrier properties and scratch resistance for corrosion protection of metallic surfaces [30]. Lignin has been incorporated in PMMA-siloxane hybrid coatings to improve anti-corrosion properties and has been shown to slightly delay the onset of damage formation during scratching [92]. Addition of graphene oxide and carbon nanotubes have shown to improve the scratch resistance, adhesion and thermal stability of PMMA-siloxane-silica anticorrosive coatings [93]. Clay has been modified with acrylic functional groups to improve the compatibility with MMA monomers, resulting in improvements in the stiffness and the scratch resistance of PMMA/clay nanocomposites [94]. Additional efforts in this area involve using functionalized multi-walled carbon nanotubes [33], acrylic rubbers [95] and plasticizers [32]. The approaches above have shown the potential to moderately improve the scratch resistance of PMMA. Typically, improvements in scratch resistance are attributed to an increase in hardness or modulus, which may not be directly correlated to the complex scratch behavior of polymers [13]. Thus, fundamental understanding about the parameters that govern the scratch behavior of PMMA composites is still needed.

Polyrotaxane (PR) is a supramolecule with rings threaded onto a backbone linear chain that is capped by bulky end groups (Figure 20) [34]. The cyclic component, cyclodextrin (CD), serves as the ring structure and it is sparsely incorporated in the backbone linear chain. CD is subsequently crosslinked on different PRs to form crosslinking junctions that exhibit a figure-of-eight shape. The crosslinking junctions can slide upon stressing allowing for stress redistribution [35]. The materials with this ability are known as slide-ring (SR) materials. The fracture energy of SR gels has been shown to be independent of Young's modulus (Figure 21), and can be enhanced by increasing the slidable distance of the movable crosslink junctions, diverging from the common behavior of conventional gels where there is a trade-off relationship between toughness and stiffness [96]. Coatings containing PR exhibit significant elastic recovery after scratching when compared against chemically crosslinked gels, showing PR can improve the scratch-proof properties of elastomeric coatings [34]. It has also been shown that both the scratch resistance and flexibility of organic-inorganic hybrid coatings can be simultaneously improved by employing PR crosslinkers [36]. Thus, showing the potential of expanding the implementation of PR into rigid polymers networks to enhance the scratch resistance.

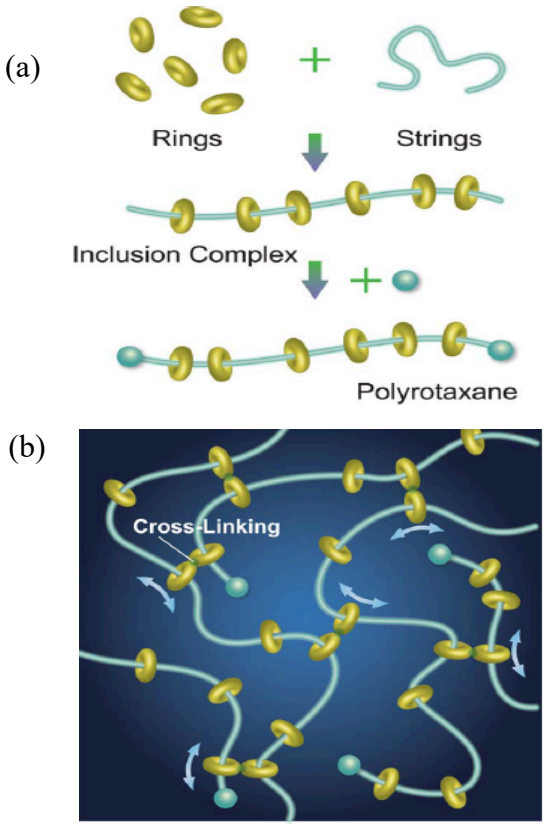

Figure 20. Schematic of (a) the constituents of polyrotaxane an (b) slide-ring gels. Reprinted with permission from J. Appl. Polym. Sci. 2014, 131, 40509. Copyright 2014. Wiley [34].

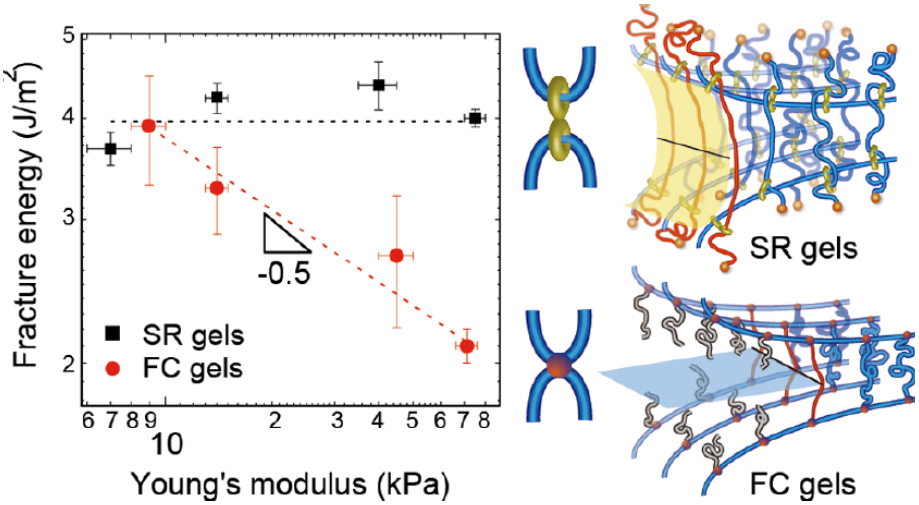

Figure 21. Fracture energy vs. Young's modulus of slide-ring and chemical gels. Reprinted with permission from ACS Macro Lett. 2017, 6, 12, 1409–1413. Copyright 2017. American Chemical Society [96].

The ASTM D7027/ISO 19252 consists of a linearly increasing normal load scratch test and has been widely used to quantitively evaluate scratch performance of polymeric systems [8, 9, 97]. By using this method, the onset normal load for different damage transitions like groove, cracking and plowing formation can be identified in one scratch. It has been shown that the onset of damage transitions due to scratch damage can be correlated to mechanical properties, such as tensile strength and compressive yield stress [13, 25, 40]. Several quantitative correlations have also been established numerically *via* finite element methods [15, 16, 42].

The objective of this work is to fundamentally understand how PR influences the scratch behavior of PMMA by first investigating the effect of PR concentration. Special attention is given to how tensile properties and frictional behavior correlate with scratch-induced crack formation. Secondly, to understand the role of each component of the PR structure, PRs with different functionalities were employed. Because of the complex molecular architecture of PR, the CD functionality on the PR was varied as follows: (1) PR with polycaprolactone (PCL)-grafted chains on CD and (2) PR partially modified with methacrylate functional groups at the terminal of the PCL grafted chains on CD. Figure 22 shows the chemical structure of the PRs and CD. For reference, the effect of the PEO main chain and CD alone on the mechanical properties of PMMA was also investigated. This work aims to understand the scratch behavior of PR-modified PMMA model systems and their structure-property relationship by correlating the scratch-induced damage with intrinsic material properties. Additionally, the possible molecular mechanisms responsible for the improvements in mechanical performance were investigated using dielectric spectroscopy and dynamic mechanical analysis. It is hoped that the knowledge gained from the present study can help develop highly scratch resistant polymers for vast engineering applications, especially for display screen and automotive glass applications.

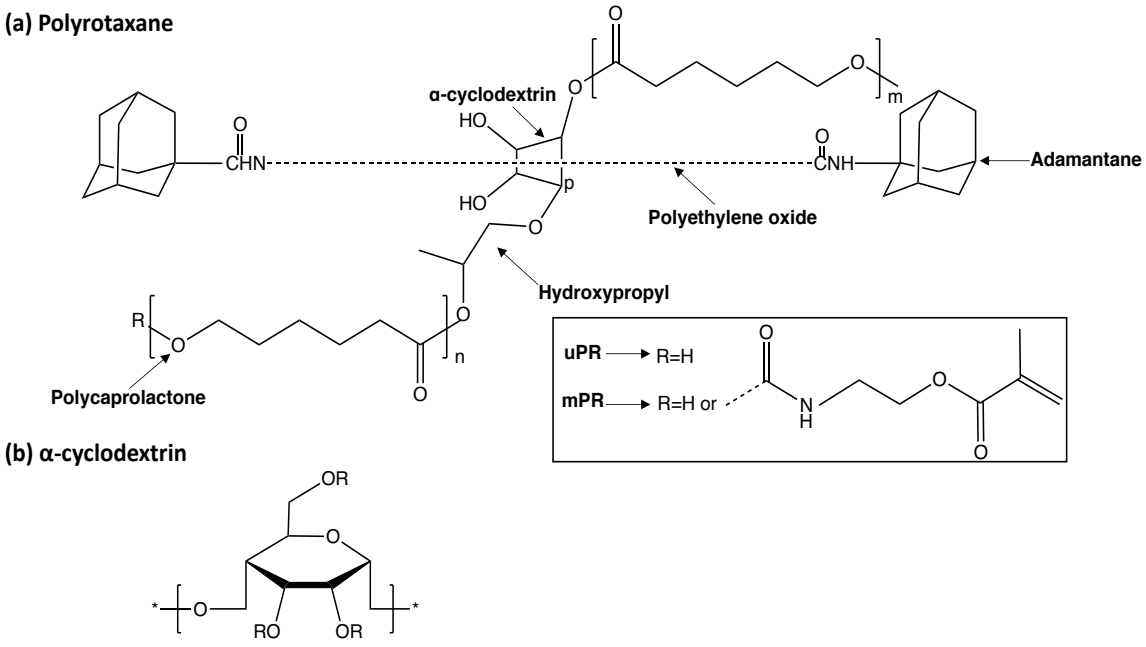

Figure 22. Chemical structure of (a) polyrotaxane and (b) α-cyclodextrin (CD). Adopted from www.asmi.jp/en/.

4.2 Materials & Methods

4.2.1 Sample Preparation

PMMA (Plexiglas® V825-100G Acrylic Resin) was donated by Arkema (M_w = 120,000 g/mol). Tetrahydrofuran (THF) was purchased from VWR. Polyrotaxanes SM1303P (M_w = 180,000 g/mol) and SH1300P (M_w = 180,000 g/mol) were obtained from ASM Inc. The M_n of the poly(ethylene oxide) (PEO) backbone linear chain was 11,000 g/mol for both polyrotaxanes. There are ~ 35 α-CD molecules per PEO chain (estimated by ^{1}H NMR). α-CD can cover two repeating units of PEO [98]. The molar ratio of α-CD to PEO repeat units is 1:7 resulting in a ring coverage of ~28% [99]. The number of caprolactone monomers on α-CD was 55.5 for both PRs (estimated by ^{1}H NMR). For PR SM1303P, 54.3% of the OH groups on the end of the PCL grafted chains on α-CD were modified with a methacrylate functional group.

To prepare the model PMMA systems containing PR modified with a methacrylate group (mPR) for scratch testing, 0.1 g of PR (SM1303P) was dissolved in 10 mL of THF. The solution was added dropwise to a 60 mL THF solution containing 10 g of PMMA in oil bath heating at 50°C and was stirred for 20 min. The mixture was sonicated for 15 min and was poured in an aluminum foil mold. The solvent was removed in a ventilated oven at 85°C for 24 hr. This sample contained 1 parts-per-hundred (phr), i.e., about 1 wt.%, of mPR and was labeled as PMMA_mPR1%. Following the same procedure, PMMA systems containing 1 phr of unmodified PR (uPR) SH1300 (PMMA_uPR1%), 1 phr of PCL-grafted α-CD (PMMA_CD1%), and a control system without PRs or CD, were prepared. PMMA containing 1 phr of PEO (M_w=3,000 g/mol) (PMMA_PEO1%) was prepared following the same procedure using acetone instead of THF. The dried material was hot-pressed in a 1 mm thick mold at 160°C for 10-15 min. For tensile testing, the dried material was hot-pressed into 0.2 mm thick films, and for compression testing, the dried material was hot-pressed using a 6 mm thick mold, both under the same molding conditions.

4.2.2 Dynamic Mechanical Analysis (DMA)

Dynamic mechanical analysis (DMA) was performed using a TA Instruments RSA-G2 using a temperature range of -140 to 165°C at a constant ramp rate of 3°C/min, a strain amplitude of 0.05% and a frequency of 1 Hz. The glass transition temperature (T_g) was defined as the peak point of the tan(δ) curve.

4.2.3 Ultraviolet-visible Spectrometer

The optical transparency of the 1 mm thick model systems was examined using an ultraviolet-visible spectrometer (Shimadzu, UV-3600) for visible wavelengths from 400-700 nm.

4.2.4 Transmission Electron Microscopy

The morphology of the samples was investigated using transmission electron microscopy (TEM). The films were embedded in an epoxy mount, stained with osmium tetroxide (OsO_4) crystals for 6 h, and rinsed in water for 12 h. A microtome (Ultracut E) and a Micro Star diamond knife were used to prepare thin sections of 70-100 nm in thickness. The particle size was measured using ImageJ software.

4.2.5 Dielectric Spectroscopy

A Novocontrol broadband dielectric spectrometer was used to investigate the dielectric relaxation of the composites ($20 \times 20 \times 1\ mm^3$) with a frequency sweep of 0.1 Hz–10 MHz at different temperatures. A temperature sweep from -80°C to 140°C was conducted at different frequencies. The samples were dried in a vacuum oven at 80°C for 5 days before conducting the dielectric measurements.

4.2.6 Tensile Stress-Strain Curves

RSA-G2 (TA Instruments) with a tensile fixture was employed to conduct the tensile tests at a speed of 2 mm/min. The 0.2 mm thick films were cut into a dog-bone shape. The true stress-strain curves were generated by measuring instantaneous cross-sectional area using digital image correlation (DIC) video setup. A black ink marker was used to generate a random speckle pattern on the gauge section of the samples. A single Canon EOS 5D Mark II DSLR camera and VIC-2D™ DIC software were used to track the deformation of the random speckle pattern on the tensile specimens during the test. This allowed for the acquisition of the true strains in tensile direction (e_{yy}) and lateral directions (e_{xx}). The true stress was obtained by dividing the applied load by the instantaneous cross-sectional area. Three tests were performed on each model system.

4.2.7 Compressive Stress-Strain Curves

Compression tests were conducted using MTS Insight® universal testing machine at a crosshead speed of 1.3 mm/min according to the ASTM D695–15 standard. The specimens were cut with a diamond saw blade to the nominal dimensions of 12 mm× 6 mm× 6 mm. Lubricant was applied on the compression fixtures before each test to minimize friction during testing. A Canon EOS 5d Mark II DSLR video camera was used to record the compression test. The images in the video were analyzed to obtain the true strains in the compression direction (e_{yy}) and lateral direction (e_{xx}). The model systems are considered to be isotropic, meaning that the strain in the thickness direction (e_{zz}) is assumed to be equal to the strain in the lateral direction (e_{xx}). At least three tests were performed on each model system.

4.2.8 Coefficient of friction (COF) and Surface Roughness (Rq)

A commercial scratch machine (Scratch 5, Surface Machine Systems, LLC) built according to the ASTM D7027/ISO 19252 standard was used to measure the COF of the model systems. The COF is also known as dynamic friction and it refers to ratio between the force required to maintain motion at a prescribed scratch speed and the force pressing the surface.[60] A flat stainless steel (10 mm × 10 mm) tip was utilized. The tests were performed at a 5 N constant normal load and the speed was 10 mm/s. Three tests were performed on each sample. The surface roughness (R_q) was measured by Keyence® VK9700 violet laser scanning confocal microscope (LSCM) using a sampling area of 675 μm × 506 μm. Five measurements were taken on each sample.

4.2.9 Scratch Test

The scratch test was conducted according to the ASTM D7027/ISO19252 methodology using a G5 scratch tester by Surface Machine Systems. A 1 mm diameter spherical stainless-steel tip was used to conduct the scratch tests. A linearly increasing normal load of 1–150 N was applied. The

scratch speed and length were 10 mm/s and 50 mm, respectively. The surface of the samples was cleaned using compressed air before scratching. Three scratches were generated on each model system. The scratch coefficient of friction (SCOF) curve was obtained by taking the ratio of the tangential load and the normal load during the scratch test. The onset of damage transitions, specifically, cracking, and corresponding damage features were identified using LSCM. The LSCM was employed to determine the residual scratch depth and the roughening along the scratch track.

4.3 Results

4.3.1 Effect of PR Concentration

The model systems containing no PR (Neat PMMA), 0.5 wt.% PR (PMMA_mPR0.5%), and 1 wt.% PR (PMMA_mPR1%) were investigated. The T_g of the model systems were 120.7°C, 118.1°C and 122.5°C for Neat PMMA, PMMA_mPR0.5%, and PMMA_mPR1%, respectively (Figure 23). The storage modulus slightly increases with PR concentration. Moreover, the sub-T_g relaxation is more pronounced for the model system containing 1 wt.% PR. Figure 24 shows the true tensile stress-strain curves of the model systems. The samples were stretched until their breaking point to determine their tensile strength. The tensile strength, elongation at break and tensile modulus increase with increasing PR concentration.

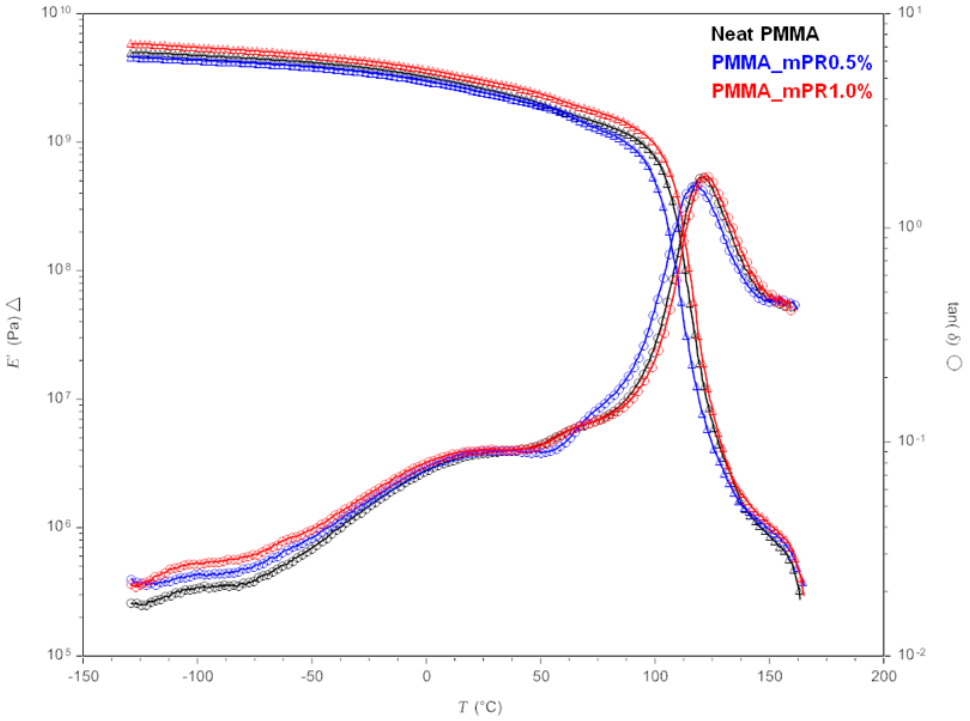

Figure 23. Storage modulus (E') and tan(δ) of model PMMA systems with varying mPR content.

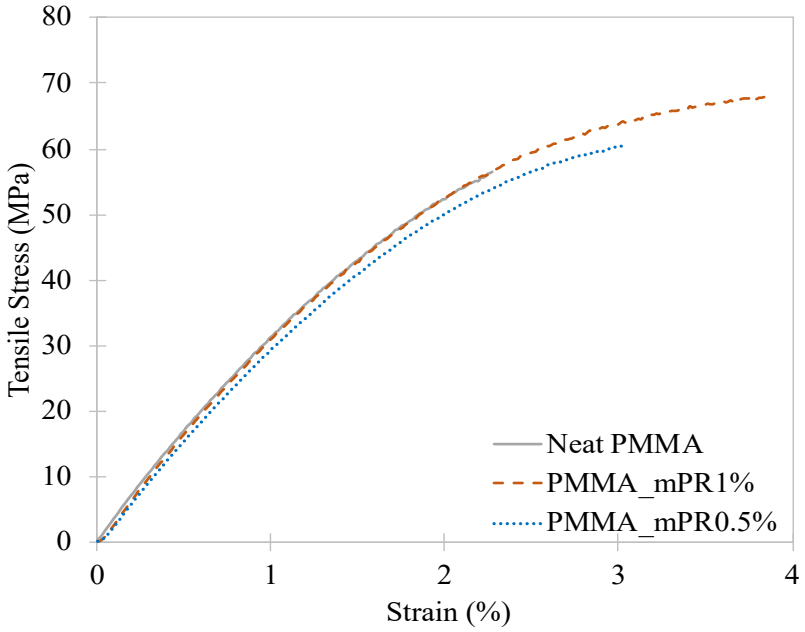

Figure 24. True stress-strain curve of model PMMA systems with varying mPR content.

As shown in Figure 25, the load required for crack formation increases as a function of PR concentration. Surprisingly, adding only 1 wt.% of PR improves the scratch resistance of PMMA by over 100%. The scratch coefficient of friction (SCOF), defined as the ratio between the tangential load and the normal load, significantly decreases due to the presence of PR, as shown in Figure 26. The results suggest that adding modified PR to PMMA dramatically affects the scratch behavior of PMMA, increasing the resistance against crack formation from 57 N (Neat PMMA) to 123 N (PMMA_mPR1%) while greatly reducing the SCOF. Previous experimental and numerical studies have shown that increasing the tensile strength increases the scratch resistance [16, 17, 25, 44]. Based on numerical studies, it has been shown that the material behind the scratch tip experience a high tensile stress during the scratch process, and that near the surface, the stress state along the scratch direction is dominated by uniaxial tension [16, 44]. In our case, the gradual increase in tensile strength with PR content may account for the observed improvement. Post-scratch analysis conducted using LCM revealed that the scratch depth of Neat PMMA is significantly higher than that of PR-containing model systems, suggesting that higher frictional forces developed during the scratch process promoting early crack formation. This is supported by Figure 26, which shows that Neat PMMA indeed exhibits a higher SCOF.

The results suggest that incorporating a PR with a methacrylate functional group at the end of the PCL-grafted chains on CD significantly alters the scratch behavior of PMMA while maintaining its transparency and the stiffness. Adding only 1 wt.% of modified PR enhances tensile strength and reduces the scratch coefficient of friction of PMMA, which delays the onset of crack formation during scratching. Future work will focus on investigating the physical mechanisms by which PR improves the mechanical properties and scratch resistance of PMMA.

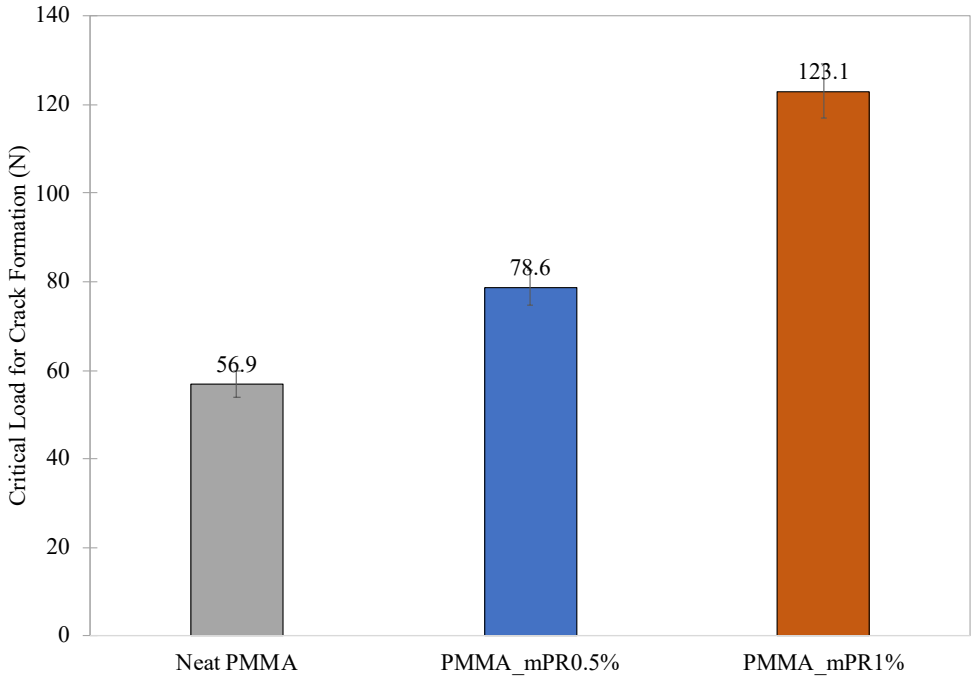

Figure 25. Onset load for scratch-induced crack formation of 1 mm thick model systems.

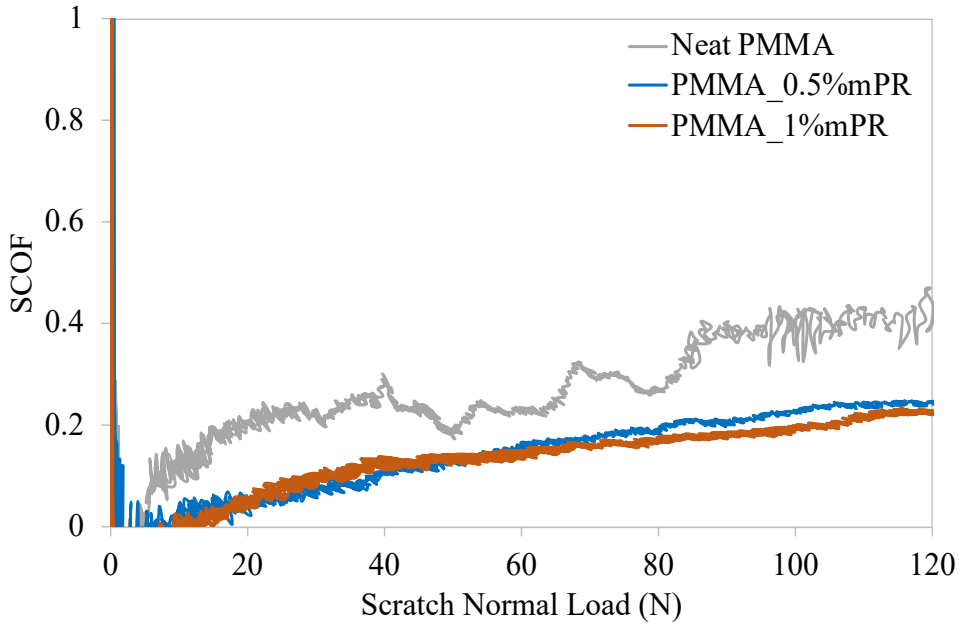

Figure 26. Scratch coefficient of friction (SCOF) curves of model PMMA systems.

4.3.2 Effect of PR Functionalization

4.3.2.1 Characterization of PR-Modified PMMA

Two model PMMA/PR systems have been prepared *via* solution casting and contained 1 phr of uPR and mPR following the procedure reported in section 4.2.1 but using PMMA (Plexiglas® V825-100G Acrylic Resin) donated by Arkema (M_w = 120,000 g/mol). Figure 22 shows the chemical structures of PRs and CD. The storage modulus (E') and tan(δ) curves of the model PMMA systems are shown in Figure 27a. The T_g of neat PMMA, PMMA/uPR and PMMA/mPR is 121, 117, and 123°C, respectively. PMMA systems containing mPR exhibits a slight increase in E' throughout the temperature range tested and show a more pronounced damping below room temperature over those of neat PMMA. Contrarily, PMMA/uPR exhibits a lower E' and a slight decrease in T_g when compared against neat PMMA. The light transmittance values within the visible light region of the 1 mm thick PMMA/mPR is similar to that of neat PMMA, while PMMA/uPR exhibits a considerable decrease (Figure 27b). TEM observation shows that PR forms sub-micron domains in the PMMA matrix ranging from 50 to 300 nm in size and that mPR appears to be better dispersed than uPR in PMMA (Figure 28). In the most miscible PR and epoxy blend, PR had a domain size from 5 to 20 nm [100]. Although mPR and PMMA are not completely miscible, the optical transparency is maintained.

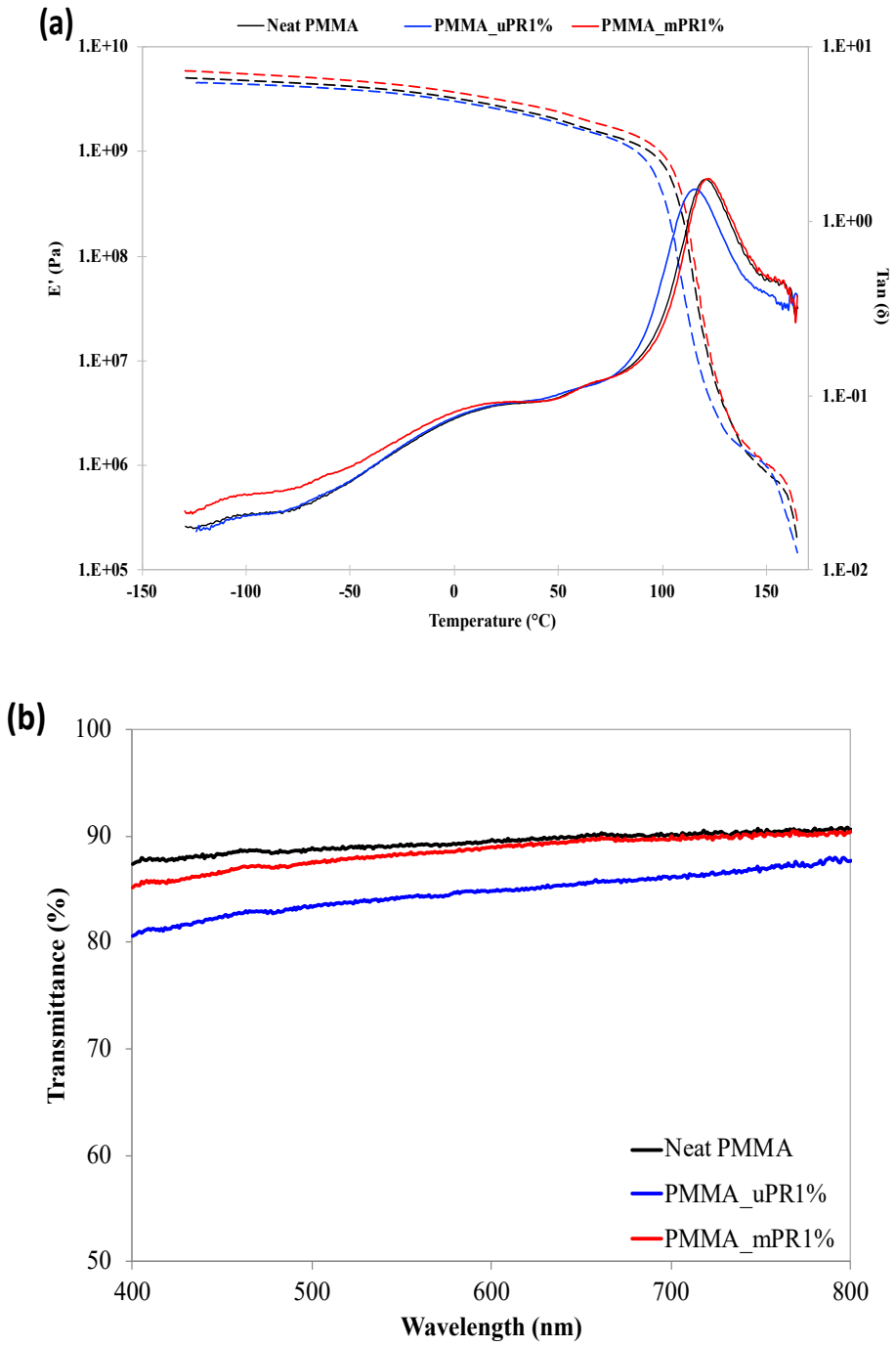

Figure 27. (a) DMA analysis and (b) transmittance (%) of the model PMMA systems. The storage modulus E' is represented by the dashed lines and tan(δ) is presented by solid lines in the DMA plot.

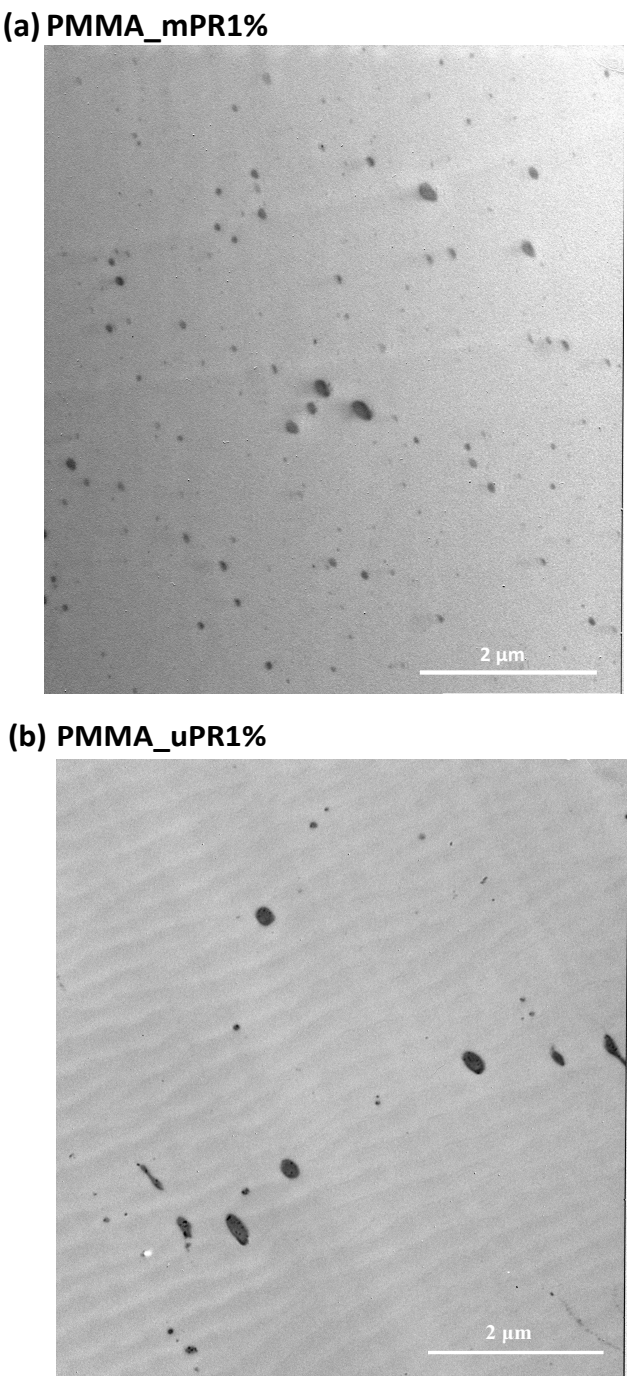

Figure 28. TEM images of PMMA containing 1 phr of (a) mPR and (b) uPR.

4.3.2.2 Mechanical Properties

Figure 29 shows the true tensile stress-strain curves for the model systems. The key tensile properties are summarized in Table 7. All the model systems have a similar tensile modulus close

to 3 GPa. Adding both types of PR moderately enhance the tensile strength and elongation at break of PMMA. Since the scratching process involves multi-axial loading with significant tensile and compressive components to induce scratch damage, the compressive properties of the model PMMA systems were also characterized. The key compressive properties are summarized in Table 8. As expected, the compressive behaviors of the model systems are drastically different from their tensile behavior (Figure 30). PMMA containing mPR exhibits a significant improvement in compressive yield stress and strength. Addition of uPR seems not to affect the compressive yield stress of PMMA but causes a substantial reduction in compressive strength. The model systems have similar compressive modulus of ≈ 4 GPa. The above findings suggest that PMMA/mPR can accommodate higher stresses before yielding and can undergo significant compressive deformation before failure at a significantly higher stress. Knowledge about both tensile and compressive behaviors of the model systems are key to understand the scratch behavior, as will be discussed later.

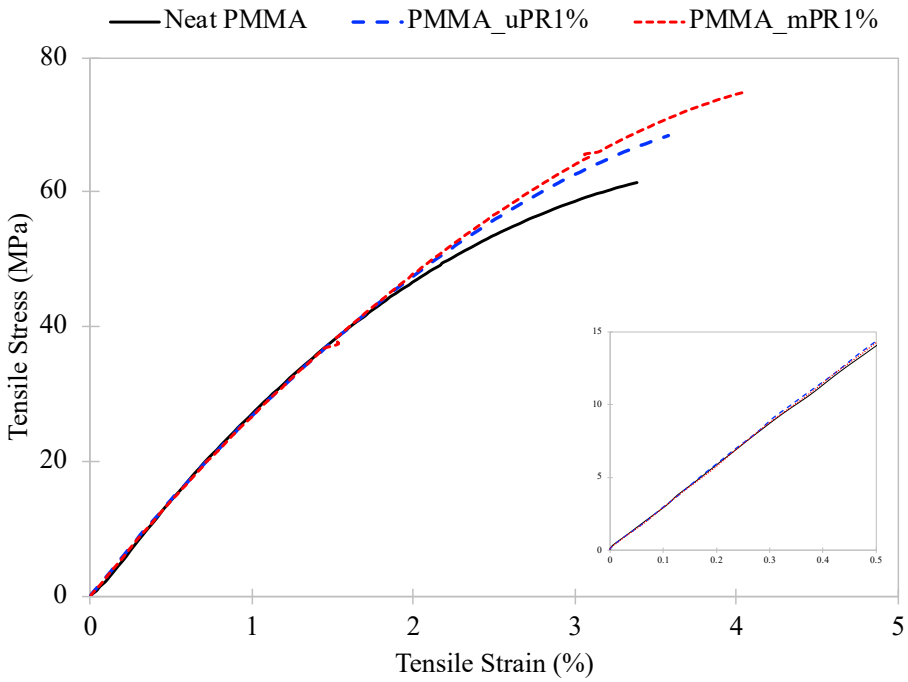

Figure 29. Tensile stress-strain curves of the model PMMA systems. The inset image shows the tensile stress up to a strain magnitude of 0.5%.

Table 7. Tensile properties of the model PMMA systems.

	Tensile Strength (MPa)	Elongation at Break (%)	Tensile Modulus (GPa)
Neat PMMA	60 ± 2	3.2 ± 0.1	2.9 ± 0.1
PMMA_uPR1%	69 ± 4	4.2 ± 0.5	2.8 ± 0.21
PMMA_mPR1%	75 ± 2	4.2 ± 0.2	3.1 ± 0.1

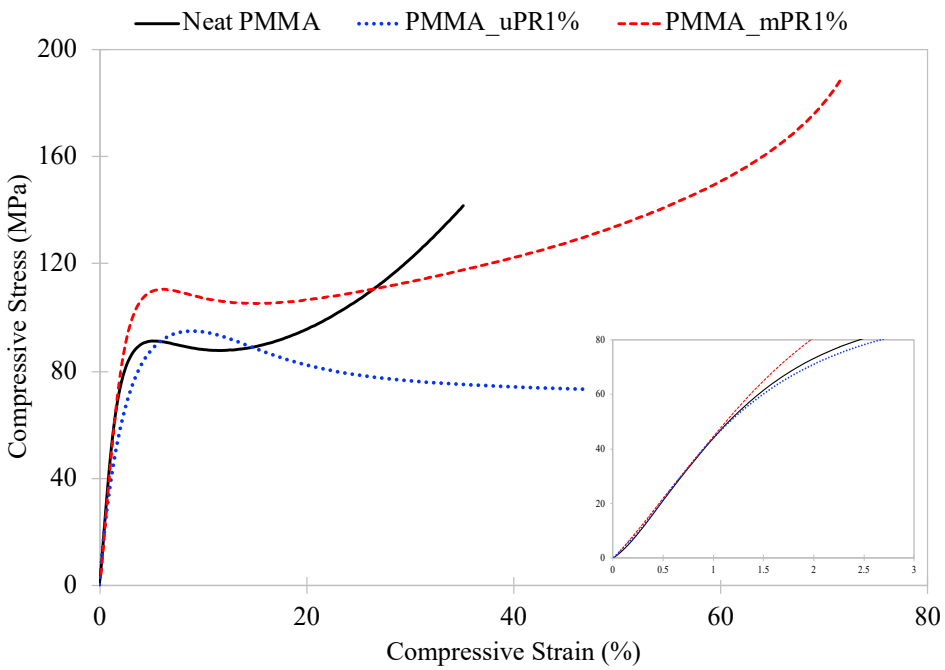

Figure 30. Compressive stress-strain curves of the model PMMA systems. The inset image shows the stresses up to a strain magnitude of 3%.

Table 8. Compressive properties of the model PMMA systems.

	Yield Stress (MPa)	Compressive Strength (MPa)	Compressive Modulus (GPa)
Neat PMMA	95 ± 4	154 ± 10	4.1 ± 0.3
PMMA_uPR1%	96 ± 1	68 ± 5	4.1 ± 0.2
PMMA_mPR1%	110 ± 2	191 ± 12	4.3 ± 0.1

4.3.2.3 Scratch Behavior

Surface properties are known to affect the scratch resistance of polymers. Surface roughness (R_q) and coefficient of friction (COF) of the model systems are shown in Figure 31. There is no significant difference in the surface properties of the model PMMA systems, indicating that the observed scratch behavior of the model systems originates from intrinsic material properties instead of surface conditions.

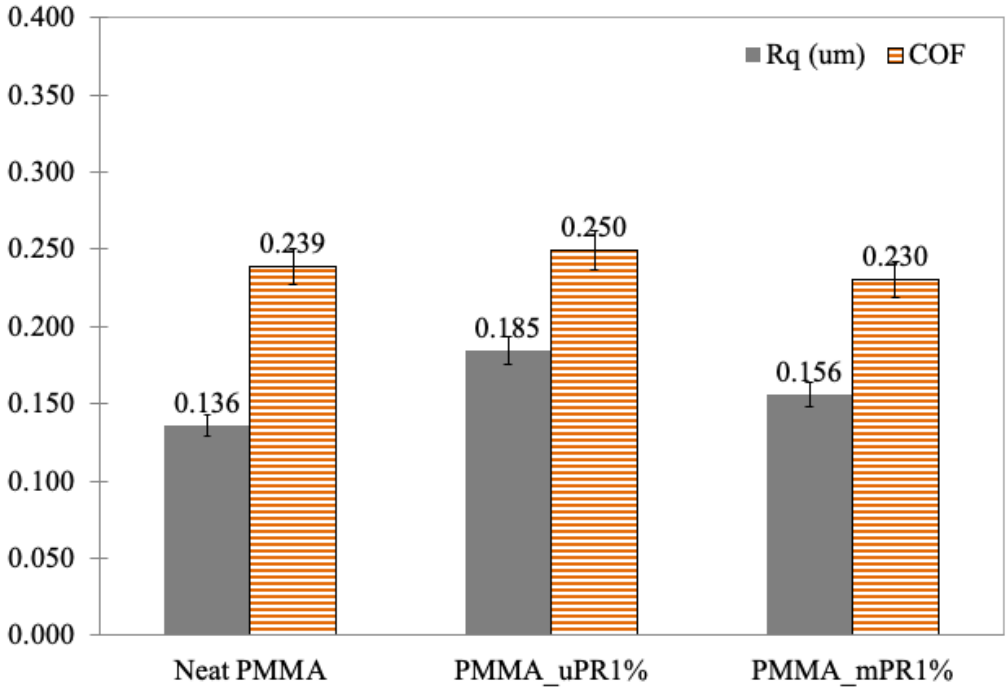

Figure 31. Surface roughness (R_q) and coefficient of friction (COF) of the 1 mm thick model PMMA systems

The scratch test was conducted on 1 mm thick samples according to the ASTM D7027/ISO 19252 method. The normal load required for crack formation during the scratch test is shown in Figure 32a. The scratch coefficient of friction (SCOF), defined as the ratio between the tangential and the normal load, is shown in Figure 32b. Post-scratch analysis, such as the scratch depth and roughening along the scratch track are shown in Figure 33a and Figure 33b, respectively. The scratch-induced damage features are shown in Figure 34. The results suggest that mPR dramatically affects the scratch resistance of PMMA, increasing the scratch resistance from 76 N for neat PMMA to 116 N for PMMA/mPR while greatly reducing the SCOF. Post-scratch analysis reveals that both the scratch depth and roughening are reduced when mPR was added to PMMA. In the case of PMMA/uPR, only a partial improvement is found in the onset of crack formation during scratching, while both the SCOF and the residual scratch depth are slightly higher than that

of neat PMMA. PMMA/mPR exhibits the best scratch performance among the model systems, delaying the onset of crack formation, reducing the SCOF, residual scratch depth and roughening. It is noted that adding both types of PR to PMMA alter the crack features, as shown in Figure 34.

Our findings suggest that in the model PMMA systems used in this study, both the tensile and compressive properties must be considered to account for the differences in their scratch behaviors. The substantial increases in tensile strength and compressive yield stress of PMMA/mPR are responsible for its low SCOF and high residual scratch depth recovery, and account for the significant improvement in scratch performance. Having higher compressive yield stress require higher loads for scratch tip to move deeper into the material during scratching. PMMA/uPR exhibits a higher tensile strength than that of neat PMMA and a slight improvement in the resistance against scratch-induced cracking. Previous experimental and numerical studies have shown that, when the compressive behaviors between two materials are similar, increasing the tensile strength usually increases the scratch resistance [16, 17, 25, 44]. However, when the compressive behaviors between two materials are substantially different, as it is the case in this study, the material with lower compressive yield stress can significantly exert high SCOF at a low scratching load and cause early crack formation process during the scratch test [13]. A low yield stress allows for the scratch tip to penetrate much deeper upon compressive yielding, which the generates much higher SCOF and promote early crack formation. This phenomenon is supported by Figure 32b and Figure 33, which shows that PMMA and PMMA/uPR indeed exhibit much higher SCOFs and higher residual scratch depth than PMMA/mPR along the scratch path. The visible light transmittance of PMMA/uPR is significantly lower than that of PMMA/mPR (Figure 27b), suggesting that uPR does not disperse well in PMMA, as shown in Figure 28b.

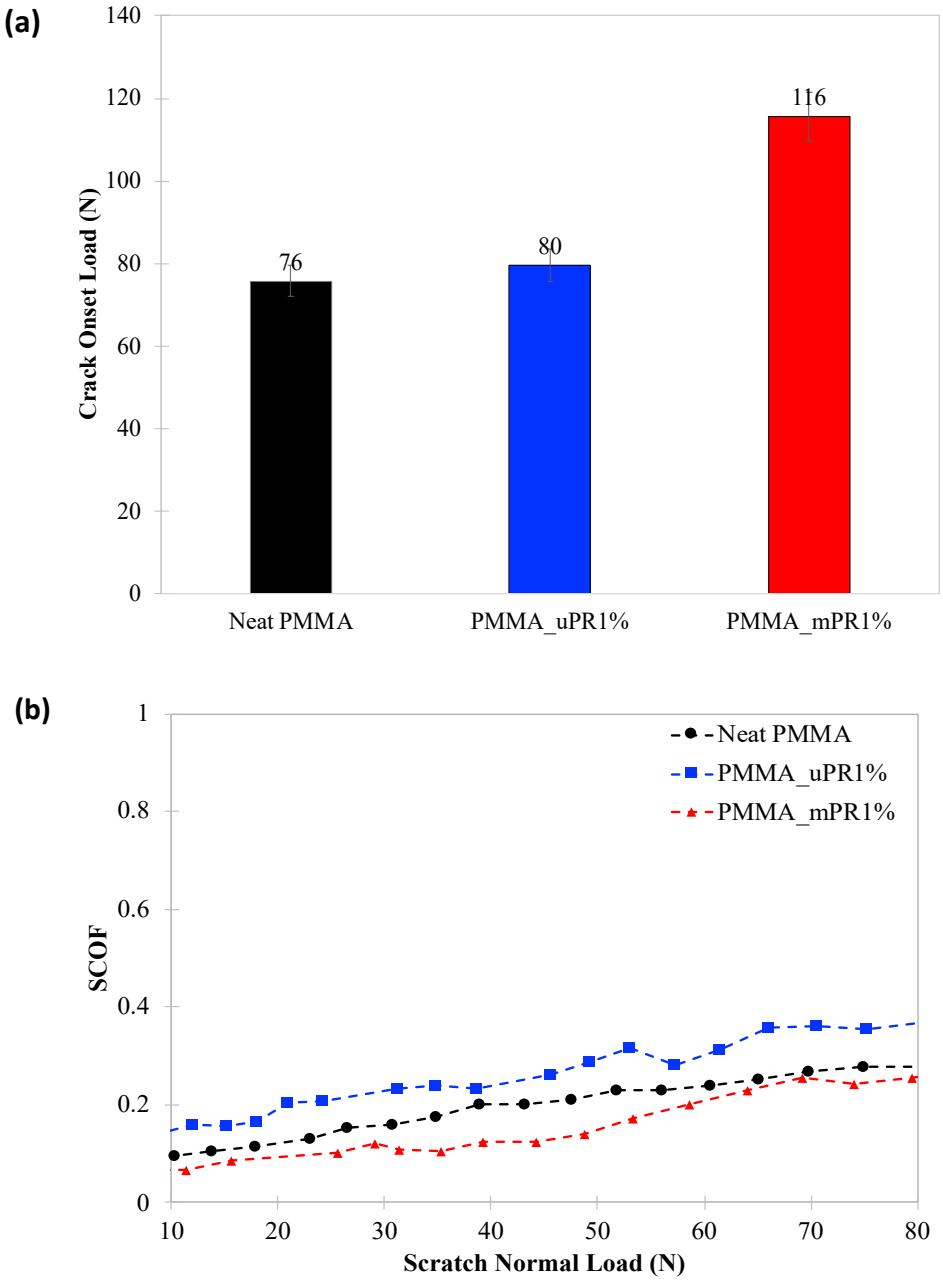

Figure 32. (a) Onset load for cracking and (b) SCOF curves of the model PMMA systems. The samples were 1 mm in thickness.

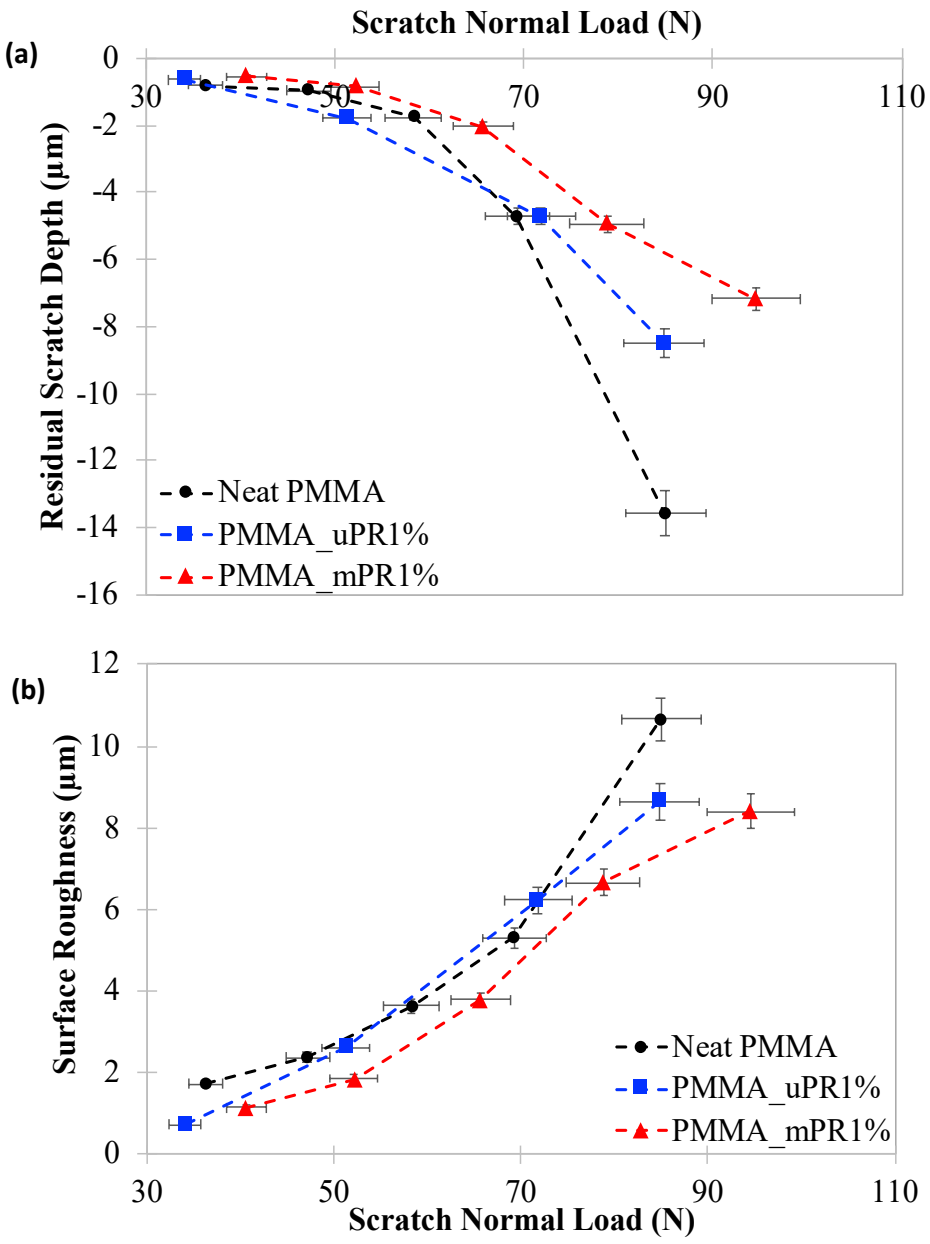

Figure 33. Post-scratch analysis *via* LSCM. (a) residual scratch depth and (b) roughening along the scratch groove as a function of scratch normal load measured by LSCM.

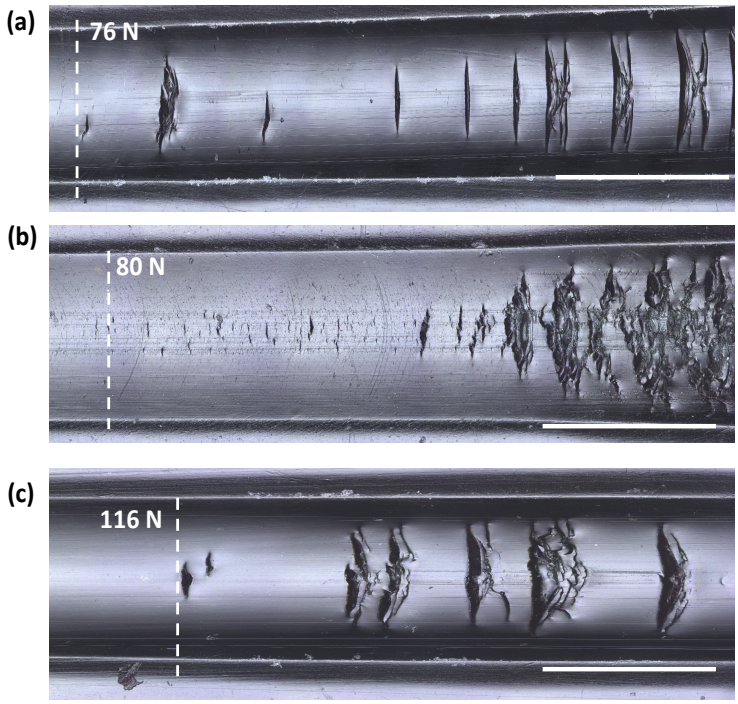

Figure 34. Onset of scratch crack formation of *via* LSCM. The scale bar is 500 μm.

To investigate the impact of each individual component of PR on PMMA properties, a model PMMA system containing 1 wt.% CD and a model PMMA system containing 1 wt.% PEO were prepared. As shown in Table 9, the tensile strength and tensile modulus are is similar to that of neat PMMA, while the scratch resistance is worsened. CD forms domains of about 100 nm in size in the PMMA matrix (Figure 36), indicating some aggregations of CD. Moreover, PMMA/PEO exhibits a slight increase in tensile strength, a significant reduction in tensile modulus, and a significant increase in elongation at break. The onset load for crack formation during scratching is about 62 N. PEO does not disperse well in PMMA with a domain size of about 7 μm (Figure 37), which significantly decreases its light transmission (Figure 35). The above findings suggest that the PEO and CD alone cannot noticeably enhance the PMMA properties. The unique combination of the PR structure with reasonable CD affinity to PMMA matrix serves to enhance the tensile, compressive, and scratch properties of PMMA/mPR.

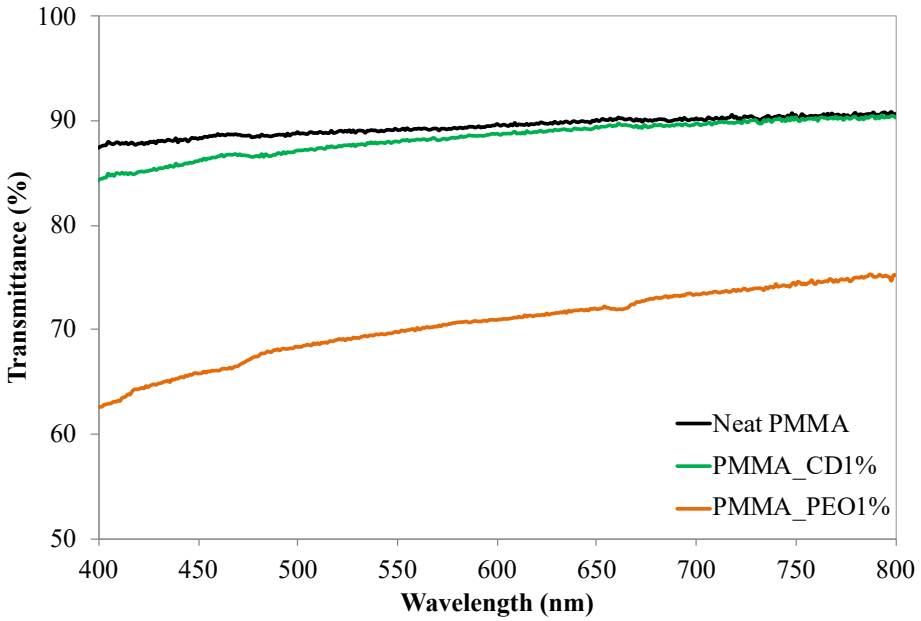

Figure 35. Transmittance (%) of neat PMMA, PMMA/CD and PMMA/PEO.

Table 9. Tensile properties and onset load for crack formation of PMMA/CD and PMMA/PEO.

	Tensile Strength (MPa)	Elongation at Break (%)	Tensile Modulus (GPa)	Onset Cracking Load (N)
PMMA_CD1%	58 ± 4	2.2 ± 0.1	3.1 ± 0.2	59 ± 6
PMMA_PEO1%	63 ± 3	4.8 ± 0.9	2.2 ± 0.4	62 ± 5

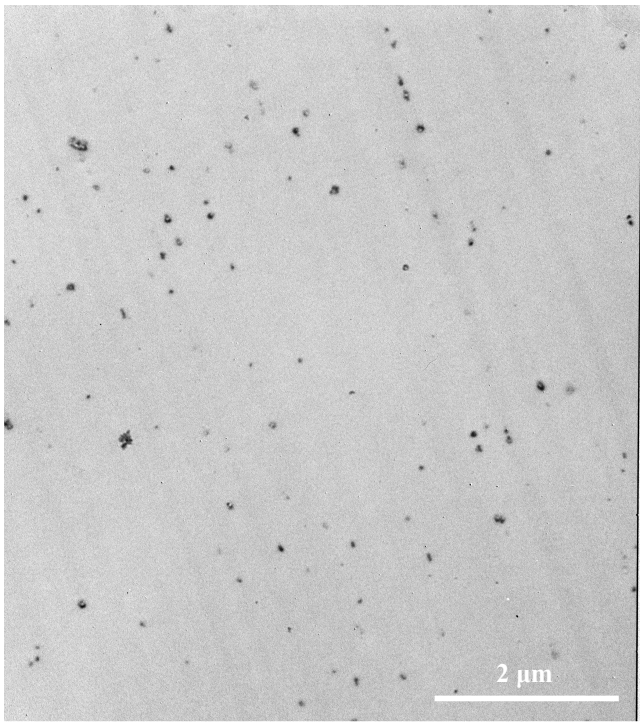

Figure 36. TEM observation of PMMA/CD.

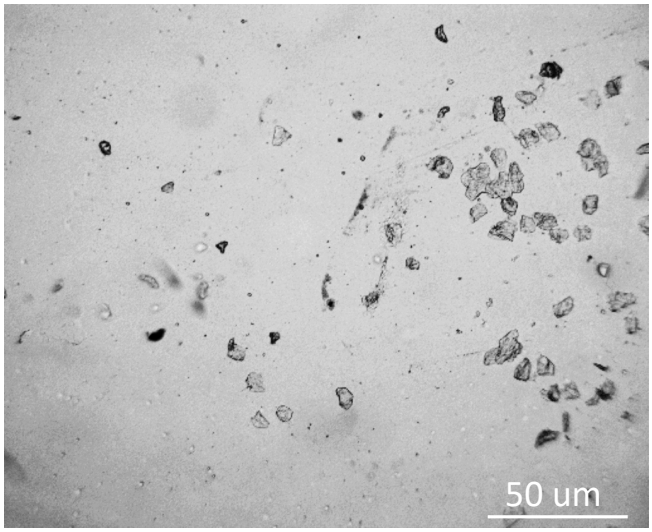

Figure 37. Optical microscope (OM) observation of PMMA/PEO.

4.3.2.4 Dielectric Relaxation Spectroscopy

To fundamentally determine why PMMA/mPR exhibits great enhancement in compressive properties and scratch performance over neat PMMA and PMMA/uPR, both DMA and dielectric spectroscopy investigations were carried out. The DMA study (Figure 27a) clearly shows that PMMA/mPR possesses a more noticeable damping characteristics than neat PMMA and PMMA/uPR at temperatures below 0°C, especially at below -50°C, suggesting the presence of mPR can greatly enhance the local molecular mobility at sub-segmental scale.

Dielectric spectroscopy can provide insights about molecular dynamics of polar polymers by monitoring the motion of dipolar species in the polymer. Numerous studies show that PMMA exhibits two main relaxation processes, α- and β-processes [101-106]. The α-process is associated with the segmental rotational micro-Brownian motion of the main chains, and the β-processes is mostly related to the micro-Brownian motion of the side groups [104, 107]. At high temperatures, these two processes merge into a complex αβ process.

Correlations between the chemical structure and the corresponding relaxation behavior of polymers have been well-established in the past. It has been shown that steric interferences and polar forces can promote intermolecular cooperativity. The chain structure, for instance, its flexibility, steric hindrance, and symmetry of the main chains and the pedant groups, influences the degree of intermolecular cooperativity on the segmental relaxation processes. Variations in the degree of cooperativity is manifested in the breadth of the dielectric dispersion [104]. Nevertheless, it is challenging to predict changes in intermolecular coupling for different polymers solely based on the chemical structure. In fact, the effect of the length of the alkyl side group of PMMA on the apparent activation energy of the β-process has been unclear [108, 109].

According to Ishida and Yamafuji [101], PMMA is considered to have a "flexible" dipole whose micro-Brownian motions are active even below T_g. PMMA has two kinds of dipoles coming from the methyl and the ester groups. The methyl groups are short and rigidly attached to the main chains, while the ester groups are long and more mobile. The dipole moment of the methyl group can be considered negligible in comparison to that of the ester group [101], and it is affected by both mobility and polarizability. Below T_g, only the micro-Brownian motion of the ester group is active, and its motion is constrained by the low mobility of the main chains, which leads to the observed β-absorption. Both the reorientation of the flexible ester group and the intermolecular environment influence the magnitude of the β-process, when observed on a timescale shorter than that of the micro-Brownian motion [107]. Since the side chains contain the electric dipole, most of the polarization relaxes through the β-relaxation. Therefore, PMMA exhibits a strong dielectric β-relaxation and a relatively weak α-relaxation [105, 110]. With increasing temperature, the micro-Brownian motion of the main chains increase, affecting the motion of the side chain ester groups, and thus, changing the behavior of the β-absorption. When near T_g, due to the segmental motion of the main chains, other modes of micro-Brownian motion of the ester groups become active and couple with the orientational motion of the methyl group dipoles, leading to the observed α-process [101].

Incorporation of reinforcing agent is a common approach to obtain polymers with improved mechanical properties. The mechanical properties of reinforced polymers are influenced by the adhesion between the phases, their morphology, inter-molecular interactions, and many other factors. Dielectric spectroscopy is an effective tool for studying the molecular dynamics and nature of the interactions between the phases. For example, Li et al. [106] studied the molecular dynamics

of PMMA/silica nanocomposites and found that the addition of silica increased the apparent activation energy for the α-process, leading to the observed increase in T_g with silica content.

The focus of the current study is to identify the possible changes in the dipole-induced relaxation processes that would help our fundamental understanding on how uPR and mPR influence the molecular relaxation of PMMA, and the corresponding mechanical behavior. The dielectric constant and dielectric loss of the three model systems are shown in Figure 38 and Figure 39, respectively. In accordance to the literature, neat PMMA exhibits a strong local process (β-process) (Figure 40a), which is originated from the partial rotation of the -$COOCH_3$ side group around the C-C bonds that link the side group to the main chain [111]. The maximum loss peak shifts to higher frequencies with increasing temperature, and the intensity of the loss peak, which is related to the population of relaxed dipoles involved in the relaxation process, tends to increase with increasing temperature (Figure 39a). At higher temperature, the α-process appears as a shoulder in the low frequency side and merges with the β-process.

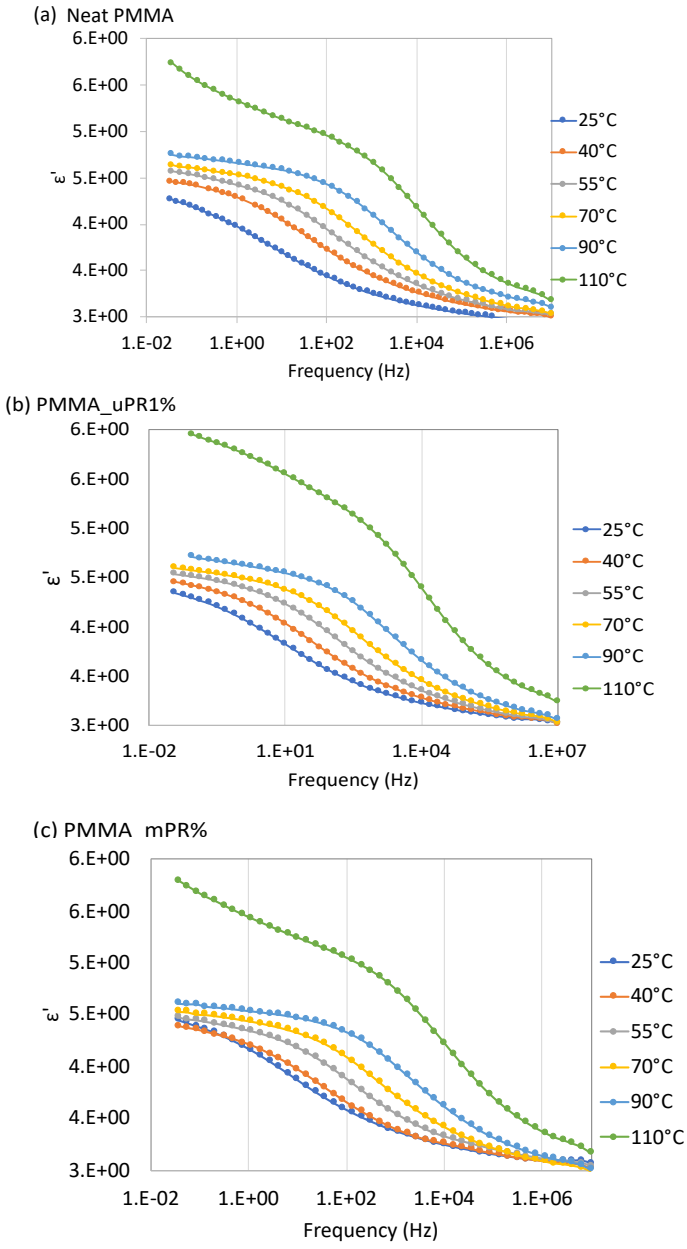

Figure 38. Dielectric constant, ***ε***', of (a) neat PMMA; (b) PMMA/uPR; and (c) PMMA_mPR.

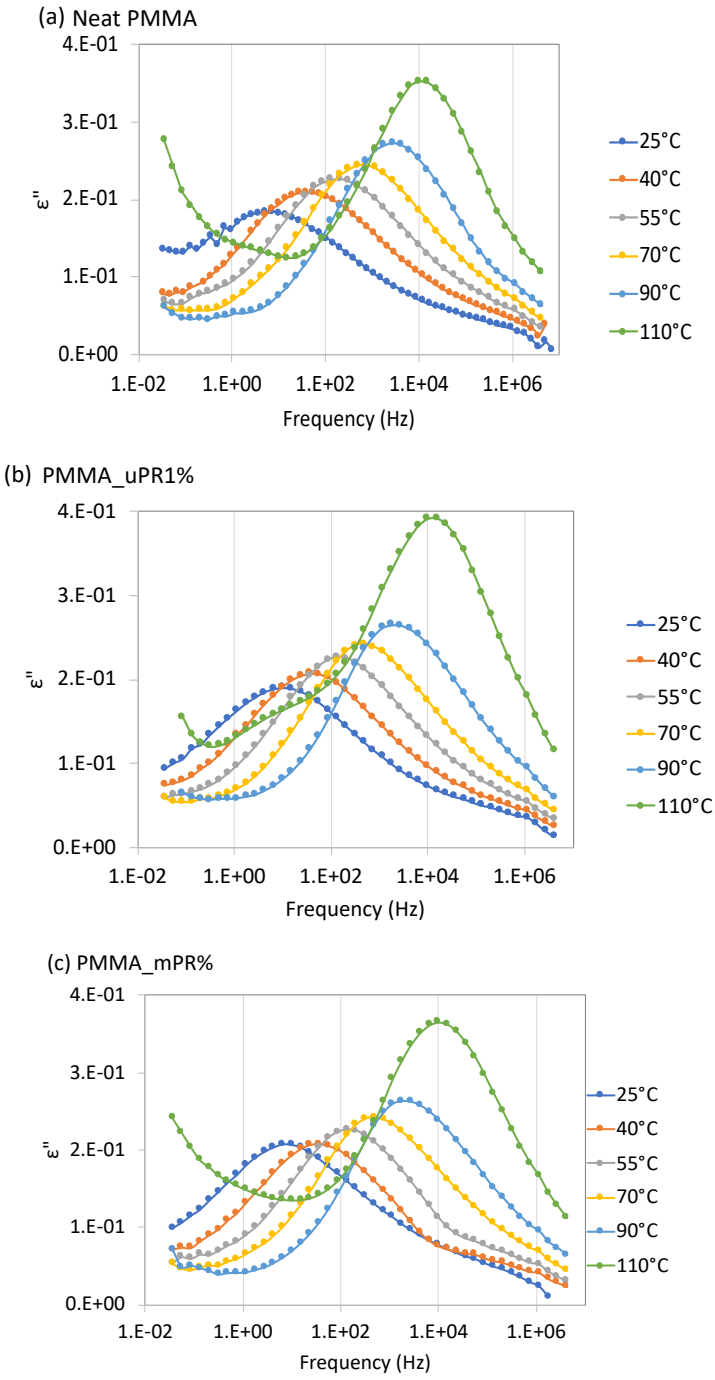

Figure 39. Dielectric loss, ***ε***", of (a) neat PMMA; (b) PMMA/uPR; and (c) PMMA/mPR.

For a more quantitative analysis of the dielectric data, the WinFIT software by Novocontrol was employed to apply the following Havriliak-Negami (HN) function [112]:

$$\varepsilon^* = \varepsilon_\infty + \frac{\Delta\varepsilon}{[1 + (i\omega\tau_{HN})^\beta]^\gamma}$$

where $\varepsilon^* = \varepsilon' - i\varepsilon''$ is the complex dielectric function, ε_∞ is the permittivity of the unrelaxed system, $\Delta\varepsilon$ is the relaxation strength, τ_{HN} is the characteristic relaxation time, ω is the angular frequency of the applied electric field, and β and γ are symmetric and asymmetric shape parameters, respectively. One or two HN functions were used to describe the α- and/or β-processes. The DC ionic conductivity contribution described as follows:

$$i\frac{\sigma_0}{\varepsilon_0\omega^s}$$

where σ_0 is dc ionic conductivity of the sample, ε_0 is the dielectric permittivity of vacuum, and s is a scaling parameter, was subtracted from the HN function.

In comparison with neat PMMA, both PMMA/uPR and PMM/mPR exhibit a noticeable high-frequency shoulder (Figure 40b and Figure 40c). This additional contribution corresponds to an additional relaxation process caused by interactions induced by the ester and/or OH groups on the grafted chains of CD. The position on the high frequency side of the spectra indicates that the PR domains have higher molecular mobility than the PMMA matrix. It is also noted that the additional relaxation process is more pronounced for PMMA/mPR than PMMA/uPR, and merges with the central peak with increasing temperature. The activation energy of the local process, estimated from the slope of the ln(τ) vs. 1000/T plot, is ~80 kJ/mol for the three model systems, suggesting that the local environment is not substantially altered by the addition of PR probably due to the low PR concentration. The results agree with our TEM observation, which show that the PRs are not completely soluble in PMMA.

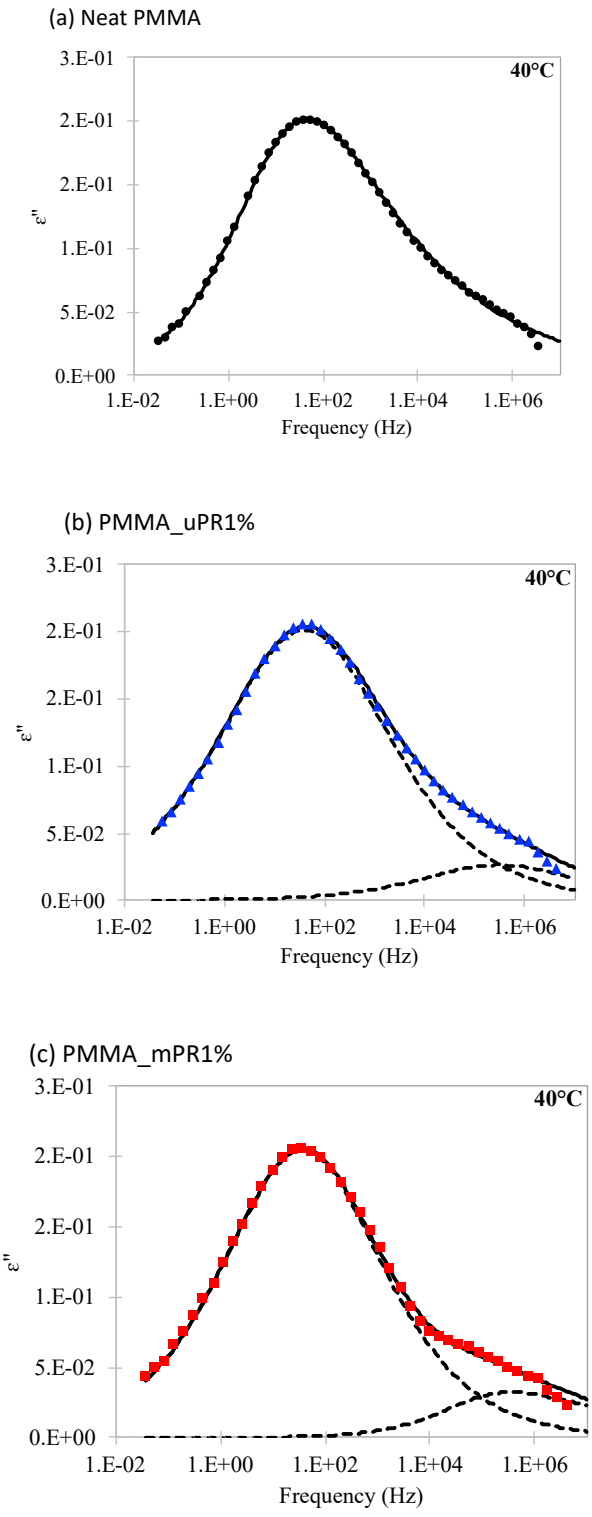

Figure 40. Dielectric loss, ε'', of (a) neat PMMA; (b) PMMA/uPR; (c) PMMA/mPR at 40°C. The symbols represent the experimental data. Depending on the temperature, i.e., the relaxations

observable in the frequency window, either one or two HN functions were used (dashed lines) while the dc ionic conductivity contribution was subtracted. The solid lines are convolutions of individual functions used to model the entire spectrum.

Significant differences between the model PMMA systems emerge at higher temperatures. To further investigate the effect of PR on the dielectric behavior of PMMA, the temperature dependence of the dielectric loss at different frequencies is shown in Figure(a-d). In accordance with the DMA results, PMMA/mPR shows a more pronounced β-relaxation. The differences among the model systems are more discernable at lower frequencies, which correspond to a larger length-scale and might be facilitated by the sliding motion of the PRs. Addition of PRs brings out significant differences in the α-relaxation process, which is related to longer length-scale molecular motion [113]. The width of the loss peak is a representation of the distribution of the relaxation times, which is associated with the homogeneity of the relaxation environment within the system [106]. A more heterogeneous relaxation environment is reflected in a wider distribution of relaxation times. As shown in Figurea-c, mPR induces a higher degree of broadening in the α-relaxation process of PMMA, indicating a less homogeneous relaxing environment. On the other hand, PMMA containing uPR exhibits a much faster relaxation dynamics likely due to the lack of affinity with PMMA Figure(c-d). This agrees with our DMA results in Figure 27a, which show that PMMA/uPR exhibits a decrease in T_g. It should be noted that there is a significant difference in the frequencies used between dielectric relaxation and DMA experiments; thus, the observed relaxation mechanisms are entirely different. The normalized spectra of the temperature dependence of the dielectric loss are shown in Figure 42. The addition of 1 phr of mPR to PMMA clearly shifts the position of the maximum loss to higher temperatures, indicating a broader molecular relaxation involving a larger length-scale molecular cooperativity. Since the β-

relaxation process correlates well with the mechanical properties of polymeric materials [114], adding both types of PR leads to an additional contribution to the local relaxation process, which is more pronounced for PMMA containing mPR (Figure 40c).

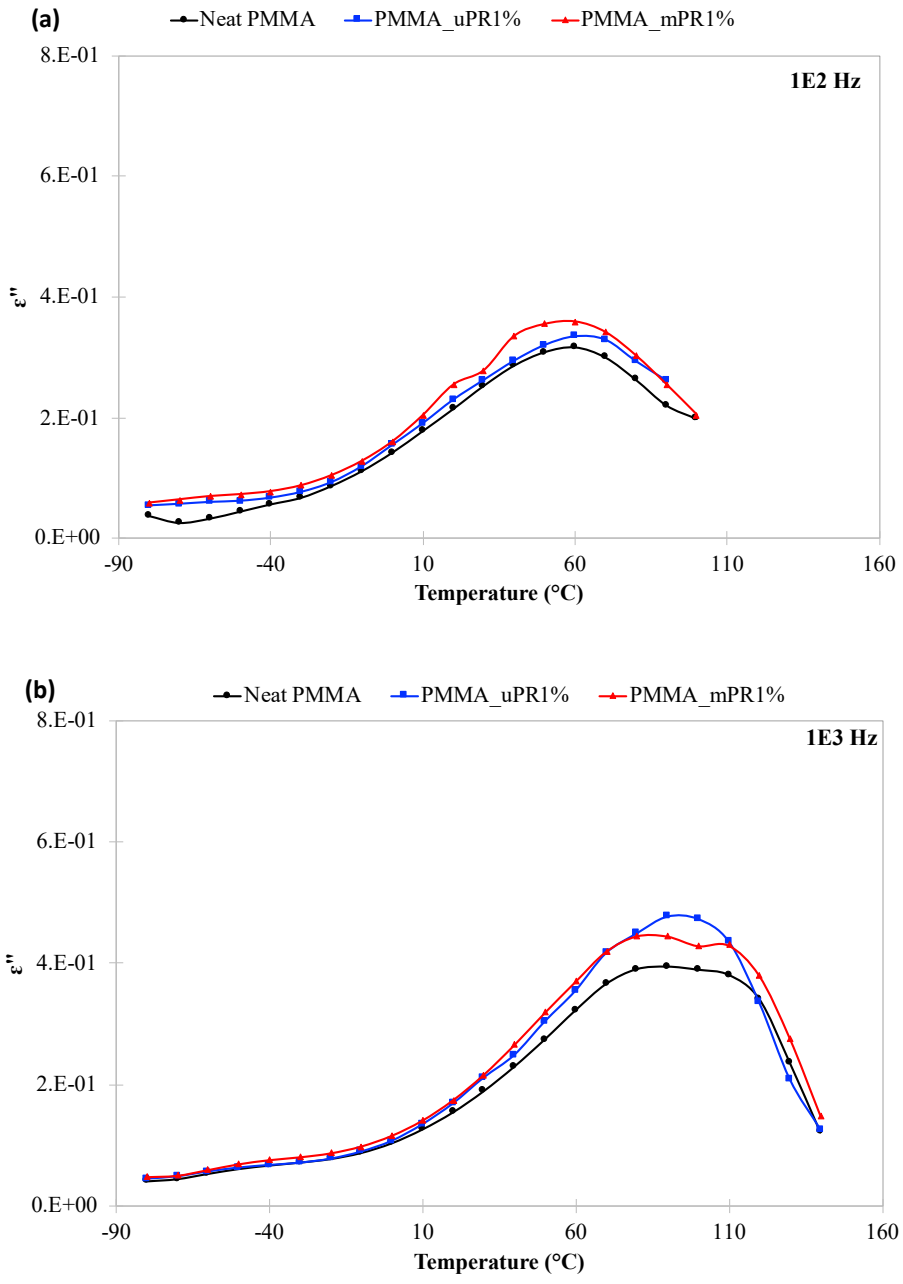

Figure 41. Temperature dependence of dielectric loss of the model PMMA systems. The tests were conducted at different frequencies: (a) 1E2 Hz; (b) 1E3 Hz; (c) 1E4 Hz; and (d) 1E5 Hz.

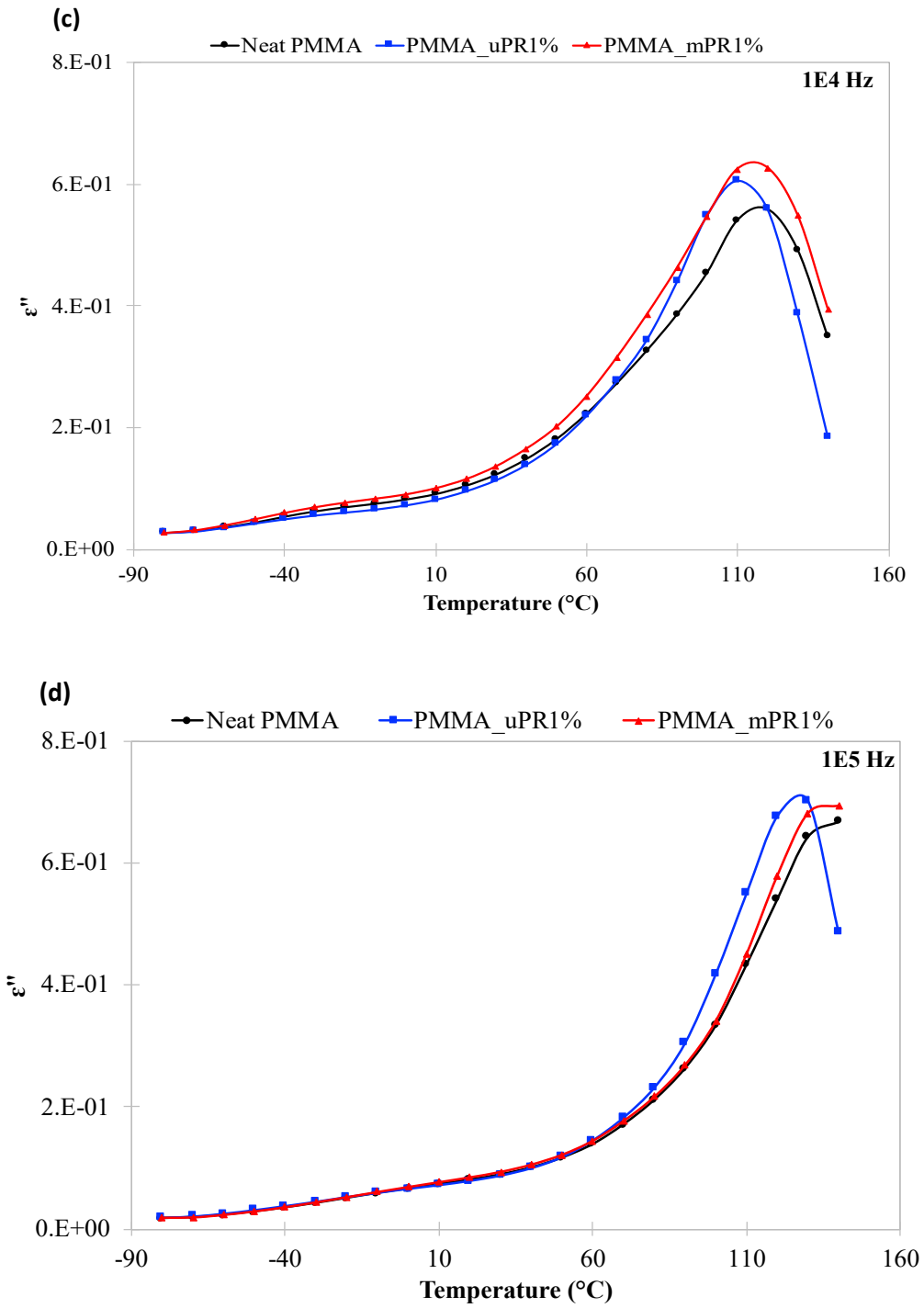

Figure 41. Continued.

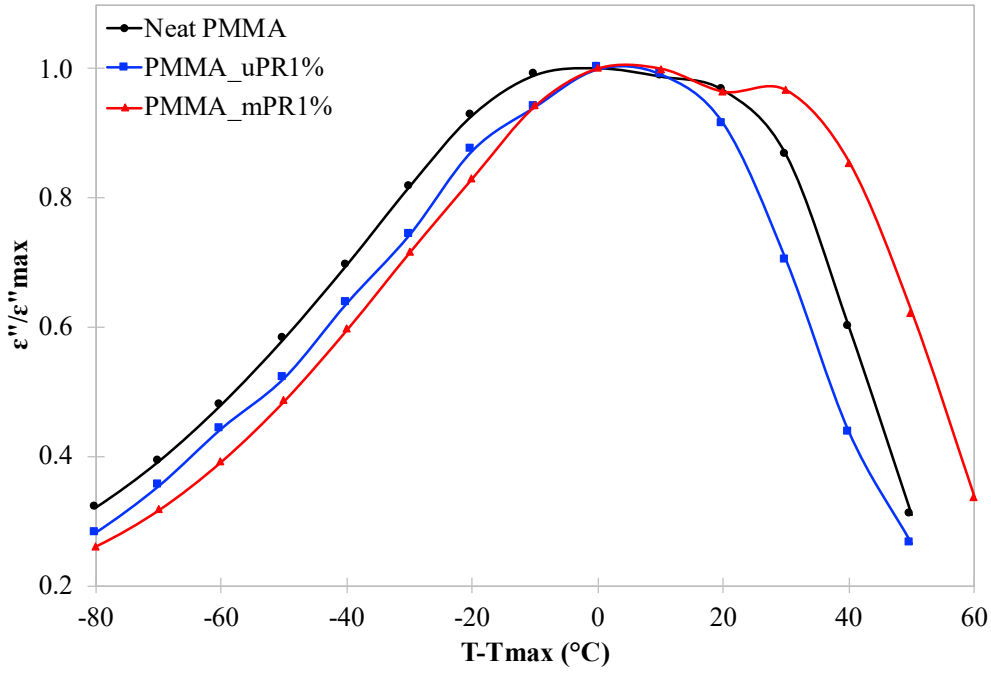

Figure 42. Normalized temperature dependence of the dielectric loss. The plot shows ε”/ε”$_{max}$ vs. T-T$_{max}$ at 1 kHz.

4.4 Discussion

Recently, Mapesa et al. [115] studied the interfacial regions of PMMA containing PMMA-grafted and nongrafted silica nanoparticles, and showed that slower or faster relaxation dynamics is strongly influenced by the nature of the interfacial zone. The mean relaxation rates for the β-relaxation were found to be similar among their neat PMMA and nanocomposite systems, which agrees with our findings. This could be understood by considering that the β-relaxation is a highly localized relaxation process and is expected to be unaffected by interactions between the matrix and the filler. Moreover, the presence of both nongrafted and grafted silica nanoparticles seemed to suppress the α-process, agreeing with our findings and with previous reports of PMMA composites [106, 111]. It was proposed that nongrafted silica particles contain hydroxyl groups

that can participate in hydrogen-bonding interactions, which leads to a formation of an interphase with reduced mobility to increase T_g.

In the present study, the differences between uPR and mPR in their interaction with PMMA leads to a different distribution of energy barriers, which is revealed by the additional peak found that can be detected despite the low PR concentration used. It was also shown that the dynamics of the α-process is strongly influenced by PRs, specifically by mPR to strongly influence the large-scale molecular motion of PMMA in a more heterogeneous fashion. These attributes are inevitably reflected on the intrinsic material characteristics of the model systems.

The observed dielectric behavior correlated well with our DMA results, both showing a more noticeable β-relaxation for PMMA containing mPR and a faster relaxation dynamic in the α-process for PMMA containing uPR. Despite its low concentration, it is evident that mPR significantly influence the relaxation dynamics of PMMA. More in-depth studies are still needed to obtain better understanding on how different modifications on PR will influence the dynamics of the α-relaxation in polymers. At this point, we propose that the presence of the methacrylate functional groups at the terminal of the PCL-grafted chains on CDs promote better coupling and affinity with the PMMA matrix, leading to a more heterogeneous relaxation environment and promote longer range molecular relaxation. In turn, PMMA containing mPR exhibits an enhancement in both the tensile strength and compressive yield stress accompanied by a significant reduction in the SCOF, which lead to greatly improved scratch performance. Having a high compressive yield stress leads to a lower penetration depth during the scratch process; as a result, the frictional forces are lower, and the onset of crack formation is delayed.

4.5 Conclusion

The scratch behavior of PMMA containing PRs with different modifications was investigated. Intrinsic material properties such as the tensile strength and the yield stress, were correlated with the onset of crack formation during scratching. Addition of only 1 wt.% of mPR enhances the compressive properties, specifically, the yield stress, of PMMA, which leads to an improvement in scratch resistance of over 100%. It was shown that partially modifying the terminal of the PCL-grafted chains on PR significantly influence the mechanical and scratch behavior of PMMA. Dielectric relaxation studies revealed that PMMA/PR systems exhibit an additional contribution to the local relaxation process. This additional contribution is more pronounced for mPR than uPR. Moreover, mPR seems to the suppress α-relaxation process, related to large-scale molecular motion. These singularities, which are a consequence of the unique and complex molecular structure of PRs, inevitably reflect on intrinsic material properties of the model systems. Future work will focus on studying the dynamics of the a-relaxation and the possible interactions at interfacial region between PMMA and PR.

CHAPTER V

CONCLUSIONS AND CONSIDERATIONS FOR FUTURE RESEARCH

5.1 Summary and Conclusion

Extensive experimental work was carried out in this study to gain fundamental understanding of the scratch behavior of different polymeric system. The focus of this research effort was the following:

- Determine the key mechanical properties that influence the scratch resistance of polymers
- Investigate how the tensile and the compressive constitutive behavior of polymers interplay during scratch deformation
- Investigate what key parameters dictate the scratch visibility resistance of polymers and how they are linked to material properties
- Apply novel material concepts like sliding-ring materials to improve to scratch resistance of PMMA
- Investigate the mechanisms behind the observed improvement in the scratch resistance of PMMA from a physics and a mechanistic point of view

By investigating a set of model epoxy systems with varying crosslinking density, fundamental structure-property relationships were established. The material properties and scratch-induced damage were correlated, and it was found that the tensile strength alone is insufficient to determine the resistance against crack formation. Both tensile strength and compressive yield stress play important roles in damage formation during scratching. Increasing the compressive yield stress can improve the scratch resistance of polymers by delaying the onset of crack formation. Additionally, other scratch testing methods were considered and compared against the ASTM

scratch test. The pencil hardness is a quick method to assess the scratch resistance of polymeric systems. However, pencil hardness results do not correlate with the intrinsic material properties of the model systems. The pencil hardness results can be influenced by many external factors, such as operator, surface characteristics of the sample and the surface finish of the pencil tip.

By investigating a set of injection molded model PC system with different tensile and compressive constitutive behaviors, it was found that the compressive yield stress strongly influences the scratch depth and shoulder height formation, which originate from the material being compressed in front of the scratch tip and displaced to the sides. Since the material in front of the tip is in compression, the groove formation and the groove geometrical parameters are closely linked to the compressive behavior rather than the tensile behavior. On the other hand, the tensile properties have a minor influence on the scratch visibility resistance of ductile polymers unless brittle-like features such as crazing and cracking occur, which will increase the roughening along the scratch path, leading to an early scratch visibility onset. In addition to mechanical properties, it was shown that the frictional behavior and surface characteristics also have a significant influence on scratch deformation. A lower COF can delay the onset of groove formation, which in turn delays the onset of visibility. Furthermore, the change in surface roughness between the scratched and the unscratched region of the samples also influences the scratch visibility. This study clearly showed that the scratch process is extremely complex and is influenced by many factors. Both the material properties and surface characteristics must be considered for a comprehensive understanding of the observed scratch behavior.

Lastly, the role of PR on the scratch resistance of PMMA was investigated. The findings indicate that a low amount of PR modified with a methacrylate group (mPR) significantly improves the scratch resistance of PMMA. The observed improvements were attributed to

increases in tensile strength and compressive yield stress, which leads to a lower SCOF and high scratch depth recovery. The molecular relaxation of the model PMMA systems was investigating using DMA and dielectric spectroscopy. In comparison to neat PMMA, PMMA/mPR shows a more pronounced β-relaxation. The differences among the model systems are more discernable at lower frequencies, which correspond to a larger length-scale and might be facilitated by the sliding motion of the PRs. Addition of PRs brings out significant differences in the α-relaxation process, which is related to longer length-scale molecular motion. PMMA/mPR also exhibits a higher degree of broadening in the α-relaxation process of PMMA, indicating a less homogeneous relaxing environment. These attributes are inevitably reflected on the intrinsic material characteristics of the model systems. It was concluded that the presence of the methacrylate functional group in PR leads to a more heterogeneous relaxation environment and promote longer range molecular relaxation. As a result, PMMA containing mPR exhibits an enhancement in the tensile strength and compressive yield stress, which manifest in a reduction in SCOF and in an improvement in scratch resistance.

5.2 Considerations for Future Research

Even though significant progress has been achieved in understanding the fundamental nature of polymer scratch behavior. There are still several aspects of polymer scratch deformation that should be addressed to enable the design of scratch resistance polymers.

5.2.1 Scratch Testing Capabilities

The standardized scratch testing has allowed for a reliable and reproducible examination of the scratch resistance of polymers. The scratch testing capabilities can be improved by incorporating additional features that allow for a deeper understanding on the physics behind the scratch phenomena. For instance, most of the scratch analysis, like scratch depth and shoulder

height, has been performed post-mortem. *In-situ* measurement of the scratch depth can provide insights about the subsequent elastic recovery behavior of polymers.

5.2.2 Finite Element Methods (FEM) Simulation

FEM enables the determination of the effect of individual or multiple material parameters on the scratch behavior in a well-controlled manner [16, 44]. Thus, the results from numerical simulations can be used to supplement experimental findings for fundamental structure-property relationship correlation. More importantly, since it is more a mechanistic approach rather than phenomenological, FEM can be used to learn exactly how the constitutive parameters influence scratch behavior. There are several challenges regarding numerical simulation. Firstly, the polymer deformation without an adequate damage criterion itself poses a big challenge. It is well known that the mechanical behavior of polymers is strain rate, temperature, and stress-state dependent. The absence of a physics-based constitutive model that is able to encompass all these factors adds complexity to the scratch problem. Current constitutive models are semi-empirical in nature, which rely on a large number of experimentally obtained parameters and assumptions. Determination of these parameters will require a long arduous experimental effort, limiting the usefulness and universal application of these models. Moreover, capturing the underlying physics associated with scratch damage formation and evolution for modeling purposes remains a challenge. Extensive research efforts are still needed.

In many polymers, such as epoxy and polycarbonate, micro-cracking is the dominant deformation mode. Therefore, it is of extreme importance to simulate scratch-induced cracking and crazing. An appropriate damage initiation criterion is required to simulate the onset of failure. Consequently, a damage evolution criterion has to be adopted to simulate the degradation of the load bearing capabilities once the damage initiation criterion has been met. Successful cracking

simulation along with a set of well-controlled model systems will allow to understand the mechanics behind scratch-induced damages. In this view, it is hoped that employing well-controlled model polymer systems and refining testing and numerical capabilities, a theorical framework on surface deformation and damage phenomena can be developed. With a framework involving material parameters and scratch mechanics, we can establish predictive model to design polymers with superior scratch performance.

5.2.3 Expanding the Use of Polyrotaxane

The work presented in Chapter IV has demonstrated that mPR can significantly improve the scratch resistance of PMMA. The tensile strength and compressive yield stress of PMMA/mPR is significantly higher than that of neat PMMA, resulting in an improvement in scratch resistance. It was also shown that PRs brings out significant differences in the long length-scale molecular motion of PMMA. Even though this study shows clear differences between the mechanical properties and molecular relaxation dynamics of PMMA and PMMA/mPR, there are still several aspects that remain unclear:

- It was shown that mPR leads to a higher degree of broadening in the α-relaxation process, determination of the activation energy of the α-relaxation can help understand how mPR influences the relaxation dynamics of PMMA, specially at lower frequencies, where the differences between them are more discernable
- Different functionalization of the ring structure of PR have shown to strongly influence the affinity between PR and PMMA, which in turn affects the mechanical properties, scratch behavior and relaxation dynamics of PMMA. Investigating possible interactions at interfacial region between PMMA and PR can help to understand how PR behaves in different polymer matrices

- Preliminary findings indicate that the molecular weight and the molecular structure of the PMMA matrix influence the mechanical and scratch behavior of PMMA/PR systems. A systematic study with well-controlled model systems should be conducted to determine why and how the PMMA matrix influence the reinforcement effect of PR
- The ultimate goal of this dissertation research is to apply the gained knowledge to design polymers with superior scratch resistance. PR could be incorporated into other engineering polymers. Proper functionalization of the ring structure in PR is required to ensure good compatibility with other polymer matrices.

REFERENCES

1. Browning, R.L., H. Jiang, and H.-J. Sue, *Scratch behavior of polymeric materials*, in *Tribology and Interface Engineering Series*. 2008, Elsevier. p. 354-373.
2. Guevin, P., *State-of-the-art instruments to measure coating hardness.* JCT, Journal of coatings technology, 1995. **67**(840): p. 61-65.
3. Vingsbo, O. and S. Hogmark, *Single-pass pendulum grooving—a technique for abrasive testing.* Wear, 1984. **100**(1-3): p. 489-502.
4. Liang, Y., et al., *Some developments for single-pass pendulum scratching.* Wear, 1996. **199**(1): p. 66-73.
5. Briscoe, B., A. Delfino, and E. Pelillo, *Single-pass pendulum scratching of poly (styrene) and poly (methylmethacrylate).* Wear, 1999. **225**: p. 319-328.
6. Chanda, A., et al., *A new parameter for measuring wear of materials.* Journal of materials science letters, 1997. **16**(20): p. 1647-1651.
7. Kody, R.S. and D.C. Martin, *Quantitative characterization of surface deformation in polymer composites using digital image analysis.* Polymer Engineering & Science, 1996. **36**(2): p. 298-304.
8. Chu, J., et al., *Scratch resistance of mineral-filled polypropylene materials.* Polymer Engineering & Science, 2000. **40**(4): p. 944-955.
9. Wong, M., et al., *A new test methodology for evaluating scratch resistance of polymers.* Wear, 2004. **256**(11): p. 1214-1227.
10. Wu, L.Y., et al., *A study towards improving mechanical properties of sol–gel coatings for polycarbonate.* Thin Solid Films, 2008. **516**(6): p. 1056-1062.

11. Hwang, D., et al., *Scratch resistant and transparent UV-protective coating on polycarbonate.* Journal of Sol-Gel Science and Technology, 2003. **26**(1-3): p. 783-787.

12. ASTM, D., *3363-05 Standard Test Method for Film Hardness by Pencil Test*. 2011, ASTM International West Conshohocken, PA.

13. Molero, G. and H.-J. Sue, *Scratch behavior of model epoxy resins with different crosslinking densities.* Materials & Design, 2019: p. 107965.

14. Astm, D., *7027–05, Standard Test Method for Evaluation of Scratch Resistance of Polymeric Coatings and Plastics Using an Instrumented Scratch Machine.* ASTM International, 2005.

15. Jiang, H., R. Browning, and H.-J. Sue, *Understanding of scratch-induced damage mechanisms in polymers.* Polymer, 2009. **50**(16): p. 4056-4065.

16. Hossain, M.M., et al., *Effect of asymmetric constitutive behavior on scratch-induced deformation of polymers.* Tribology Letters, 2012. **47**(1): p. 113-122.

17. Browning, R., et al., *Effects of acrylonitrile content and molecular weight on the scratch behavior of styrene-acrylonitrile random copolymers.* Polymer Engineering & Science, 2011. **51**(11): p. 2282-2294.

18. Bucaille, J.-L., et al., *The influence of strain hardening of polymers on the piling-up phenomenon in scratch tests: experiments and numerical modelling.* Wear, 2006. **260**(7-8): p. 803-814.

19. Jiang, H., et al., *Finite element method parametric study on scratch behavior of polymers.* Journal of Polymer Science Part B: Polymer Physics, 2007. **45**(12): p. 1435-1447.

20. Hossain, M.M., H. Jiang, and H.-J. Sue, *Effect of constitutive behavior on scratch visibility resistance of polymers—A finite element method parametric study.* Wear, 2011. **270**(11-12): p. 751-759.

21. Hutchings, I., P. Wang, and G. Parry, *An optical method for assessing scratch damage in bulk materials and coatings.* Surface and Coatings Technology, 2003. **165**(2): p. 186-193.

22. Rangarajan, P., et al., *Scratch visibility of polymers measured using optical imaging.* Polymer Engineering & Science, 2003. **43**(3): p. 749-758.

23. Wong, M., et al., *Study of surface damage of polypropylene under progressive loading.* Journal of materials science, 2004. **39**(10): p. 3293-3308.

24. Chrisman, J., et al., *Testing and evaluation of mar visibility resistance for polymer films.* Polymer Testing, 2018. **69**: p. 238-244.

25. Xiao, S., et al., *Scratch behavior of model polyurethane elastomers containing different soft segment types.* Materials & Design, 2017. **132**(Supplement C): p. 419-429.

26. Liang, Y.L., H.J. Sue, and R. Minkwitz, *Rubber content effect on scratch behavior in acrylonitrile-styrene-acrylate copolymers.* Journal of Applied Polymer Science, 2012. **126**(3): p. 1088-1096.

27. Ali, U., K.J.B.A. Karim, and N.A. Buang, *A review of the properties and applications of poly (methyl methacrylate)(PMMA).* Polymer Reviews, 2015. **55**(4): p. 678-705.

28. Lalande, L., et al., *Microdeformation mechanisms in rubber toughened PMMA and PMMA-based copolymers.* Engineering Fracture Mechanics, 2006. **73**(16): p. 2413-2426.

29. Qu, M., et al., *Tailoring and probing particle–polymer interactions in PMMA/silica nanocomposites.* Soft Matter, 2011. **7**(18): p. 8401-8408.

30. Dos Santos, F.C., et al., *On the structure of high performance anticorrosive PMMA–siloxane–silica hybrid coatings.* RSC advances, 2015. **5**(129): p. 106754-106763.

31. Fabre-Francke, I., et al., *Hybrid PMMA combined with polycarbonate inside interpenetrating polymer network architecture for development of new anti-scratch glass.* Materials Today Communications, 2019. **21**: p. 100582.

32. Mansha, M., et al., *The effect of plasticization by fatty acid amides on the scratch resistance of PMMA.* Wear, 2011. **271**(5-6): p. 671-679.

33. Chakraborty, H., et al., *Indentation and scratch behavior of functionalized MWCNT–PMMA composites at the micro/nanoscale.* Polymer composites, 2014. **35**(5): p. 948-955.

34. Noda, Y., Y. Hayashi, and K. Ito, *From topological gels to slide-ring materials.* Journal of Applied Polymer Science, 2014. **131**(15).

35. Ito, K., *Slide-ring materials using topological supramolecular architecture.* Current Opinion in Solid State and Materials Science, 2010. **14**(2): p. 28-34.

36. Seo, J., et al., *Foldable and extremely scratch-resistant hard coating materials from molecular necklace-like cross-linkers.* ACS applied materials & interfaces, 2019.

37. Hamdi, M., X. Zhang, and H.-J. Sue, *Fundamental understanding on scratch behavior of polymeric laminates.* Wear, 2017. **380-381**(Supplement C): p. 203-216.

38. Wong, J.S., et al., *Scratch damage of polymers in nanoscale.* Acta Materialia, 2004. **52**(2): p. 431-443.

39. Jiang, H., et al., *Quantitative evaluation of scratch visibility resistance of polymers.* Applied Surface Science, 2010. **256**(21): p. 6324-6329.

40. Liang, Y.-L., et al., *Effect of high temperature annealing on scratch behavior of acrylonitrile styrene acrylate copolymers.* Polymer, 2012. **53**(2): p. 604-612.

41. Xiao, S., et al., *Physical correlation between abrasive wear performance and scratch resistance in model polyurethane elastomers.* Wear, 2019. **418**: p. 281-289.

42. Hossain, M.M., et al., *Quantitative modeling of scratch-induced deformation in amorphous polymers.* Polymer, 2014. **55**(23): p. 6152-6166.

43. Hossain, M.M., R. Minkwitz, and H.J. Sue, *Minimization of surface friction effect on scratch-induced deformation in polymers.* Polymer Engineering & Science, 2013. **53**(7): p. 1405-1413.

44. Hossain, M.M., H. Jiang, and H.-J. Sue, *Effect of constitutive behavior on scratch visibility resistance of polymers—A finite element method parametric study.* Wear, 2011. **270**(11): p. 751-759.

45. Chandelia, V.K., H.-J. Sue, and M.M. Hossain, *FEM Modeling on Scratch Behavior of Multiphase Polymeric Systems.* Tribology Letters, 2018. **66**(2): p. 1-16.

46. Brostow, W., et al., *Molecular dynamics computer simulation of scratch resistance testing of polymers: visualization.* Polymer bulletin, 2013. **70**(4): p. 1457-1464.

47. Gómez-del Río, T. and J. Rodríguez, *Compression yielding of epoxy: strain rate and temperature effect.* Materials & Design, 2012. **35**: p. 369-373.

48. Mayr, A.E., W.D. Cook, and G.H. Edward, *Yielding behaviour in model epoxy thermosets—I. Effect of strain rate and composition.* Polymer, 1998. **39**(16): p. 3719-3724.

49. Radhakrishnan, S., N. Sonawane, and C. Siju, *Epoxy powder coatings containing polyaniline for enhanced corrosion protection.* Progress in Organic Coatings, 2009. **64**(4): p. 383-386.

50. Lei, F., et al., *Scratch behavior of epoxy coating containing self-assembled zirconium phosphate smectic layers.* Polymer, 2017. **112**: p. 252-263.

51. Joshi, M. and U. Chatterjee, *Polymer nanocomposite: An advanced material for aerospace applications*, in *Advanced Composite Materials for Aerospace Engineering*. 2016, Elsevier. p. 241-264.

52. Bilyeu, B., W. Brostow, and K.P. Menard, *Epoxy thermosets and their applications I: chemical structures and applications.* Journal of Materials Education, 1999. **21**(5/6): p. 281-286.

53. Zhao, S. and M.M. Abu-Omar, *Renewable epoxy networks derived from lignin-based monomers: effect of cross-linking density.* ACS Sustainable Chemistry & Engineering, 2016. **4**(11): p. 6082-6089.

54. Choi, J.H., et al., *Effect of crosslink density on thermal conductivity of epoxy/carbon nanotube nanocomposites.* Journal of Applied Polymer Science, 2017. **134**(4).

55. Garcia, F.G., et al., *Mechanical properties of epoxy networks based on DGEBA and aliphatic amines.* Journal of Applied Polymer Science, 2007. **106**(3): p. 2047-2055.

56. Bilyeu, B., W. Brostow, and K.P. Menard, *Epoxy thermosets and their applications II. Thermal analysis.* Journal of Materials Education, 2000. **22**(4/6): p. 107-130.

57. Bilyeu, B., W. Brostow, and K.P. Menard, *Separation of gelation from vitrification in curing of a fiber-reinforced epoxy composite.* Polymer Composites, 2002. **23**(6): p. 1111-1119.

58. *Standard Test Method for Film Hardness by Pencil Test*. 2011.

59. Chattopadhyay, D., S.S. Panda, and K. Raju, *Thermal and mechanical properties of epoxy acrylate/methacrylates UV cured coatings.* Progress in Organic Coatings, 2005. **54**(1): p. 10-19.

60. Brostow, W., et al., *Tribology with emphasis on polymers: friction, scratch resistance and wear.* Journal of Materials Education, 2003. **25**(4/6): p. 119-132.

61. Standard, A., *D695: Standard Test Method for Compressive Properties of Rigid Plastics.* ASTM International, West Conchohocken, 2008.

62. Oleinik, E.F., *Epoxy-aromatic amine networks in the glassy state structure and properties*, in *Epoxy resins and composites IV*. 1986, Springer. p. 49-99.

63. Vallo, C.I., P.M. Frontini, and R.J. Williams, *Elastic modulus and yield stress of epoxy networks in the glassy state.* Polymer Gels and Networks, 1993. **1**(4): p. 257-266.

64. Yamini, S. and R.J. Young, *The mechanical properties of epoxy resins.* Journal of materials science, 1980. **15**(7): p. 1823-1831.

65. Lesser, A.J. and R.S. Kody, *A generalized model for the yield behavior of epoxy networks in multiaxial stress states.* Journal of Polymer Science Part B: Polymer Physics, 1997. **35**(10): p. 1611-1619.

66. Bucaille, J.-L., E. Felder, and G. Hochstetter, *Experimental and three-dimensional finite element study of scratch test of polymers at large deformations.* J. Trib., 2004. **126**(2): p. 372-379.

67. Fortuna, S.V., et al., *Microstructural features of wear-resistant titanium nitride coatings deposited by different methods.* Thin Solid Films, 2000. **377**: p. 512-517.

68. Martin-Palma, R., et al., *Optical and compositional analysis of functional SiOxCy: H coatings on polymers.* Thin Solid Films, 2006. **515**(4): p. 2493-2496.

69. Wu, L.Y., et al., *Synthesis and characterization of transparent hydrophobic sol-gel hard coatings.* Journal of sol-gel science and technology, 2006. **38**(1): p. 85-89.

70. Schmidt, H., *Inorganic-organic composites by sol-gel techniques.* MRS Online Proceedings Library (OPL), 1989. **171**.

71. Lee, T.-H., E.-S. Kang, and B.-S. Bae, *Catalytic effects of aluminum butoxyethoxide in sol-gel hybrid hard coatings.* Journal of sol-gel science and technology, 2003. **27**(1): p. 23-29.

72. Robertson, M., et al., *Mechanical and thermal properties of organic/inorganic hybrid coatings.* Journal of sol-gel science and technology, 2003. **26**(1): p. 291-295.

73. Fabbri, P., et al., *Improvement of the surface properties of polycarbonate by organic–inorganic hybrid coatings.* Journal of applied polymer science, 2008. **108**(3): p. 1426-1436.

74. Fabbri, P., et al., *Enhancing the scratch resistance of polycarbonate with poly (Ethylene oxide)–silica hybrid coatings.* Advances in Polymer Technology: Journal of the Polymer Processing Institute, 2008. **27**(2): p. 117-126.

75. Le Bail, N., et al., *Scratch-resistant sol–gel coatings on pristine polycarbonate.* New Journal of Chemistry, 2015. **39**(11): p. 8302-8310.

76. Sowntharya, L., et al., *Investigations on the mechanical properties of hybrid nanocomposite hard coatings on polycarbonate.* Ceramics International, 2012. **38**(5): p. 4221-4228.

77. Boentoro, W., A. Pflug, and B. Szyszka, *Scratch resistance analysis of coatings on glass and polycarbonate.* Thin Solid Films, 2009. **517**(10): p. 3121-3125.

78. Seong, D.-W., J.-S. Yeo, and S.-H. Hwang, *Fabrication of polycarbonate blends with poly(methyl methacrylate-co-phenyl methacrylate) copolymer: Miscibility and scratch resistance properties.* Journal of Industrial and Engineering Chemistry, 2016. **36**: p. 251-254.

79. Stuart, B. and B. Briscoe, *Scratch hardness studies of poly (ether ether ketone).* Polymer, 1996. **37**(17): p. 3819-3824.

80. Briscoe, B.J., et al., *Scratching maps for polymers.* Wear, 1996. **200**(1-2): p. 137-147.

81. Zhang, J., et al., *In-situ observation of temperature rise during scratch testing of poly (methylmethacrylate) and polycarbonate.* Tribology International, 2016. **95**: p. 1-4.

82. Misra, R., R. Hadal, and S. Duncan, *Surface damage behavior during scratch deformation of mineral reinforced polymer composites.* Acta Materialia, 2004. **52**(14): p. 4363-4376.

83. Jiang, H. and H. Sue, *ASV© User's Manual V. 1.4.* College Station, TX, 2009.

84. Crist, B., *Yield processes in glassy polymers*, in *The physics of glassy polymers*. 1997, Springer. p. 155-212.

85. Capaccio, G. and I. Ward, *Effect of molecular weight on the morphology and drawing behaviour of melt crystallized linear polyethylene.* Polymer, 1975. **16**(4): p. 239-243.

86. Govaert, L. and T.A. Tervoort, *Strain hardening of polycarbonate in the glassy state: influence of temperature and molecular weight.* Journal of Polymer Science Part B: Polymer Physics, 2004. **42**(11): p. 2041-2049.

87. Nunes, R.W., J.R. Martin, and J.F. Johnson, *Influence of molecular weight and molecular weight distribution on mechanical properties of polymers.* Polymer Engineering & Science, 1982. **22**(4): p. 205-228.

88. Wills, A., G. Capaccio, and I. Ward, *Plastic deformation of polypropylene: Effect of molecular weight on drawing behavior and structural characteristics of ultra-high-modulus products.* Journal of Polymer Science: Polymer Physics Edition, 1980. **18**(3): p. 493-509.

89. Boyce, M.C., D.M. Parks, and A.S. Argon, *Large inelastic deformation of glassy polymers. Part I: rate dependent constitutive model.* Mechanics of materials, 1988. **7**(1): p. 15-33.

90. Hamilton, G.M. and L. Goodman, *The stress field created by a circular sliding contact.* 1966.

91. Hamilton, G.M., *Explicit equations for the stresses beneath a sliding spherical contact.* Proceedings of the Institution of Mechanical Engineers, Part C: Journal of Mechanical Engineering Science, 1983. **197**(1): p. 53-59.

92. Harb, S.V., et al., *Siloxane–PMMA hybrid anti-corrosion coatings reinforced by lignin.* Surface and Coatings Technology, 2015. **275**: p. 9-16.

93. Harb, S.V., et al., *A comparative study on graphene oxide and carbon nanotube reinforcement of PMMA-siloxane-silica anticorrosive coatings.* ACS applied materials & interfaces, 2016. **8**(25): p. 16339-16350.

94. Tsai, T.-Y., et al., *Effects of modified clay on the morphology and thermal stability of PMMA/clay nanocomposites.* Materials chemistry and Physics, 2013. **138**(1): p. 230-237.

95. An, J., et al., *Observation and evaluation of scratch characteristics of injection-molded poly (methyl methacrylate) toughened by acrylic rubbers.* Tribology International, 2014. **77**: p. 32-42.

96. Liu, C., et al., *Unusual fracture behavior of slide-ring gels with movable cross-links.* ACS Macro Letters, 2017. **6**(12): p. 1409-1413.

97. *Standard Test Method for Evaluation of Scratch Resistance of Polymeric Coatings and Plastics Using an Instrumented Scratch Machine*.

98. Harada, A. and M. Kamachi, *Complex formation between poly (ethylene glycol) and α-cyclodextrin.* Macromolecules, 1990. **23**(10): p. 2821-2823.

99. Harada, A., J. Li, and M. Kamachi, *Preparation and properties of inclusion complexes of polyethylene glycol with. alpha.-cyclodextrin.* Macromolecules, 1993. **26**(21): p. 5698-5703.

100. Pruksawan, S., et al., *Homogeneously dispersed polyrotaxane in epoxy adhesive and its improvement in the fracture toughness.* Macromolecules, 2019. **52**(6): p. 2464-2475.

101. Ishida, Y. and K. Yamafuji, *Studies on dielectric behaviors in a series of polyalkyl-methacrylates.* Kolloid-Zeitschrift, 1961. **177**(2): p. 97-116.

102. Sasabe, H. and S. Saito, *Dielectric relaxations and electrical conductivities of poly (alkyl methacrylates) under high pressure.* Journal of Polymer Science Part A-2: Polymer Physics, 1968. **6**(8): p. 1401-1418.

103. Williams, G. and D.C. Watts, *Molecular motion in the glassy state. The effect of temperature and pressure on the dielectric β relaxation of polyvinyl chloride.* Transactions of the Faraday Society, 1971. **67**.

104. Ngai, K. and C. Roland, *Chemical structure and intermolecular cooperativity: dielectric relaxation results.* Macromolecules, 1993. **26**(25): p. 6824-6830.

105. Bergman, R., et al., *Dielectric relaxation in PMMA revisited.* Journal of non-crystalline solids, 1998. **235**: p. 580-583.

106. Li, C., et al., *Effect of inorganic phase on polymeric relaxation dynamics in PMMA/silica hybrids studied by dielectric analysis.* European polymer journal, 2004. **40**(8): p. 1807-1814.

107. Williams, G. and D.C. Watts, *Molecular motion in solid amorphous polymers. The dielectric relaxation of a poly-nonyl methacrylate and poly-n-lauryl methacrylate as a*

function of frequency, temperature and applied pressure. Transactions of the Faraday Society, 1971. **67**: p. 2793-2801.

108. De Brouckere, L. and G. Offergeld, *The dielectric properties of solid polymers.* Journal of Polymer Science, 1958. **30**(121): p. 105-118.

109. Mikhailov, G., *Dielectric losses and polarization of polymers.* Journal of Polymer Science, 1958. **30**(121): p. 605-614.

110. Bergman, R., et al., *The merging of the dielectric α-and β-relaxations in poly-(methyl methacrylate).* The Journal of chemical physics, 1998. **109**(17): p. 7546-7555.

111. Madbouly, S.A., *Broadband Dielectric Spectroscopy for Poly (methyl methacrylate)/Poly (α-methyl styrene-co-acrylonitrile) Blend.* Polymer journal, 2002. **34**(7): p. 515-522.

112. Havriliak, S. and S. Negami, *A complex plane representation of dielectric and mechanical relaxation processes in some polymers.* Polymer, 1967. **8**: p. 161-210.

113. Schönhals, A. and E. Schlosser, *Dielectric relaxation in polymeric solids Part 1. A new model for the interpretation of the shape of the dielectric relaxation function.* Colloid and Polymer Science, 1989. **267**(2): p. 125-132.

114. Landry, C.J. and P.M. Henrichs, *The influence of blending on the local motions of polymers. Studies involving polycarbonate, poly (methyl methacrylate), and a polyester.* Macromolecules, 1989. **22**(5): p. 2157-2166.

115. Mapesa, E.U., et al., *Wetting and Chain Packing across Interfacial Zones Affect Distribution of Relaxations in Polymer and Polymer-Grafted Nanocomposites.* Macromolecules, 2020. **53**(13): p. 5315-5325.